Technical Report CHL-98-10
May 1998

US Army Corps of Engineers
Waterways Experiment Station

Joint Wind Wave Height-Frequency-Direction Statistics at Two Disparate Sites

by Charles E. Long

Prepared for Headquarters, U.S. Army Corps of Engineers

The contents of this report are not to be used for advertising, publication, or promotional purposes. Citation of trade names does not constitute an official endorsement or approval of the use of such commercial products.

The findings of this report are not to be construed as an official Department of the Army position, unless so designated by other authorized documents.

Technical Report CHL-98-10
May 1998

Joint Wind Wave Height-Frequency-Direction Statistics at Two Disparate Sites

by Charles E. Long

U.S. Army Corps of Engineers
Waterways Experiment Station
3909 Halls Ferry Road
Vicksburg, MS 39180-6199

Final report

Approved for public release; distribution is unlimited

Prepared for U.S. Army Corps of Engineers
Washington, DC 20314-1000

Under Civil Works Research Work Unit 32484

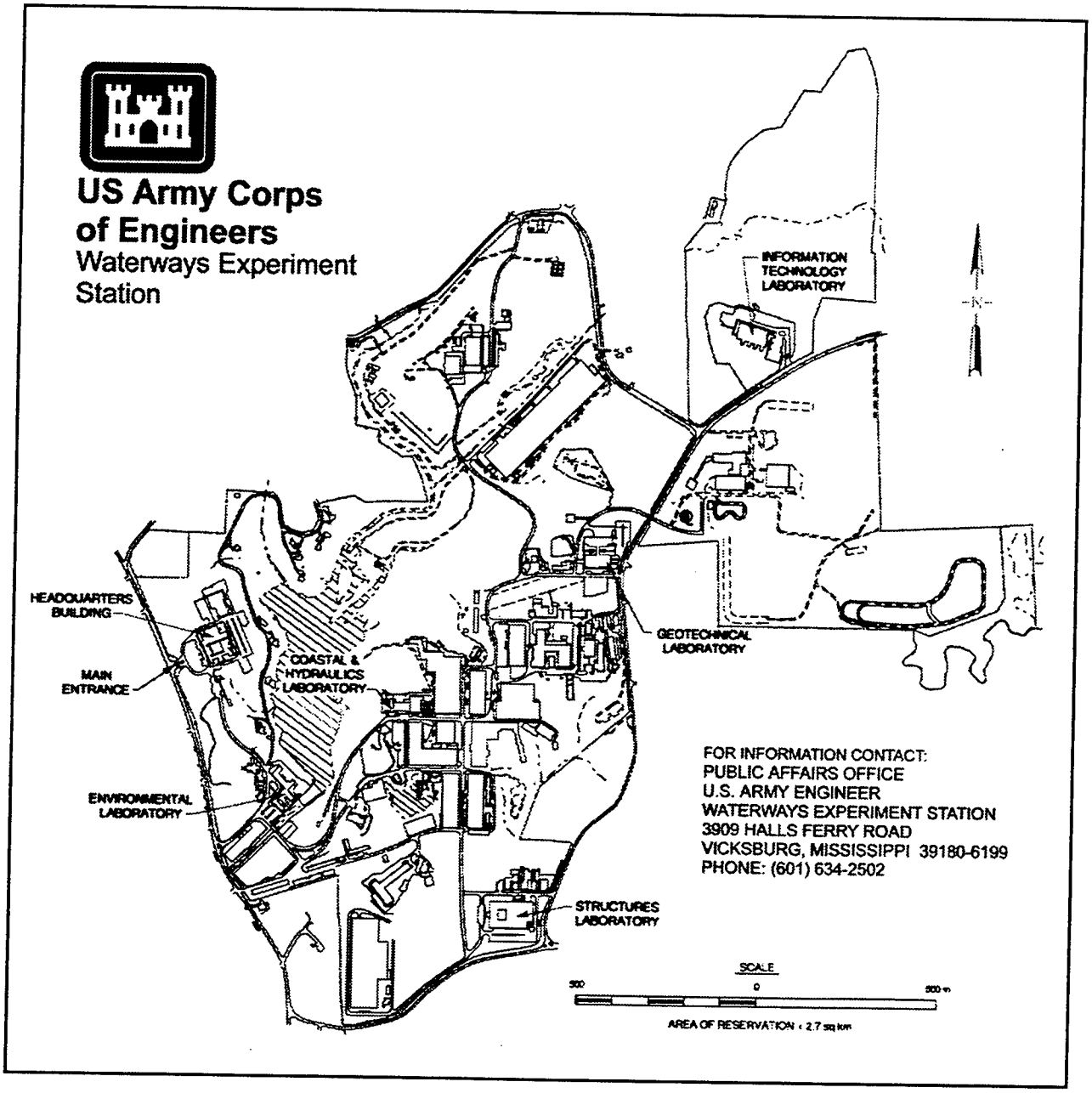

Waterways Experiment Station Cataloging-in-Publication Data

Long, Charles E.
Joint wind wave height-frequency-direction statistics at two disparate sites / by Charles E. Long ; prepared for U.S. Army Corps of Engineers.
107 p. : ill. ; 28 cm. — (Technical report ; CHL-98-10)
Includes bibliographic references.
1. Wind waves — North Carolina — Duck — Statistics. 2. Wind waves — California —Point Conception — Statistics. I. United States. Army. Corps of Engineers. II. U.S. Army Engineer Waterways Experiment Station. III. Coastal and Hydraulics Laboratory (U.S. Army Engineer Waterways Experiment Station) IV. Title. V. Series: Technical report (U.S. Army Engineer Waterways Experiment Station) ; CHL-98-10.
TA7 W34 no.CHL-98-10

Contents

Preface

In response to a need stated in the Shore Protection Manual, this report provides estimates of joint probabilities of characteristic wave height, frequency, and direction based on data from the U.S. Army Engineer Waterways Experiment Station (WES) Coastal and Hydraulics Laboratory (CHL) Field Research Facility (FRF) and Texaco Oil Company's Harvest Platform. This effort was authorized by Headquarters, U.S. Army Corps of Engineers (HQUSACE), under Civil Works Coastal Navigation Hydrodynamics Program Research Work Unit 32484, "Directionality of Waves in Shallow Water." Funds were provided through WES under the program management of Ms. Carolyn M. Holmes, CHL. Messrs. John H. Lockhart, Jr. (retired), Charles Chesnutt, and Barry W. Holliday were HQUSACE Technical Monitors.

This report was prepared by Dr. Charles E. Long, under the direct supervision of Mr. William A. Birkemeier, Chief, FRF, and Mr. Thomas W. Richardson, Chief, Coastal Sediments and Engineering Division, CHL. General supervision was provided by Dr. James R. Houston and Mr. Charles C. Calhoun, Jr., Director and Assistant Director, CHL, respectively.

At the time of publication of this report, Director of WES was Dr. Robert W. Whalin. Commander was COL Robin R. Cababa, EN.

1 Introduction

Extremely useful in coastal engineering project design is knowledge of the statistical wind wave climate in the vicinity of a project site. With such information, physical and numerical models used to test proposed project designs can be driven with meaningful conditions, including most probable wave conditions and rarer, but more destructive, conditions. Tests for conditions that do not occur can be avoided. To execute any of these models, one needs a set of descriptors that adequately represents prototype wave conditions during periods of time that are short, relative to typical storms, tidal variations, and other wave-modifying events, and yet are long enough to be statistically meaningful. These are the same requirements used to define wave record lengths in field measurements. Though the complete wave field during the time of a single sample can be quite complex (Long and Oltman-Shay 1991, Long 1995), it is sufficient for many engineering purposes to represent such a sample by a small number of characterizing parameters. Most of the engineering guidance in the *Shore Protection Manual* (SPM) (1984) is based on three characterizing parameters to represent wave conditions at a particular time. The three parameters are characteristic wave height, wave frequency (or period) of the most energetic waves, and an attack or propagation direction that is representative of a wave field.

Though many of the analysis tools in the SPM (1984) are based on three parameters, examples of statistical characterizations given by the SPM are in terms of wave height alone, owing primarily to the limited data sets available at the time of its 1984 publication. However, the SPM emphasizes the importance of and need for three-parameter statistical climatologies to characterize project study sites. In response to that stated need, this report describes and interprets three-parameter wave climatologies for two somewhat disparate sites.

One of the study sites is near the U.S. Army Engineer Waterways Experiment Station Coastal and Hydraulics Laboratory's Field Research Facility (FRF), located on the Outer Banks of North Carolina, near the village of Duck (Figure 1). Long-term observations from a high-resolution directional wave gauge centered on the 8-m depth contour about 900 m offshore of the FRF are used to characterize conditions typically just outside the surf zone at a shallow east coast site adjacent to a broad continental shelf and exposed to local storms as well as waves radiating from processes in the deep Atlantic Ocean, including hurricanes.

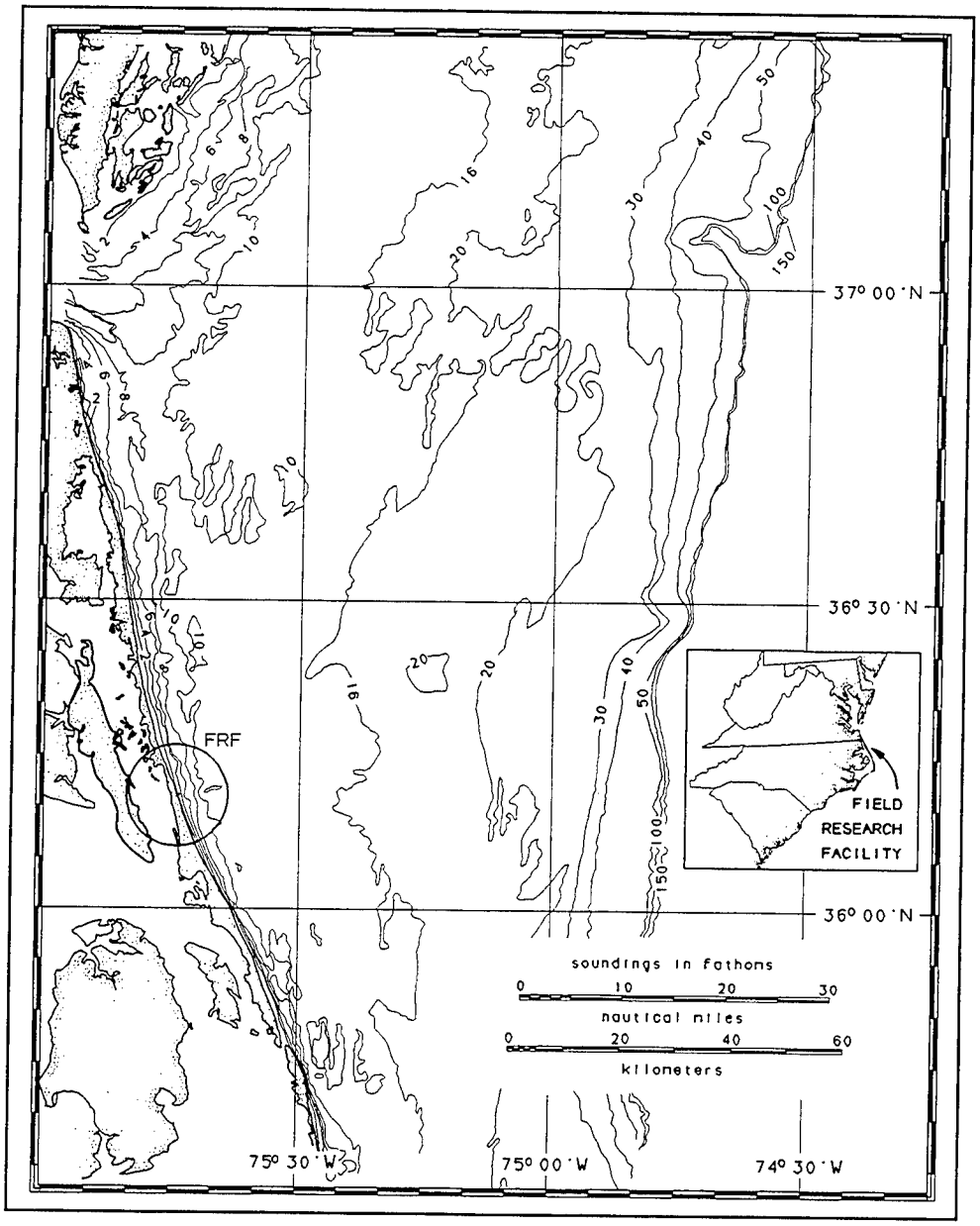

Figure 1. FRF location map

The other site is the Texaco Oil Company oil-production facility known as Harvest Platform, located about 20 km west of Point Conception, California, in water that is 200 m deep (Figure 2). A 3-year database of high-resolution directional wave observations is used to characterize this deepwater west coast site which is exposed to open Pacific Ocean wave conditions along an arc ranging from northwest to west to south and to waves from the southeast originating in the Santa Barbara Channel. The Pacific Ocean exposure of the Harvest Platform gauge makes its observations useful in characterizing open-ocean wave conditions that impinge on the region of the Southern California Bight.

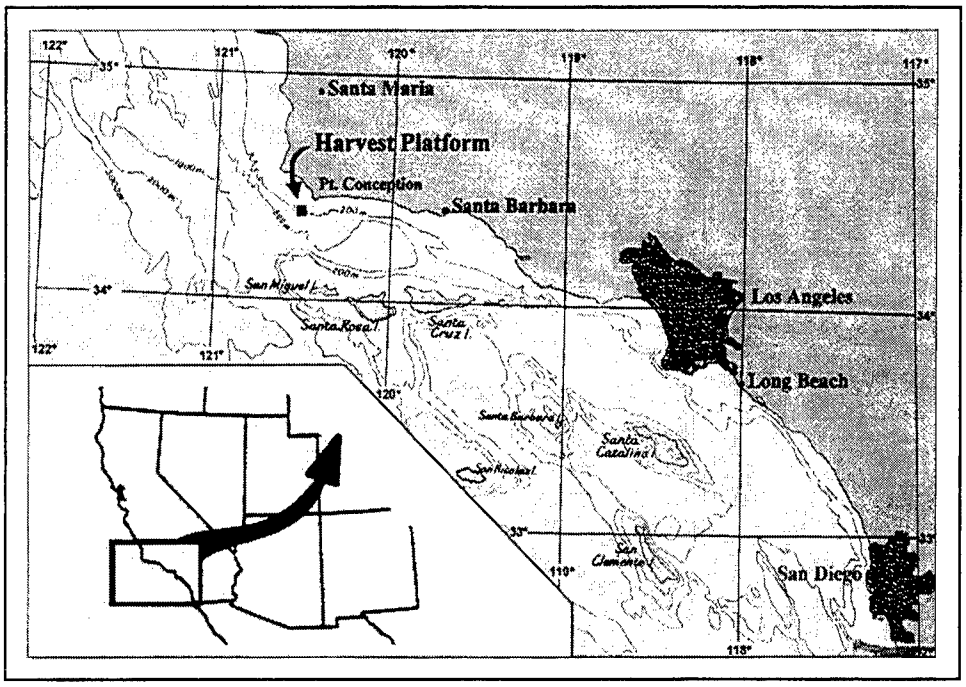

Figure 2. Harvest Platform location map

Though the observational databases from the two sites are formally specific to their particular locations, they may be representative of sites having similar forcing and boundary conditions. For the FRF 8-m array, this may include many sites along the U.S. east coast, and, for Harvest Platform, the deduced climatology may be typical of open Pacific Ocean conditions outside much of the Southern California Bight. Where other climatological data are missing, results of the present study can thus provide guidance for studies of a number of other sites.

The climatologies developed herein are expressed in the form of joint probability densities among the parameters that characterize wave height, frequency, and direction. While the formality and terminology of joint statistical distributions can seem somewhat daunting, the concepts are quite simple. What is sought is some measure, such as fraction of all observed cases, where waves have heights in a certain range, with characteristic frequencies in a certain range, and arrive from a particular range of directions.

Computation of this fraction can be thought of as creating a conceptual cube made up of a number of smaller cubes or cells. The three dimensions of the main cube are associated with the three parameters, height, frequency, and direction. Ranges of values along each axis are large enough to encompass all of the observed data. Each axis is then divided into a number of conveniently sized discrete increments, like tick marks on a graphic axis. A three-dimensional grid with grid lines passing through these tick marks divides the entire space into cells with each of the three cell dimensions representing some incremental range of wave height, frequency, or direction. Each observation will then fall uniquely into one of these cells. Passing through all observations, and counting the

number that accumulate in each cell, results in the basic entity from which a discrete joint probability density is formed. If the case count in a cell is divided by the total number of observations in the data set, the result is an estimate of the probability that a randomly chosen wave condition will have height, frequency, and direction within the parameter ranges that bound the three sides of that cell.

Results of this study are necessarily empirical, because there is no basic theory for the distribution of wave parameters at an arbitrarily chosen site. In a recent thesis, Leyden (1997) discusses some studies of statistical distributions of various wave parameters and notes that there is little consensus among investigators as to a general analytic model for the distribution of characteristic wave height alone, independent of any joint statistics with frequency or direction. This makes sense, because characteristic wave heights at any location depend on the frequency and nature of local storms; the distribution, paths, and intensities of distant storms; and, in shallow water, the specific character of wave-steering bathymetry between deep water and the site being studied. Statistical descriptions of conditions at distinctively different sites, such as the two sites considered in the present study, are thus expected to be different. Sites subject to the same storm climates, with similar continental shelf bathymetries, and adjacent to the same main ocean basin may have more nearly the same statistical descriptions. Thus, results found in this study may be somewhat more than just site-specific but are not expected to have global applicability.

This report is organized as follows. Chapter 2 discusses the sources, nature, quality, and amount of basic data used in this study. Chapter 3 describes the mathematical tools employed to convert basic data into desired statistical forms. Examined in Chapter 4 are the distributions of characteristic wave heights alone, because this is of historical importance, and because it is of interest to compare empirical height distributions to several common probability functions. In Chapters 5 and 6, two-parameter joint distributions between characteristic wave height and frequency, and wave height and direction, respectively, are examined for insights into the wave climates at the two study sites. In Chapter 7, three-parameter joint statistics of height, frequency, and direction are examined as site descriptors. Findings are summarized in Chapter 8. For archiving purposes, basic case counts (the cell contents discussed earlier) are included as tables in Appendixes A and B for the FRF 8-m array and Harvest Platform sites, respectively. Appendix C lists the notations used in this report.

2 Observational Databases

Climatologies developed in this report are derived from large sets of wave observations at the FRF and at Harvest Platform, each of which has a subsurface array of pressure gauges that are used collectively to determine wave direction. Observations consist of discrete, sea-surface displacement frequency spectra $S(f_r)$ and frequency-direction spectra $S(f_r, \theta_m)$, where f_r and θ_m are center values of discrete frequency bands and direction arcs, respectively[1]. Each observation is based on 8,192 sec (2 hr 16 min 32 sec) of data sampled simultaneously from all gauges in each array. Pressure gauge data are Fourier transformed in 1,024-sec segments, surface corrected according to linear wave theory, and converted to frequency spectra following Bendat and Piersol (1971) and to frequency-direction spectra by the iterative maximum likelihood estimator of Pawka (1983). Frequency spectra are smoothed over ten adjacent frequency bands, resulting in a nominal 160 degrees of freedom for all spectral estimates, with a final resolution frequency bandwidth Δf = 0.00977 Hz. Directional spectral estimates are made for arc widths $\Delta\theta$ = 2 deg.

Ranges of independent variables differ for the two sites because of gauge depths and array geometries. For spectra at both sites, discrete frequency band center values can be expressed as $f_r = f_{min} + (r - 1)\,\Delta f$ for $r = 1, 2, \ldots, R$, where f_{min} = 0.044 Hz. Differences occur at the high-frequency cutoffs, dictated by R. For the FRF 8-m array, R = 29, and observations cover the full wind wave frequency range from 0.044 to 0.319 Hz. At Harvest Platform, gauges were deployed at a depth that allowed resolution of large waves but resulted in a restriction in the frequency at which pressure data could be surface corrected. Consequently, R = 13 for Harvest Platform data, and the operational range of frequency is from 0.044 to 0.162 Hz.

A general expression for discrete direction axes is $\theta_m = \theta_{min} + (m - 1)\,\Delta\theta$ for $m = 1, 2, \ldots, M$, but both θ_{min} and M are different for the two sites. The FRF directional gauge is a one-dimensional linear array that can only estimate wave energy arriving from deeper water and is thus restricted to incident wave angles from -90 to +90 deg (measured counterclockwise from shore normal), in which case, θ_{min} = -90 deg and M = 91. The Harvest Platform array is a two-dimensional spatial array and can resolve waves propagating in all directions. Its

[1] For convenience, symbols and abbreviations are listed in the notation (Appendix C).

directional range is thus from -180 to +180 deg (measured counterclockwise from true north), so that θ_{min} = -180 deg and M = 181.

The directional constraint on FRF results does not have severe consequences, as little energy is reflected from the local shoreline (Long 1997a, and references therein). More serious is the frequency constraint on observations from Harvest Platform. Because the high-frequency part of the wind wave frequency band is truncated, estimates of characteristic wave height will be biased toward lower values than would be obtained if the high-frequency part of the spectrum was included. Characteristic frequencies that might exist in this part of the spectrum will not exist in the database, but will necessarily be replaced by one of the frequencies in the low-frequency part of the spectrum. Characteristic directions, which key on characteristic frequencies, will likewise be misrepresented when true characteristic frequencies are in the high-frequency part of the spectrum. Frequency and direction errors are most severe in the early stages of local storms with low background swell. Wave height errors are significant at these times and also in later stages of local storms when considerable energy is contained in the high-frequency part of the spectrum. The effect of these biases cannot be assessed from the existing database. There is an evident tendency for day-to-day conditions to be dominated by swell from distant sources (Long 1997b, and references therein), which helps to mitigate the lack of high-frequency information. However, the deduced climatology from Harvest Platform must be viewed with some caution because all wave heights are underestimated to some extent, and early storm cases are not necessarily well represented.

Parameter Definitions

In this study, the three parameters used to characterize an observation are spectrum-based wave height H_m , spectral peak frequency f_p, and mean wave direction θ_0 derived from the directional spectrum at the spectral peak frequency. In terms of discrete frequency spectra and frequency-direction spectra that constitute the fundamental databases, characteristic wave height is defined in the usual way as

$$H_{mo} = 4\sqrt{\sum_{r=1}^{R} S(f_r)\,\Delta f} \tag{1}$$

Representative frequency f_p is simply the discrete frequency at which $S(f_r)$ is a maximum. Note that this parameter defaults to one of R discrete frequencies and thus forms a convenient way to classify observations in terms of wave frequency. Characteristic direction θ_0, described by Kuik, van Vledder, and Holthuijsen (1988) as the first circular sine moment of a directional distribution function, is defined in discrete form from the frequency-direction spectrum as the direction that satisfies

$$\sum_{m=1}^{M} \sin(\theta_m - \theta_0) S(f_p, \theta_m) \Delta\theta = 0 \tag{2}$$

On expanding the sine term in Equation 2, rearranging the results, and solving for θ_0, one obtains

$$\theta_0 = \tan^{-1}\left[\frac{\sum_{m=1}^{M} \sin(\theta_m) S(f_p, \theta_m)}{\sum_{m=1}^{M} \cos(\theta_m) S(f_p, \theta_m)}\right] \tag{3}$$

Note that in Equations 2 and 3, the frequency-direction spectrum is evaluated at frequency f_p.

Data Requirements

A large number of observations of H_{mo}, f_p, and θ_0 are required to create a joint probability function that portrays a wave climate reasonably well. The SPM (1984) suggests that a database made of six observations per day for one year is adequate to describe a wave-height climate to the 1 percent level of occurrence. Clearly, more observations are desirable if a suite of observations associated with wave heights in a given range are to be subdivided into groupings of wave period and characteristic direction in the estimation of joint statistics. Thus, multiple years of data are preferable. There are other constraints, as well. It is important that data from an integral number of years is used to avoid biasing results by having excessive samples during parts of the annual cycle having wave conditions that are distinctive by season (e.g., low-energy, low-frequency summer swell or fall storms at the FRF).

It is also important that the sampling of wave conditions be uniform in time, again to avoid misrepresenting particular wave conditions. An example of this is the sampling pattern used at the FRF prior to October 1991. Wave gauges were sampled regularly at 6-hr intervals except when H_{mo} exceeded 2 m, during which times the sampling interval was reduced to 3 hr. Empirical statistics based on this sampling scheme would clearly be biased toward high-wave conditions because the database would contain an undue number of such samples. Beginning in October 1991, FRF sampling was set at 3-hr intervals (8 samples per day) for all conditions. FRF data collected since that time thus have both the uniformity and sampling density desired for estimating climatological statistics.

FRF Data

Of the consequently available data, subject to the annual cycle constraint, a 5-year database was selected to characterize wave climatological statistics at the

FRF 8-m array. Extending from 1 January 1992 to 31 December 1996, a total of 13,941 observations of H_{mo}, f_p, and θ_0 were used. Table 1 shows the number of observations by month and year for this database and indicates uniformity of sampling. At 8 collections per day, a 30-day month would ideally have 240 observations, and a 31-day month would have 248. Examination of Table 1 indicates that numbers of observations in most months are at or near these ideal values. Occasional losses of observations occurred because of downtime of the data collection system. These losses occurred randomly in time and so would not necessarily bias statistical estimates but do preclude absolutely complete data

Table 1
Number of Observations by Month and Year for FRF 8-m Array

Month	Year					Total
	1992	1993	1994	1995	1996	
January	241	229	243	245	248	**1,206**
February	231	223	223	220	232	**1,129**
March	244	241	246	228	169	**1,128**
April	237	240	229	239	238	**1,183**
May	243	245	245	246	246	**1,225**
June	235	239	233	237	227	**1,171**
July	239	240	229	244	237	**1,189**
August	244	89	244	248	244	**1,069**
September	228	56	235	240	240	**999**
October	241	246	248	248	248	**1,231**
November	240	239	240	236	240	**1,195**
December	228	248	245	247	248	**1,216**
Total	**2,851**	**2,535**	**2,860**	**2,878**	**2,817**	**13,941**

coverage. More significant shortages occurred in August and September 1993, when the 8-m array was being rebuilt in preparation for the DUCK94 experiment, and in March 1996, when a new interface building was being installed on the FRF pier. Typical March data include a broad variety of wave conditions, and loss of such data may have a somewhat uniform effect on deduced statistics, not affecting greatly any particular grouping of data. August and September tend to be low-energy months, however, and the loss of such data will result in a slight underestimation of low-wave conditions in a deduced climatology. Though the data set is not perfect, it is remarkably complete,

uniform, and of sufficient duration to provide a meaningful estimate of wave climate at the FRF.

Harvest Platform Data

Routine high-resolution directional wave observations at Harvest Platform, which began in November 1992, were established at regular 3-hr intervals from the beginning. Exceptions to this pattern occurred on a few occasions of about a day's duration when a tsunami alert was issued for the Pacific Ocean, whereupon collections occurred at 2-hr intervals. This pattern resulted in 12 collections per day instead of 8, and frequency-direction spectral estimates, based on records of durations longer than 2 hr, overlapped somewhat and were not completely independent. However, these events were rare enough that no serious degradation of deduced statistics occurred. Processing of high-resolution results from Harvest Platform terminated on schedule in September 1996. Of data collected during this project, a set of 7,066 observations encompassing almost 3 years, from 1 January 1993 to 12 December 1995, was isolated for climatological analysis.

Table 2 shows the distribution of these observations by month and year. In contrast to Table 1, the month-to-month variation in case counts is broader for

Table 2
Number of Observations by Month and Year for Harvest Platform

Month	Year			Total
	1993	1994	1995	
January	160	180	210	**550**
February	201	154	211	**566**
March	225	189	241	**655**
April	212	190	206	**608**
May	209	161	228	**598**
June	175	200	177	**552**
July	151	181	213	**545**
August	190	181	224	**595**
September	206	188	218	**612**
October	226	220	221	**667**
November	201	232	217	**650**
December	157	244	67	**468**
Total	**2,313**	**2,320**	**2,433**	**7,066**

this data set, and no one month has all of the cases one would ideally expect. The main reason for shortages was sporadic errors in data transmission from Harvest Platform to the land-based data collection computer. These errors were not related to any particular wave condition and so should not result in any specific biases in statistical analysis. It is noted that, with one exception, all months in all years have at least 63 percent of the expected number of cases, so that data coverage is sufficiently complete for a first estimate of wave climate. The exceptional month is December 1995 wherein a major local storm with characteristic wave heights nearing 6 m damaged the Harvest Platform gauges, precluding subsequent data collection until February 1996. This is unfortunate because waves in this storm were the most extreme in the whole data set, and it is desirable to have adequate coverage of extreme events within any sampling duration. Nevertheless, the Harvest Platform observations are sufficiently dense and adequately uniform and span enough annual cycles to develop a rough approximation of wave statistics for the eastern North Pacific Ocean.

3 Theoretical Considerations

To describe a wave climate as a statistical probability involving the three parameters H_{mo}, f_p, and θ_0, the entity that is sought is a joint probability density function $p(H_{mo}, f_p, \theta_0)$ that describes the simultaneous behavior of the argument variables. If an analytic form of p is known, a formal expression for the probability that $H_1 \le H_{mo} \le H_2, f_1 \le f_p \le f_2$, and $\theta_1 \le \theta_0 \le \theta_2$ is

$$Prob[H_1 \le H_{mo} \le H_2, f_1 \le f_p \le f_2, \theta_1 \le \theta_0 \le \theta_2] = \int_{H_1}^{H_2} \int_{f_1}^{f_2} \int_{\theta_1}^{\theta_2} p(H_{mo}, f_p, \theta_0)\, d\theta\, df\, dH \quad (4)$$

where H_1 and H_2 are the boundaries of an arbitrary range of wave height, f_1 and f_2 bound an arbitrary range of frequency, θ_1 and θ_2 are the limits of an arbitrary range of direction, and *Prob*[ ] means "the probability that." All relevant statistics, including moments of individual parameters, marginal distributions, and moments of pairs of marginal parameters can then be computed using p with standard statistical definitions. In the present study, however, p is not known *a priori*, and an estimate of p, denoted $\hat{p}$, must be computed from the observational database described in Chapter 2. Such an estimate is found by extending to three dimensions the method described by Bendat and Piersol (1971) for estimation of joint probability functions in two dimensions. The estimate is expressed as

$$\hat{p}_{ijk}(H_{mo}, f_p, \theta_0) = \frac{n_{ijk}}{N \Delta H \Delta f \Delta \theta} \quad (5)$$

where

$\hat{p}_{ijk}$ = an element of a three-dimensional matrix containing discrete estimates of the joint probability density of H_{mo}, f_p, and θ_0 with discrete bins or cells of these variables indexed by the integers i, j, and k, respectively

i = integer index of discrete values of the wave height dimension

j = integer index of discrete values of the frequency dimension

k = integer index of discrete values of the direction dimension

n_{ijk} = an element of a three-dimensional matrix of integers containing the number of occurrences where a triplet of observed parameters H_{mo}, f_p, and θ_0 corresponds to the i^{th} wave height cell, j^{th} frequency cell, and k^{th} direction cell

N = total number of triplets H_{mo}, f_p, and θ_0 in a data set

ΔH = discrete cell width used to define the wave height dimension

Δf = discrete cell width used to define the frequency dimension

$\Delta\theta$ = discrete cell width used to define the direction dimension

Discretization of the three coordinate dimensions representing wave height, frequency, and direction is accomplished by defining the center points of the cells into which the coordinates are divided. The coordinate representing wave height is divided into I cells of width ΔH, such that the set of discrete coordinate positions is defined by

$$H_i = (i - \tfrac{1}{2})\Delta H \qquad i = 1, 2, \ldots, I \tag{6}$$

A characteristic wave height associated with index i thus falls in the range from $H_i - \frac{1}{2}\Delta H$ to $H_i + \frac{1}{2}\Delta H$. The lower limit of the first cell ($i = 1$) is 0.0 m. The upper limit of the last cell ($i = I$) is $I\,\Delta H$symbolically, and, in this study, is set to be 6 m to span the total range of observed wave heights. Values of the individual parameters I and ΔHvary in this study and are defined in association with the analyses described in Chapters 4 - 7.

Frequency coordinate positions default to the set of discrete frequencies arising from frequency-direction spectral analysis and are defined by

$$f_j = f_{min} + (j - 1)\Delta f \qquad j = 1, 2, \ldots, J \tag{7}$$

where f_{min} = 0.044 Hz is the lowest of the range of wind wave frequencies retained and Δf = 0.00977 Hz is the final resolution bandwidth in spectral analysis of both FRF 8-m and Harvest Platform data. Parameter J establishes the bin representing the highest frequencies analyzed. For the FRF 8-m array, the high-frequency bin was centered at 0.318 Hz such that J = 29. For Harvest Platform the high-frequency bin was centered at 0.162 Hz and J = 13.

Parameters f_{min}, Δf, and J were kept constant for each site in all parts of this study.

The direction coordinate was discretized in the form

$$\theta_k = \theta_{min} + (k - 1)\Delta\theta \qquad k = 1, 2, \ldots, K \tag{8}$$

Direction bin width $\Delta\theta$ was kept constant at 5 deg in all analyses of data from both sites. Ranges of possible characteristic direction differed between the two sites, so parameters θ_{min} and K were different from site to site, but these parameters were held constant for all computations for a given site. For the FRF site, θ_0 could take on values ranging from -90 deg to +90 deg , so $\theta_{min} = -90$ deg , and $K = 37$. For Harvest Platform, $\theta_{min} = -180$ deg , and $K = 73$, consistent with the ability of data from that site to detect waves from any direction. Note that for Harvest Platform, the direction coordinate spans a full circle, such that information associated with index $k = 1$ is the same as that for $k = K$ and so is redundant. This redundancy is retained here for clarity in displaying results, but in computations involving integrations of $\hat{p}_{ijk}$ with respect to the direction coordinate, information in either bin 1 or bin 73 should be ignored.

Elements of the case counting matrix n_{ijk} in Equation 5 are found from the N observed triplets H_{mo}, f_p, and θ_0 in a data set and the coordinate discretizations defined by Equations 6, 7, and 8. In making this computation, all elements of n_{ijk} are initially set equal to zero. Each observed parameter triplet represents one case and can be identified uniquely with a single element of n_{ijk}. That element is defined by indexes i , j , and k, which are found for a given triplet H_{mo}, f_p, and θ_0 from relationships based on inversions of Equations 6, 7, and 8. These relationships are

$$i = nint\left[\frac{H_{mo} + \frac{1}{2}\Delta H}{\Delta H}\right] \tag{9}$$

$$j = 1 + nint\left[\frac{f_p - f_{min}}{\Delta f}\right] \tag{10}$$

and

$$k = 1 + nint\left[\frac{\theta_0 - \theta_{min}}{\Delta\theta}\right] \tag{11}$$

where $nint[\ ]$ is the nearest integer operator, which rounds the entity in square brackets to the nearest whole number. With bin indexes i, j, and k identified by Equations 9, 10, and 11, respectively, for a particular triplet of observations H_{mo}, f_p, and θ_0, case count matrix element n_{ijk} is incremented by 1. By considering all of the N triplets of observations in turn, the various elements of the case count matrix will contain integers indicating the total number of cases where triplets of observations uniquely fit particular ranges of height, period, and direction. High counts indicate more commonly occurring, or more probable, combinations of these parameters, low counts indicate rarer occurrences, and counts of zero indicate combinations of parameters that do not exist in the observed data set. When the case count elements are incorporated in Equation 5, the result is an estimate of the joint probability density function for the study site.

As noted by Bendat and Piersol (1971), quality of the estimate $\hat{p}$ in Equation 5 is a function of the choice of the discretization parameters ΔH, Δf, and $\Delta\theta$. If these cell dimensions are made too big, all of the observations will fall into a small number of matrix elements, and the result will lack detail of the structure of the joint probability function. If the cell dimensions are made too small, no matrix element will have more than a few counts, and it becomes difficult to distinguish high-probability conditions from low-probability regimes. Values of the discretization parameters used in this study were established by trial and error to be intermediate between the two extremes, yielding probability function estimates that are reasonably smooth and yet retain enough detail for engineering design purposes.

Study results can be cast in several forms for storage, publication, and illustration purposes. Clearly, the most fundamental result is the case count matrix n. All subsequent results are derived from this matrix, coupled with the coordinate discretization parameters used in Equations 6, 7, and 8. Because the case count matrix is simply a set of integers, it is the easiest form of quantitative result to publish, and that is the form of the output from this study shown in Appendixes A and B for the FRF 8-m array and Harvest Platform, respectively. Another convenient form of result is percent occurrence, which is found by dividing each element of the case count matrix by the total number of observations and multiplying the result by 100 percent. This result yields the percentage of all observations that reside in each height-frequency-direction classification cell and enables an intuitive form of graphic display. Elements of the percent occurrence matrix are computed from n by

$$(\text{percent occurrence})_{ijk} = 100\,\frac{n_{ijk}}{N} \tag{12}$$

or, equivalently, from the probability density estimate of Equation 5 by

$$(\text{percent occurrence})_{ijk} = 100\,\hat{p}_{ijk}\,\Delta H\,\Delta f\,\Delta\theta \tag{13}$$

The third form of result is the probability density estimate of Equation 5, which is useful for intercomparing the probability densities found in this study with either analytic models or estimates from other sources.

While joint height-frequency-direction probability density estimates are primary results of this study, it is insightful to examine subsets of the observational database. One type of subset is the probability density of H_{mo} alone, which, by virtue of relative ease of measurement, is one of the most common wave climatological characterizations. Other types of subsets are the joint distributions of height and frequency or height and direction. Though each of these subsets can be computed from a primary set of observations by simply ignoring the parameters not being considered, they are formally called marginal distributions and arise by integrating $p(H_{mo}, f_p, \theta_0)$ with respect to the unwanted variables over the full ranges of these variables. The term marginal indicates that distributions of only a few of the full set of system parameters are being considered. In this study, it is assumed that wave climate can be characterized by height, frequency, and direction parameters. Examination of the behavior of only one or two of these variables excludes some essential information. Thus, results of such examinations are termed marginal.

In terms of the discrete estimate $\hat{p}_{ijk}(H_{mo}, f_p, \theta_0)$ in Equation 5, marginal distributions are estimated by summing the contents of all cells representing the unwanted variables. For example, an estimate of the distribution of wave height alone $\hat{p}_i(H_{mo})$ is found by summing the right-hand side of Equation 5 with respect to the indexes representing frequency and direction, or

$$\hat{p}_i(H_{mo}) = \sum_{j=1}^{J} \sum_{k=1}^{K} \hat{p}_{ijk} \Delta f \Delta\theta \tag{14}$$

where the single subscript indicates a function of one variable, and, as before, the subscript i is associated with wave height. If the expression on the right-hand side of Equation 5 is substituted into Equation 14, the simplified result is

$$\begin{aligned} \hat{p}_i &= \sum_{j=1}^{J} \sum_{k=1}^{K} \frac{n_{ijk}}{N \Delta H} \\ &= \frac{n_i}{N \Delta H} \end{aligned} \tag{15}$$

where n_i is a one-dimensional matrix containing case counts of all observed H_{mo} in bins defined by the coordinate discretization of Equation 6. The second equality in Equation 15 is the computation that would be performed if wave height data alone were available. In Chapter 4, marginal distributions of observed characteristic wave heights for the two study sites are displayed and compared to several common analytic probability functions.

Marginal distributions representing the joint distributions of wave height and frequency $\hat{p}_{ij}(H_{mo}, f_p)$, useful for examining how wave energy is distributed in each discrete frequency bin without regard to wave direction, are found by integrating the three-dimensional joint probability estimate of Equation 5 over all possible directions, or

$$\begin{aligned}\hat{p}_{ij}(H_{mo}, f_p) &= \sum_{k=1}^{K} \hat{p}_{ijk} \Delta\theta \\ &= \sum_{k=1}^{K} \frac{n_{ijk}}{N \Delta H \Delta f}\end{aligned} \tag{16}$$

where the subscripts i and j on the left-hand side indicate a two-dimensional function of wave height and frequency, respectively. Surfaces representing this marginal probability function for the two study sites are illustrated and described in Chapter 5. These surfaces are expressed in terms of percent occurrence, which, for joint height-frequency distributions, is defined as

$$\begin{aligned}(\text{percent occurrence})_{ij} &= 100\, \hat{p}_{ij} \Delta H \Delta f \\ &= 100 \sum_{k=1}^{K} \frac{n_{ijk}}{N}\end{aligned} \tag{17}$$

In similar fashion, marginal distributions showing joint distributions of wave height and direction $\hat{p}_{ik}(H_{mo}, \theta_0)$ are found by integrating the frequency dependence from the joint probability estimate of Equation 5. Computationally,

$$\begin{aligned}\hat{p}_{ik}(H_{mo}, \theta_0) &= \sum_{j=1}^{J} \hat{p}_{ijk} \Delta f \\ &= \sum_{j=1}^{J} \frac{n_{ijk}}{N \Delta H \Delta\theta}\end{aligned} \tag{18}$$

where subscripts i and k indicate dependence on wave height and direction, respectively. The two-dimensional function $\hat{p}_{ik}$ indicates how wave energy is distributed in direction without regard to further distinction by frequency. Surfaces representing this function in terms of percent occurrence, defined as

$$\begin{aligned}(\text{percent occurrence})_{ik} &= 100\, \hat{p}_{ik} \Delta H \Delta\theta \\ &= 100 \sum_{j=1}^{J} \frac{n_{ijk}}{N}\end{aligned} \tag{19}$$

are pictured and discussed in Chapter 6.

The marginal probability function estimates $\hat{p}_i(H_{mo})$, $\hat{p}_{ij}(H_{mo}, f_p)$, and $\hat{p}_{ik}(H_{mo}, \theta_0)$ are introductory and interesting examinations of the data sets from the FRF and Harvest Platform study sites. These examinations lead up to

presentation of the full three-dimensional joint probability function estimates $\hat{p}_{ijk}(H_{mo}, f_p, \theta_0)$, which are depicted and discussed in Chapter 7.

4 Wave Height Distributions

Estimates of characteristic wave height marginal probability density functions $\hat{p}_i(H_{mo})$ for the two data sets used in this study were computed using Equations 9 and 15 with the height dimension discretized according to Equation 6 in $I = 60$ bins of width $\Delta H = 0.1$ m. This discretization spans the wave height range from 0.0 to 6.0 m and encompasses all observations from both data sets. Results are shown as the stepped curves in Figure 3, with the FRF estimate in the upper graph and the Harvest Platform estimate in the lower graph.

The two representations of wave climate are distinctively different. The FRF has a modal peak probability near 0.6 m, whereas the Pacific Ocean site has its highest probability near 1.7 m, indicating a much higher-energy regime. The FRF is subject to some very low-energy conditions, with occasional wave heights as low as 0.2 m, but at Harvest Platform, the lowest waves are about 0.6 m, roughly equal to the most common waves at FRF. Both sites experience waves in the range from 3 to 6 m, but the probability of such waves is clearly much higher at Harvest Platform. These observations are consistent with similar observations reported and discussed in the SPM (1984).

It is of interest to compare observed estimates to a number of analytic probability density functions to see if any one model consistently represents both data sets. There is considerable interest in finding such a model (Leyden 1997, and references therein) because it could be applied to characterize project sites where long term observations are not available. A problem with seeking such a model is that its adequacy must be deduced empirically, there being no underlying principle or assumption that leads to the derivation of an analytic model. For example, the distribution of heights of individual waves in a typical wave record was derived by Longuet-Higgins (1952), and verified by many observations since, to follow a Rayleigh probability density based on the single, simple assumption that the wave field is confined to a narrow range of frequencies. In contrast, characteristic wave heights derived from wave records collected at several-hour intervals and spanning many years will have distributions that depend on many climatological variables. Among these are frequency and intensity of local wave-generating storms, frequency, intensity, and spatial distribution of storms in the ambient major ocean basin, and, at coastal sites, the nature of wave-modifying bathymetry and coastal currents. Given the number and ranges of these variables from site to site, it is unlikely that a single, simple model (one having a small number of controlling parameters) can be found that universally represents all sites. Nevertheless, it

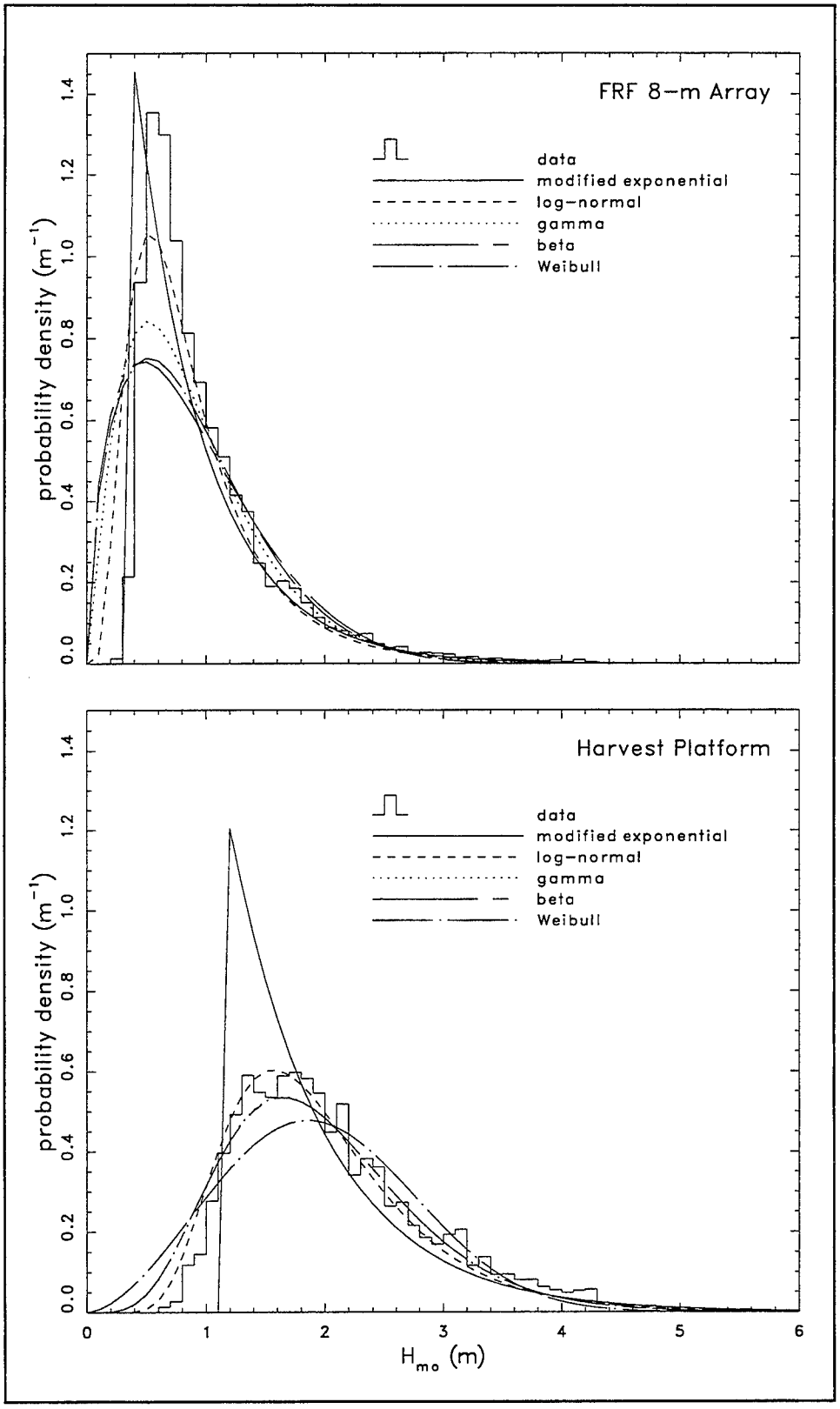

Figure 3. Estimated and modeled wave height probability density functions

may be that sites subject to similar forcing conditions will have distributions of characteristic wave heights that are not too different so that one of a small suite of models will be adequate for any project site of interest. Thus, it is useful to compare results from the two sites in the present study to some simple analytic models.

Shown in Figure 3 for each of the two data sets are five analytic probability density functions that are commonly used to characterize random processes. One of the models is the *modified exponential* distribution, described in the SPM (1984) as being a useful representation of wave climates in shallow water. The other four models, named *log-normal*, *gamma*, *beta*, and *Weibull*, are commonly described in elementary statistics texts, the one by Miller and Freund (1985) being referenced here. All five models are simple in the sense that they require only two parameters in their definitions, and , for each model, these parameters can be evaluated from the mean μ and standard deviation σ of an observed data set. For the two data sets examined in this study, μ and σ are computed following conventional methods and are listed in Table 3.

Model Definitions

The modified exponential probability density function can be found by manipulating the exceedance probability reported in the SPM (1984). Its two parameters are μ and σ identically, and the function is defined by

$$p(H_{mo}) = \begin{cases} 0 & H_{mo} \le \mu - \sigma \\ \dfrac{1}{\sigma e} e^{-\left(\frac{H_{mo} - \mu}{\sigma}\right)} & H_{mo} > \mu - \sigma \end{cases} \tag{20}$$

The log-normal probability density is

$$p(H_{mo}) = \begin{cases} 0 & H_{mo} \le 0 \\ \dfrac{1}{\sqrt{2\pi}\,\beta\,H_{mo}} e^{-\frac{(\ln H_{mo} - \alpha)^2}{2\beta^2}} & H_{mo} > 0 \end{cases} \tag{21}$$

with parameters α and β related to μ and σ through the expressions

$$\mu = e^{\alpha + \frac{1}{2}\beta^2} \tag{22}$$

and

$$\sigma^2 = e^{2\alpha + \beta^2}(e^{\beta^2} - 1) \tag{23}$$

Table 3
Data Set and Model Parameters from Analysis of Characteristic Wave Heights

Parameter	Data Source	
	FRF 8-m Array	Harvest Platform
Data Set		
μ (m)	0.90	1.97
σ (m)	0.59	0.80
d (m)	8.00	200.00
Modified Exponential Distribution		
H_{min} (m)	0.31	1.17
Log-Normal Distribution		
α (ln m)	-0.28	0.60
β	0.60	0.39
Gamma Distribution		
α	2.33	6.06
β (m)	0.39	0.32
Beta Distribution		
H_{max} (m)	4.44	111.11
α	1.65	5.94
β	6.51	329.01
Weibull Distribution		
α (m^{β})	1.00	0.12
β	1.56	2.65

The gamma probability density is

$$p(H_{mo}) = \begin{cases} 0 & H_{mo} \le 0 \\ \dfrac{1}{\beta^{\alpha}\Gamma(\alpha)} H_{mo}^{\alpha-1} e^{-\frac{H_{mo}}{\beta}} & H_{mo} > 0 \end{cases} \tag{24}$$

where Γ is the gamma function (see, e.g., Abramowitz and Stegun 1970), and parameters α and β are related to μ and σ by

$$\mu = \alpha \beta \tag{25}$$

and

$$\sigma^2 = \alpha \beta^2 \tag{26}$$

The beta probability density function is unique among the models considered herein because it is bounded to have finite values only where its argument is in the range from 0 to 1. This feature suggests that this model may be useful in shallow water, where wave heights are known to be limited by water depth. To apply this model to the data at hand, it is assumed that there is a maximum characteristic wave height H_{max} below which all observations must reside. It is further assumed that the maximum individual wave height in any observation is equal to the water depth d and that the distribution of individual wave heights in any observation follows a Rayleigh probability function. Under these conditions, H_{mo} is approximately equal to $H_{1/3}$ as defined by Longuet-Higgins (1952), and the extreme individual wave is approximately $1.8\,H_{mo}$. Combining these assumptions leads to the expression $H_{max} = d/1.8$. The beta probability density function takes the form

$$p(H_{mo}) = \frac{1}{H_{max}} \frac{\Gamma(\alpha + \beta)}{\Gamma(\alpha)\Gamma(\beta)} \left(\frac{H_{mo}}{H_{max}} \right)^{\alpha - 1} \left(1 - \frac{H_{mo}}{H_{max}} \right)^{\beta - 1} \tag{27}$$

for $0 < H_{mo} < H_{max}$, and $p(H_{mo}) = 0$ elsewhere. Parameters α and β relate to μ, σ, and H_{max} through the relationships

$$\frac{\mu}{H_{max}} = \frac{\alpha}{\alpha + \beta} \tag{28}$$

and

$$\frac{\sigma^2}{H_{max}^2} = \frac{\alpha \beta}{(\alpha + \beta)^2 (\alpha + \beta + 1)} \tag{29}$$

The Weibull probability density function is defined as

$$p(H_{mo}) = \begin{cases} 0 & H_{mo} \le 0 \\ \alpha \beta H_{mo}^{\beta - 1} e^{-\alpha H_{mo}^{\beta}} & H_{mo} > 0 \end{cases} \tag{30}$$

with parameters α and β related to μ and σ by

$$\mu = \alpha^{-\frac{1}{\beta}} \Gamma\left(1 + \frac{1}{\beta}\right) \tag{31}$$

and

$$\sigma^2 = \alpha^{-\frac{2}{\beta}} \left[\Gamma\left(1 + \frac{2}{\beta}\right) - \Gamma^2\left(1 + \frac{1}{\beta}\right)\right] \tag{32}$$

For each of the five models, expressed by Equations 20, 21, 24, 27, and 30, parameters α and β were found by simultaneous solution of the associated expressions for μ and σ. Resulting parameters for all models for both data sets are given in Table 3. For the depth-dependent beta probability density, a constant nominal depth was used for each observation site, resulting in a single value of H_{max} for each of the two study sites. This approach is adequate for a preliminary comparison of the beta distribution with observations, but may be somewhat incorrect for the high-energy region of the FRF observations. In shallow water, high waves are often accompanied by storm-induced setup, and, coupled with tidal variations, true depths are then greater than the nominal value used here. This type of behavior means that there is a distinct H_{max} for every observation, and a formal examination of the beta distribution should be done in terms of a data set based on the ratio H_{mo} / H_{max} instead of just H_{mo}, as was done in this study. Such a formal approach may be worth pursuing if only the distribution of H_{mo} is of interest. However, for joint statistics, populations of the discrete H_{mo} bins illustrated in Figure 3 are further distributed in frequency and direction. Except in the unlikely event that the joint probability densities for the two study sites consist of products of independent probability functions, it is rather moot to examine detailed behavior of marginal distributions of wave height alone. Thus, the simplified approach using a constant depth d and corresponding H_{max} for each of the two study sites is justified here. Values of these parameters used in this study are given in Table 3.

Probability Densities

Curves for the five analytic models using the parameters listed in Table 3 are shown as patterned lines for each data set in Figure 3. Curiously, all of the models bear some resemblance to the observations, having modal values at or near those of the data, and high-energy tail regions that are somewhat alike. The model that qualitatively most resembles the FRF observations is the modified exponential, whose results add validity to its use in shallow water as recommended by the SPM (1984). That same model does not appear to replicate the Harvest Platform data very well, overpredicting and displacing the modal peak, clipping the lower wave heights, and underpredicting much of the

high-energy tail region. The single model that best represents both data sets is the log-normal, though it underpredicts slightly the modal peak and overpredicts the low-energy waves of the FRF observations. The gamma, beta, and Weibull models consistently tend to underpredict modal peaks and overpredict the low-energy tails in both data sets. The Weibull curve also overpredicts part of the high-energy tails of data from both sites.

Percent Exceedances

Of particular interest are high-energy waves, which, though of low probability, can be most damaging to coastal projects. To examine model-data comparisons in the high-energy tail regions of the distributions, it is useful to cast all information in the form of exceedance probabilities, which are the probabilities that a random observation will exceed a specific value. If these probabilities are multiplied by 100 percent, one obtains percent exceedance $Q(H_{mo})$, which is an indication of the percentage of a number of random observations that exceed a specific value. For an analytic model, like any of the five discussed above, percent exceedance is formally found from the expression

$$Q(H_{mo}) = 100 \int_{H_{mo}}^{\infty} p(x)\,dx \tag{33}$$

where p is one of the models expressed in Equations 20, 21, 24, 27, and 30 and x is the dummy variable of integration. Not all of the model expressions were readily integrable in analytic form, so all were integrated numerically using the trapezoid rule (Abramowitz and Stegun 1970, or any basic calculus text), working backward in steps of 0.01 m from an upper limit of 10 m, where, for the model parameters used here, all probability densities were small enough not to bias the integrations. For a set of N observations of H_{mo}, an estimate $\hat{Q}(H_{mo})$ of percent exceedance is found by ordering the set of H_{mo} from smallest to largest, numbering them as $H_{mo}(n)$, $n = 1, 2, \ldots, N$, then ascribing to each of them the estimate computed by

$$\hat{Q}\left[H_{mo}(n)\right] = 100\left(1 - \frac{n}{N+1}\right) \tag{34}$$

Comparisons of observed and modeled percent exceedances for both study sites are shown in Figure 4, which is cast in the same form as Figure 4-20 in the SPM (1984) for ease of comparison. In this semi-logarithmic form, an exponential curve will appear as a straight line, and, above about a 0.3-percent probability of exceedance, the FRF observations (upper graph in Figure 4) appear to follow this pattern, which is anticipated by the modified exponential model recommended by the SPM. Furthermore, the FRF observations in this linear region are nearly identical to the curve in Figure 4-20 of the SPM for Nags

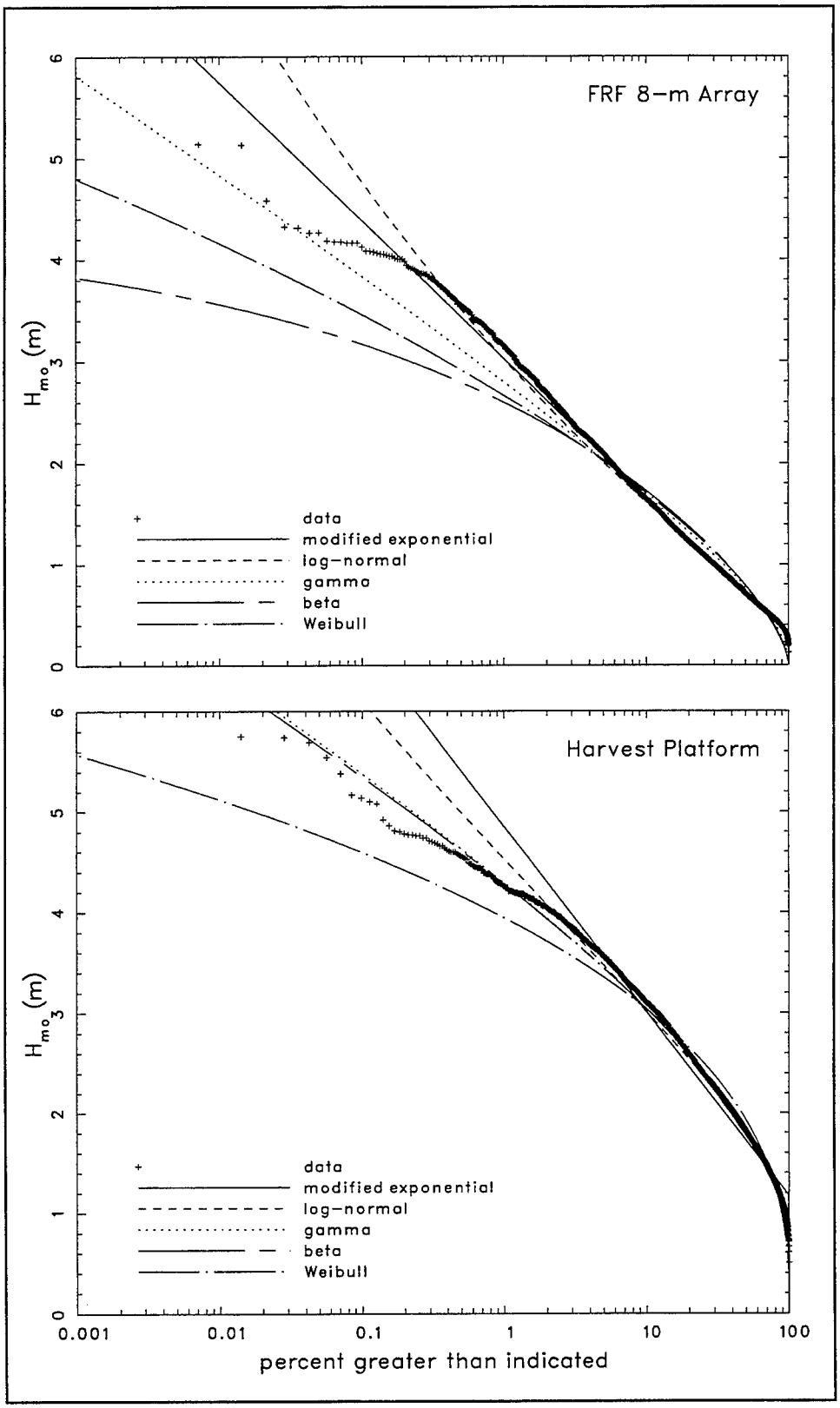

Figure 4. Estimated and modeled wave height exceedance functions

Head, NC, about 40 km south of the FRF, based on measurements taken roughly 20 years ago. These findings add credibility both to SPM guidance for wave height behavior in shallow water and to the hypothesis that wave height distributions will be similar for sites subject to the same forcing and boundary conditions.

In close agreement with the FRF observations and the modified exponential model is the log-normal model. This model appears slightly closer to observations than the modified exponential model for exceedances ranging from about 0.3 to 1.0 percent, but deviates more at higher exceedance levels and much more at lower exceedance percentages. The FRF observations have a rather abrupt break in slope near the point where wave heights begin to exceed 4 m. This behavior may be an indication of depth limitation, which is expected for heights of order half the water depth. While the observations span too short a duration to reflect accurately the behavior of the most extreme wave heights, the change in slope occurs where there are enough observations to provide a meaningful indication of depth-limiting conditions. It is notable that none of the models shown in Figure 4 characterize this break in slope very well. This result suggests that a model more elaborate than the simple two-parameter models shown here is required to characterize fully the FRF observations. Of the models shown with the FRF data, the most reasonable is the SPM-recommended modified exponential, which appears quite valid for wave heights up to about half the water depth and makes conservative projections of higher waves.

In contrast, observations from Harvest Platform (lower graph in Figure 4) have no significant depth limitation and, because of the site's exposure to conditions in the open Pacific Ocean, may be representative of some deepwater sites where waves have not been transformed by shoaling or refraction. The exceedance distribution for the Harvest Platform observations appears to vary smoothly over its full range of values. It has no particular region that follows a straight line in Figure 4, indicating that an exponential distribution is not appropriate for these data, although the modified exponential model does approximate the observations reasonably well for exceedances ranging from 5 to 80 percent. The log-normal curve does somewhat better, representing the data quite nicely for exceedances greater than 2 percent. Neither modified exponential nor log-normal models adequately represent the high-wave, low-probability tail of the Harvest Platform observations. This data region appears to be better represented by the gamma and beta distributions, which are nearly indistinguishable for the particular set of parameters used. However, these two models deviate more from the probability density data shown in Figure 3 than does the log-normal curve. Thus, of the models tested here, there is no single distribution that represents all of the Harvest Platform observations.

Comment on Wave Height Distributions

For both Harvest Platform and FRF data, one could combine or modify these models or develop other models to represent the marginal distributions of characteristic wave height better than the curves shown in Figures 3 and 4. For example, Leyden (1997) examined log-normal and gamma distributions shifted

along the wave-height axis to improve representation of observations at the FRF and achieved modest success. Such efforts are fine if only distributions of wave heights are of interest. However, wave height is only part of the wave climate. When considering joint distributions of wave height with characteristic frequency, peak direction, or both, populations of wave height bins discussed in this chapter are further subdivided into bins representing the other independent variables, and the primary quantities of interest become the surface or volume populations in these multidimensional spaces. Except in the absence of other information, as decried in the SPM (1984), or in the highly unlikely case where the wave height distribution is independent of the other variables, the marginal distribution of wave height alone is only of passing interest.

5 Joint Distributions of Wave Height and Frequency

Considerably more informative than the distribution of wave height alone is the marginal distribution representing the joint probability of characteristic wave height and spectral peak frequency. This distribution is marginal in the sense that there is no directional information, but it has use in engineering applications where wave direction is not used. For example, in designing a suite of wave flume model tests of breakwater stability, all waves travel in the same direction, so the relevant design parameters are wave height and frequency. Knowledge of how these parameters are jointly distributed at a site of interest allows specification of test conditions that include the most common (highest probability) conditions as well as less common, but potentially more damaging, combinations of wave height and frequency. Furthermore, it allows exclusion of expensive tests involving parametric combinations that do not exist.

Parametric data from the FRF and Harvest Platform study sites can be used in Equation 16 for a formal estimate of joint height-period probability densities $\hat{p}_{ij}(H_{mo}, f_p)$, but, for display and engineering design purposes, it is sufficient to cast results in the form of percent occurrence as defined by Equation 17. As with wave height data, there are N = 13,941 observations of height and period for the FRF site and 7,066 parameter pairs from Harvest Platform. The wave height coordinate for two-parameter joint statistics is defined using Equation 6 with I = 30 bins of width ΔH = 0.2 m for both study sites. These bins are wider than the ΔH = 0.1 m used in evaluation of wave height alone to ensure a reasonably smooth result for data that are now distributed in two dimensions. The frequency coordinate is defined using Equation 7 with f_{min} = 0.044 Hz and Δf = 0.00977 Hz for both data sets, J = 29 frequency bins for FRF data, and J = 13 bins for Harvest Platform data.

Results are shown in Figure 5, where FRF observations are displayed in the two graphs on the left-hand side and Harvest Platform observations are shown in the two graphs on the right-hand side. For each study site, the upper graph represents a three-dimensional surface showing percent occurrence of conditions in each of a grid of discrete cells denoting coordinates f_p and H_{mo}. The lower graphs are contour maps of corresponding three-dimensional surface plots with

contours drawn at 0.25-percent intervals. Results from both study sites are drawn at the same scale for comparison purposes.

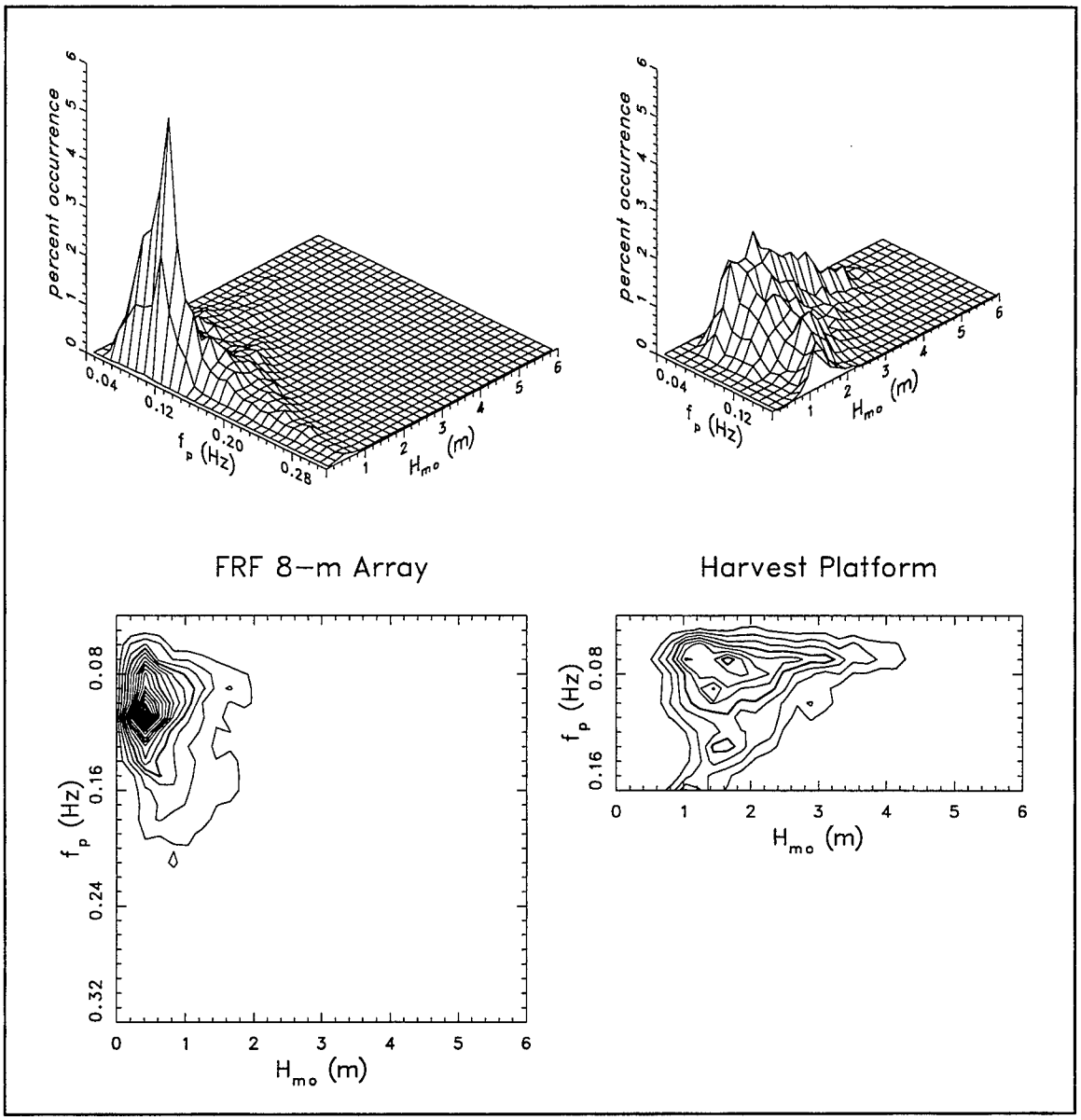

Figure 5. Joint probabilities of wave height and frequency

FRF results shown in Figure 5 indicate a strong tendency for characteristic waves with heights of 0.4 to 0.6 m and frequencies near 0.11 Hz. Contour lines are closely spaced in this region, and, by summing contents of adjacent bins, it is seen that approximately 90 percent of all observations are bounded by peak frequencies in the range 0.08 to 0.13 Hz and have characteristic wave heights less than 1 m. Rarer, but still dynamically important, conditions reside well away from the primary modal peak. A number of cases occur where spectral

peak frequencies are quite high. As evidenced by a low ridge paralleling the frequency axis at low values of H_{mo}, these conditions occur in the initial stages of storms, are usually transient, and, though of low energy, may be efficient in freeing nearshore surface sediments for subsequent storm transport. At intermediate wave heights between 1 and 2 m, there appear to be two groupings, one near 0.16 Hz, representing common peak frequencies for local wind seas, and one near 0.09 Hz, a typical swell frequency. High-energy conditions, with $H_{mo} > 2$ m, are shown diffusely scattered with low probabilities at low frequencies in the three-dimensional graph, and do not appear at all at the interval used in the contour graph (note that quantitative percentages can be deduced from the case count tables for FRF data in Appendix A).

In contrast to the FRF results, Harvest Platform data indicate very few conditions with $H_{mo} < 1$ m and a high percentage of 1- to 4-m waves with peak frequencies between 0.05 and 0.08 Hz. Waves with higher peak frequencies are accompanied by a narrower range of wave heights, consistent with early storm conditions. As noted in Chapter 2, gauge deployment depths precluded detection of wind wave signals at frequencies above 0.16 Hz for Harvest Platform so the climatology of the high end of the wind wave frequency band remains unknown. As suggested by the three-dimensional graph, and quantifiable through the case count tables for Harvest Platform in Appendix B, waves with the greatest heights occur at frequencies in the range 0.06 to 0.07 Hz.

The two climates represented by Figure 5 indicate that most of the FRF observations can be represented by conditions near the single, dominant modal peak of the probability distribution, whereas Harvest Platform is subject to a broad variety of conditions having nearly equal probability. Both sites are subject to high-energy, low-frequency waves and relatively lower energy, high-frequency waves. These conditions would need to be considered in structural reliability tests. Tests that could be excluded are clearly revealed in Figure 5 as regions in the wave height-frequency planes where there are no observations.

These results are insightful, and may be useful in unidirectional flume tests, but they are not complete because directional information is missing. In the full three-dimensional joint probability function involving wave height, frequency, and direction, the contents of each wave height-frequency bin shown in Figure 5 are further distributed by peak direction. Results of such a computation are discussed in Chapter 7, but first, it is useful to examine the directional counterpart of the joint height-frequency distribution, the joint height-direction distribution. This distribution is shown and discussed in Chapter 6.

6 Joint Distributions of Wave Height and Direction

Though less directly applicable than joint distributions of height and frequency, marginal distributions involving joint probabilities of height and direction are extremely informative in that they reveal directions along which the most energetic waves travel, as well as directions that are virtually devoid of wave energy. By neglecting frequency information, these distributions give an indication of the general directional climatology in terms of various energy levels represented by wave heights. Sites for which wave energy is tightly bound in direction, or prone to arrive from more than one dominant direction, are thus revealed.

A formal estimate of joint height-direction probability $\hat{p}_{ik}(H_{mo}, \theta_0)$ can be obtained using site-specific databases in Equation 18, but it is simpler, and just as meaningful, to compute percent occurrence using Equation 19. For Equation 19 and the coordinate axis representing wave height, Equation 6, parameters N, I, and ΔH remain the same as in Chapter 5. For the direction axis, Equation 8, $\Delta\theta$, θ_{min}, and K are as described for the FRF and Harvest Platform sites in the text following Equation 8.

Results are displayed in Figure 6, where FRF observations are displayed in the two graphs on the left-hand side and Harvest Platform observations are shown in the two graphs on the right-hand side. For each site, the upper graph depicts a three-dimensional surface of percent occurrence as a function of H_{mo} and θ_0. The lower graphs are contour maps of corresponding three-dimensional plots with 0.25-percent contour intervals. Results from both sites are drawn at the same scale.

Direction axes indicate directions from which waves are coming in a conventional trigonometric coordinate system where direction increases counterclockwise when viewed from above. The zero directions differ for the two study sites. For the FRF, the shoreline is a highly relevant physical boundary so the directional origin is set to be the shore-normal azimuth. In this directional system (refer to Figure 1 for geophysical orientation), waves propagating directly onshore have θ_0 = 0 deg. Waves propagating parallel to the coast from northward to southward have θ_0 = 90 deg, and waves moving

from southward to northward parallel to the coast have θ_0 = -90 deg. Note that resolution of the FRF directional gauge limits the range of characteristic direction to be $|\theta_0| \leq 90$ deg so that all waves represented in the FRF database used here have an onshore propagating component. This resolution constraint does not exist for the Harvest Platform directional gauge, which can detect waves propagating in any direction. Because it is in relatively open water, the directional origin for Harvest Platform results is simply aligned with true north (see Figure 2). Thus, waves from the north have θ_0 = 0 deg. Then, for counterclockwise-increasing directions, waves from the west have θ_0 = 90 deg, waves from the south have θ_0 = 180 deg, or, by the cyclic nature of direction, θ_0 = -180 deg, and waves from the east have θ_0 = -90 deg.

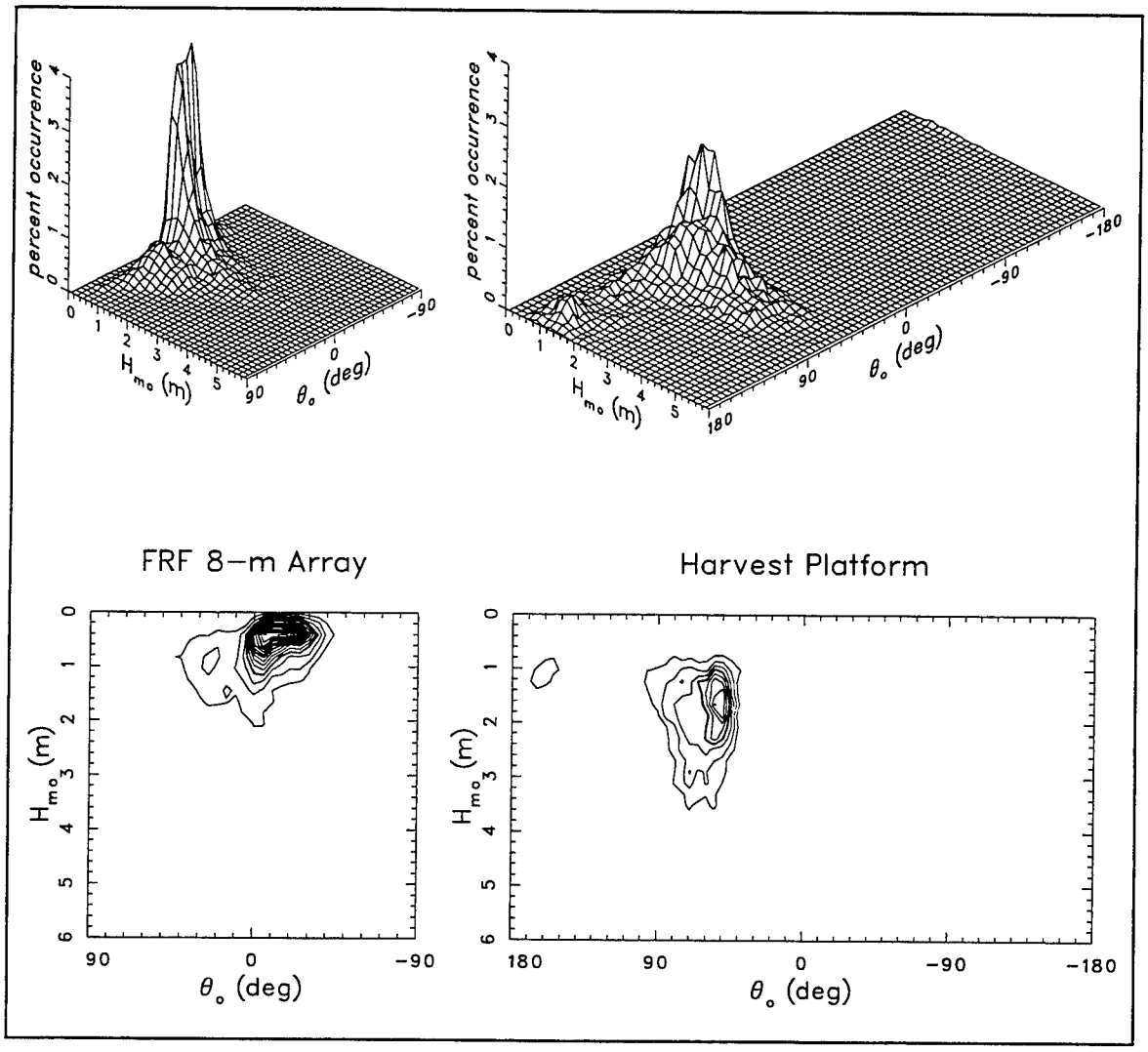

Figure 6. Joint probabilities of wave height and direction

The FRF directional climate revealed in Figure 6 shows a dominant peak of low-energy waves bounded between the directions 0 deg and -30 deg. The reason for this is that, in the absence of storms, the primary waves reaching the FRF consist of long-period, low-amplitude swell originating from distant storms in the deep Atlantic Ocean. To reach the FRF, these waves must pass over the continental shelf. As shown in Figure 1, the shelf break is oriented roughly along a north-south line, while the local coastline follows a line roughly 20 deg west of north. Long waves from deep water refracting at the shelf break, then approach the FRF from about 20 deg south of shore normal, or at θ_0 = -20 deg in the coordinates used for Figure 6. The probability peak is large because such waves occur through most of the summer, much of the winter, and frequently in the spring and fall storm seasons.

A weaker, secondary probability peak occurs in the FRF data for H_{mo} near 1 m and θ_0 in the range 20 to 30 deg. These conditions occur in the initial stages of dominant storm patterns, locally called *northeasters*, owing to the wind direction, and waves thus generated respond in part to the direction of wind forcing and in part to bathymetric steering. At the peaks of such storms, and when hurricanes pass near the FRF, wave heights become much larger, and wavelengths longer. These waves are much more strongly coupled to local bathymetry and tend to become almost, but not quite, shore normal, as evidenced by the high-energy tail of the FRF probability function shown in Figure 6.

The Harvest Platform data also indicate two dominant directional modes in the low-energy regime, but for a very different reason. There is a primary peak in the probability function for H_{mo} between 1 and 2 m and θ_0 in the range 40 to 70 deg. As can be deduced from Figure 2, these waves are arriving from the northern Pacific Ocean with geophysical directions ranging from northwest to west-northwest, an arc to which the Harvest Platform site is well exposed. It is also exposed to a range of directions in an extension of that arc from 70 deg to 180 deg, and, with somewhat reduced probabilities but about the same range of wave heights, waves do arrive from these directions. There is a minimum (but not a zero) in the probability near 140 deg and a small secondary maximum centered near 160 deg. Though frequency information is not displayed in Figure 6, it is known that this secondary maximum is due to a phenomenon known as *southern swell*, long-traveled waves from large storms in the southern Pacific Ocean. Part of the ridge of probability for 1- to 2-m waves between 90 and 180 deg is due to the co-occurrence of southern swell and swell from the northwest in individual collections. When the mean direction θ_0 is computed for such cases, a direction intermediate between and dependent on individual strengths of the two swell trains is obtained [see Long (1995) for examples of such cases and Long (1994) for a discussion of hazards encountered when trying to characterize complicated directional wave observations with only three parameters]. The effect in climatological estimates is a smearing of observations between primary peak directions as evidenced in Figure 6.

As can be seen in Figure 2, waves are not expected to arrive at Harvest Platform from the east through northeast to north, azimuths of -90 to 0 deg in Figure 6, owing to blockage by the California land mass. Waves are further

blocked by the so-called Channel Islands of San Miguel, Santa Rosa, and Santa Cruz to the south and southeast of Harvest Platform, -180 to -135 deg in Figure 6. This leaves a small arc of directions from -135 to -90 deg, southeast to east in Figure 2, from which waves generated between the Channel Islands and the mainland can arrive. Though faintly seen in Figure 6 (but quantified in Appendix B), there are some relatively rare occasions when waves with heights between 1 and 3 m, probably generated by local storms, arrive at Harvest Platform from within this arc. Waves at high energy, with $H_{mo} > 3$ m, have characteristic directions primarily in the range 40 to 90 deg, indicating major energy sources in the north Pacific Ocean.

Somewhat striking about the two study sites is the fact that the bulk of observations, roughly 90 percent in both cases, reside in a narrow range of characteristic directions, roughly 30 deg wide, from shore normal to 30 deg south of shore normal at the FRF and from 40 to 70 deg at Harvest Platform. While this might suggest that the two directional climates are simple to characterize, such characterization would preclude the less probable, but dynamically important, cases on the fringes of the distributions. At sites like the FRF, minor variations in mean wave direction in the vicinity of shore normal can have strong effects on resulting nearshore dynamic processes (Long 1994), so it is important that details of these distributions be considered in modeling or project design. Furthermore, the views of the observations provided by Figure 6 are just the marginal distributions involving wave height and direction. While of interest for a bulk characterization of the data, they do not include information about the way data in each height-direction cell are distributed in frequency. The full three-dimensional distributions that are most revealing are displayed and discussed in Chapter 7.

7 Joint Distributions of Wave Height, Frequency, and Direction

The complete statistical characterization of wave climate within the scope of this report is the joint probability density of characteristic wave height, frequency, and direction. In the simplest application, this information can be used to understand what conditions do and do not exist at a particular site. In project design, this information can be used to define a suite of realistic numerical or physical model tests with which to quantify structural response or beach fill endurance. Tests could include common, highly probable conditions and rarer, but possibly more critical, combinations of wave height, frequency, and direction that would stress structural integrity or beach erodability. It is understood that for a given combination of these three parameters, there can be an infinite variety of actual wave conditions, including various degrees of directional spread in the wave field, distribution of wave energy with respect to frequency, or multiple modes in frequency-direction spectra, suggesting more than one source or generation mechanism for wave energy. Nonetheless, the simple characterization presented herein is far more advanced than guidance given in the SPM (1984), which emphasizes the need for and utility of joint, three-parameter statistical descriptions of wave climates at, or representative of, project sites.

The formal estimate of the joint height-period-direction probability density $\hat{p}_{ijk}(H_{mo}, f_p, \theta_0)$ is given by Equation 5 with coordinate axes for H_{mo}, f_p, and θ_0 given by Equations 6, 7, and 8, respectively. However, as with the marginal probabilities discussed in Chapters 4, 5, and 6, it is just as instructive for display purposes to compute percent occurrence, which is defined by Equation 12. The central element in estimates of both probability density and percent occurrence is the case count matrix n_{ijk}. The entities defined by Equations 5 and 12 are derived using this matrix, the constants ΔH, Δf, and $\Delta\theta$ relating to coordinate axis discretization, and the number of parameter triplets N in a given data set. For height-period-direction computations, parameters N, f_{min}, Δf, J, θ_{min}, $\Delta\theta$, and K are given the same values as previously defined. Because the number of observations stays the same, but is distributed in three-dimensional space, it has been found necessary to increase the wave-height discretization increment

ΔH to 0.5 m (from the 0.1 m used in Chapter 4 and the 0.2 m used in Chapters 5 and 6) to gain a clear characterization of the probability distributions. To span all wave-height observations from 0 to 6 m, parameter I of Equation 6 is then set equal to 12 in analysis of data from both study sites. Values of parameters used in three-dimensional analysis are summarized in Table 4. Case-count matrices n_{ijk} tabulated in Appendixes A and B are based on the coordinate-discretization parameters given in Table 4. Together, Table 4 and Appendixes A and B form the archival results of this study.

Table 4
Parameters Used for Estimation of Joint Height-Frequency-Direction Probability Functions

Parameter	Data Source	
	FRF 8-m Array	Harvest Platform
N	13,941	7,066
ΔH (m)	0.5	0.5
I	12	12
f_{min} (Hz)	0.044	0.044
Δf (Hz)	0.00977	0.00977
J	29	13
θ_{min} (deg)	-90	-180
$\Delta\theta$ (deg)	5	5
K	37	73

Displaying results graphically and meaningfully is a challenge. Results are functions ($\hat{p}_{ijk}$, percent occurrence, or n_{ijk}) of the three coordinate dimensions H_{mo}, f_p, and θ_0 and so cannot readily be depicted in a single graph. However, a sequence of three-dimensional plots, each showing a function in terms of two coordinates, with the sequence based on discretized ranges of the third coordinate, is one way to illustrate four-dimensional information. Here, it is useful to depict percent occurrence as a function of f_p and θ_0 for each of the 12 discrete ranges, or bins, representing H_{mo}. This graphic format is used in Figures 7 and 9.

FRF Results

Figure 7 shows results from the FRF 8-m array with the wave-height sequence in columnar form. Low-energy conditions are shown on the left-hand side, high-energy conditions are on the right-hand side, and, in each column, wave height increases from top to bottom. To augment information in Figure 7, contours of the three-dimensional surfaces are shown in Figure 8. The single height-frequency-direction bin with the highest population contains about 1.7 percent of the observations. A convenient contour interval is 0.1 percent, which, with two exceptions, is the interval used in Figure 8. The exceptions arise because it is important to be able to identify both the very low-population bins, those having only one or two cases represented, and the extreme edges of information-containing bins, which may likewise have very low populations. Following Equation 12, a cell with one case in a population of more than 13,000 has an estimated occurrence percentage of less than 0.01. Consequently, an extreme contour line has been drawn in the plots in Figure 8 at 0.001 percent. An intermediate line at 0.01 percent has been drawn to help emphasize the fringe areas. With this plotting scheme, all cells with a population of one or more cases are identifiable by having at least one contour line.

As seen in Chapter 4, the most common wave conditions at the FRF site have characteristic heights less than 1 m. In Chapters 5 and 6, it was seen that populations of these waves tend to concentrate near a frequency of 0.11 Hz and arrive at the FRF array over a small arc of directions from shore normal to slightly south of shore normal. This pattern is iterated in Figures 7 and 8, but now is added the very interesting behavior of the high-frequency, high-angle-of-attack waves which constitute the tails of distributions shown in Figures 5 and 6. Low-energy conditions are shown in the upper graphs on the right-hand side of Figures 7 and 8, where the statistical distributions are more diffuse than any of the graphs related to higher energy. At high frequencies, there is a strong tendency for waves to arrive from within one of two ranges of direction, one range consisting of positive angles (waves from the northeast) and the other range being negative (waves from the southeast). Clearly there is a tendency for angle of attack to increase with increasing frequency and a distinct gap where there are very few shore-normal peak directions for peak frequencies greater than about 0.20 Hz.

The bulk of these low-energy observations are related to two primary wave sources at the FRF. One is long-traveled swell from the deep Atlantic Ocean. The other relates to local wind forcing arising from a common pattern in weather frontal systems that cross the FRF site. Low-energy, low-frequency swell waves at low incidence angles are present virtually all the time, arising from numerous distributed sources, including equatorial and north Atlantic Ocean storms, hurricanes migrating northward and offshore of the U.S. east coast, and major frontal systems moving eastward off the North American continent. Such conditions are often masked by local storms, but clearly dominate populations of low-energy conditions, and, in fact, all conditions, by their very persistence.

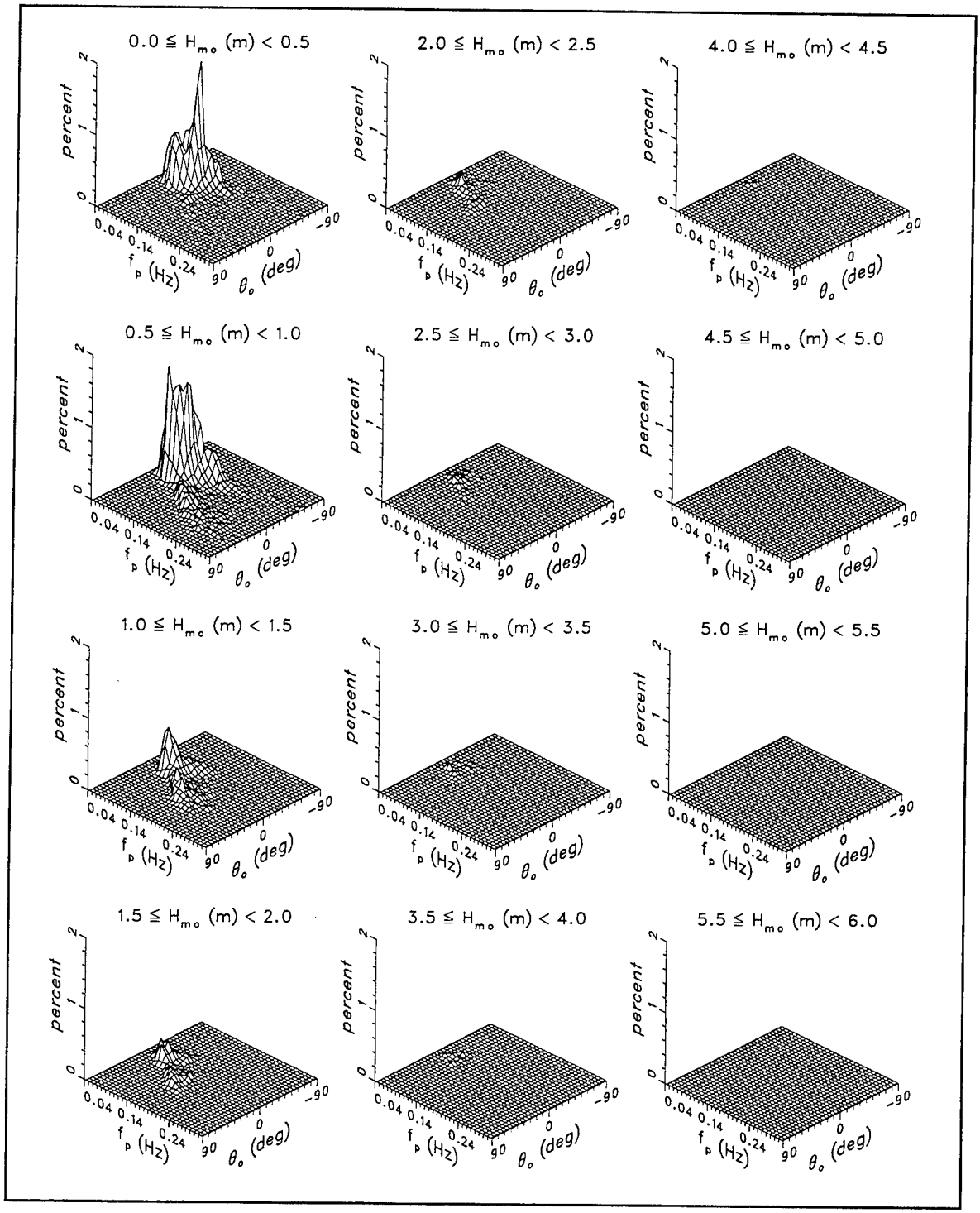

Figure 7. Estimated joint wind wave height-frequency-direction probability function based on data from the FRF 8-m array

High-frequency, high-angle-of-attack waves at low energy occur under the influence of local wind forcing. Local wind events commonly arise from the eastward migration of northeast-southwest-oriented weather fronts. As such a front approaches the FRF, winds tend to come from the southwest (see Figure 1).

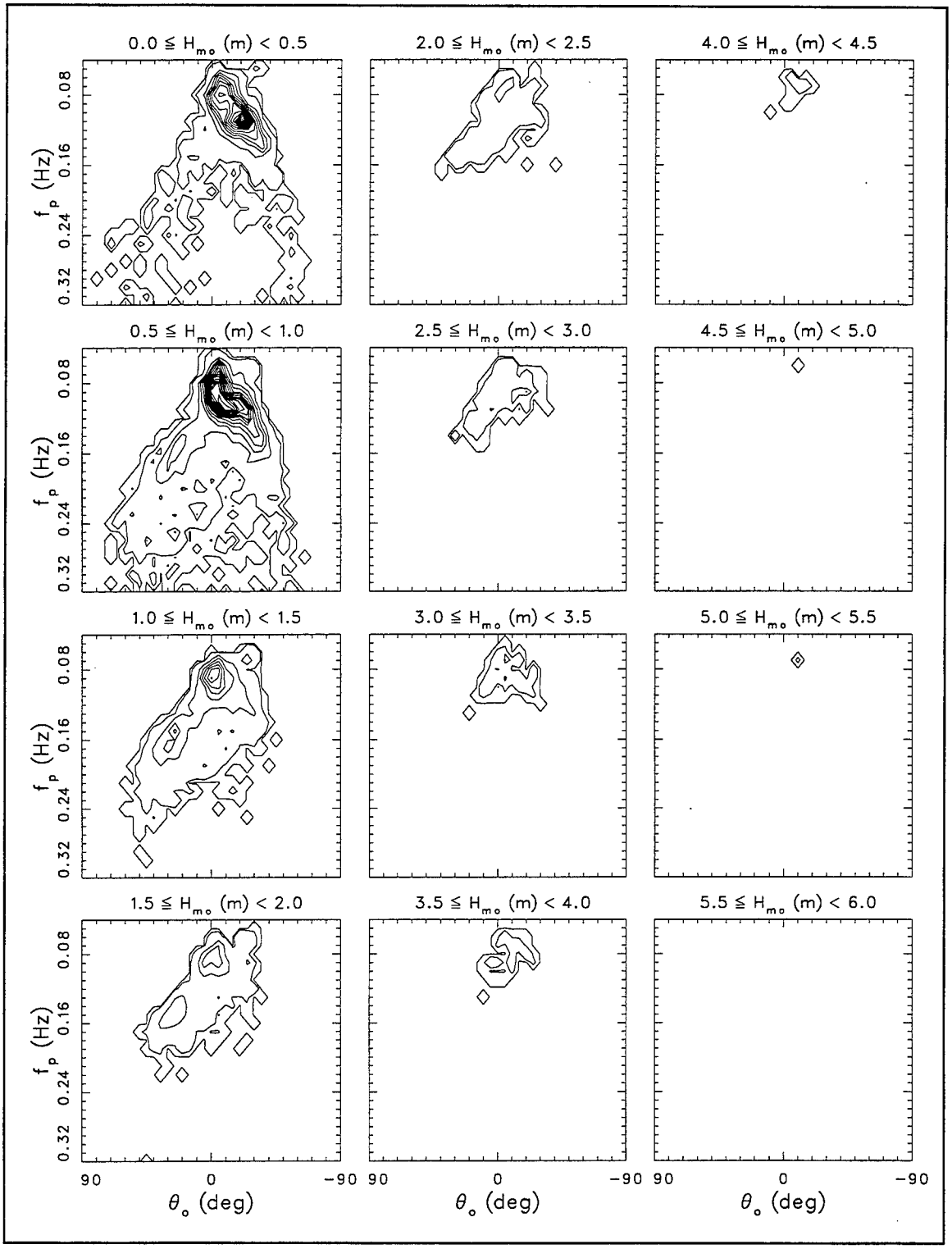

Figure 8. Contour plots of surfaces shown in Figure 7

Curiously, such winds begin to build local seas that appear at the FRF 8-m array as coming from the southeast, roughly at right angles to the wind. A physically consistent explanation for this is that a wind from the southwest can be

decomposed into an offshore-directed component and an alongshore-directed component. The offshore component is severely fetch-limited, but the alongshore component has no such restriction, so there is a tendency for the wind to build waves moving northward parallel to the coast. As the wind sea builds, its peak frequency decreases and its associated peak wavelength increases. Because water is quite shallow nearshore, such waves rapidly achieve sizes where they are influenced by the bottom. As soon as that happens, the longshore traveling waves tend to refract so as to be propagating toward shallower water, and thus appear to be arriving from the southeast. These are the only waves that can be detected with the FRF 8-m array because the array consists of bottom-mounted pressure sensors and can only detect waves with signals that reach the bottom. Visual observations at the FRF indicate that the usual surface wind signatures consisting of wind streaks, cat's paws (capillary waves), and very high-frequency waves that cannot be detected with the 8-m array do tend to propagate downwind, but that waves at the high-frequency end of the wind wave band appear to arrive from an offshore source, consistent with directions detected with the 8-m array.

Waves at the highest frequencies resolvable with the 8-m array are the shortest and least refracted by the deeper bathymetry offshore of the 8-m depth contour. Thus, these waves are perceived by the directional array as propagating most nearly parallel to the coast. As the wind persists, spectral peak frequencies move lower. These longer waves interact with deeper offshore bathymetry and so are more refracted when crossing the 8-m array, appearing to arrive from progressively more shore-normal directions. The persistence of this pattern of behavior results in the ridge of finite probabilities visible for low-energy conditions at negative θ_0 in Figures 7 and 8. It is interesting to note that, while the observations and heuristic description of this process are consistent with known physical processes, few conventional wave generation models replicate this nearshore behavior, all tending to generate waves that propagate downwind, not crosswind. This shortcoming may not be severe in the energetic sense because these conditions only occur in the initial stages of wave generation when wave heights are small, i.e., for the two wave-height bins for which $H_{mo} \leq 1$ m in Figures 7 and 8. However, in some coastal navigation applications, especially those related to small craft attempting to land on an open beach, proper modeling of these low-wave conditions may be critical. Furthermore, replication of this type of behavior could be used as a test of the adequacy of the physics represented in future improvements to nearshore wave generation models.

A similar ridge of probability is seen for low-energy, high-frequency waves with positive θ_0. On this side of the shore-normal direction, two front-related processes act, both related to conditions after a front has passed the FRF. If a frontal system is sufficiently curved, winds tend to blow normal to the frontal line, leading to wind directions from the northwest. In these cases, the process is identical to the response to southwest winds, except that waves come from northeasterly directions, symmetric about shore normal to the distribution for southeasterly waves. For more linear fronts positioned east of the FRF, winds tend to come from the north to northeasterly directions, and waves are then driven more directly in the downwind direction with no fetch limitation. Such

waves are still subject to refraction, however, so that, for the same reasons given in the previous paragraph, waves at the highest frequencies can have characteristic directions that span the whole northeast quadrant from 0 to 90 deg. Waves at intermediate frequencies, evolving either as parts of weak storms or in the spin-down stages of larger storms, are more restricted by refraction effects, and are bound to angles of incidence nearer to 0 deg. High-frequency waves at low energy are not physically precluded from angles of attack near 0 deg, and the relative scarcity of observations in this region in Figures 7 and 8 indicates that initial wave forcing by due-easterly winds is quite rare.

As local storms evolve, spectral peak frequencies tend to move to lower values, and wave energy increases. The frequency-dependent restriction on wave direction still holds so that, as wave energy increases, ranges of both peak frequency and characteristic direction are reduced. This is quite obvious in the contour plots of Figure 8 where frequency-direction patterns become gradually smaller as characteristic wave height increases. This is presented sequentially as the lower two graphs on the left-hand side of Figure 8, then down the center column of graphs, and into the upper graphs in the right-hand column. The highest waves in the data set are in the wave height bin spanning 5.0 to 5.5 m (there are no FRF observations in the 5.5- to 6.0-m wave height bin, which is included in computational analysis to span both FRF and Harvest Platform data sets). These wave conditions reside in the frequency bin centered near 0.07 Hz and the direction bin centered at -10 deg, a directional characteristic typical of waves that come from deep water and refract at the continental shelf break. Note that the low-frequency waves from all of the intermediate- and high-wave bins cluster in the directional bins ranging from -30 to 0 deg. This is consistent with what was seen in the wave height-direction marginal probability function of Figure 6, except that now it is seen that such behavior is restricted to low-frequency waves. Waves at sequentially higher characteristic frequencies span correspondingly increasing directional arcs until, at the extreme of low energy and high frequency, the range of mean direction covers almost the entire incident-wave semicircle.

Though the probabilities of intermediate and high waves are small relative to the large number of cases of low swell shown in Figure 7, high waves are important dynamically because such waves are capable of inflicting considerable structural damage and moving large amounts of sediment over their relatively short durations. What is clear in Figures 7 and 8 is that low-frequency waves at all energy levels tend to come from slightly south of shore normal, intermediate- and high-frequency waves at low energy tend to arrive from both sides of shore normal, and mid-frequency waves at moderate energy can arrive from shore normal to modestly high angles of attack to the north of shore normal.

In simple nearshore process models, wave-driven currents and sediment transport are quite sensitive to all three parameters used here to characterize wave climate at the FRF. Even in this elementary depiction, the system is quite complicated, as evidenced by results shown in Figures 7 and 8. With this quantification of occurrence probabilities of the various wave height-frequency-direction regimes, and assuming that three parameters are adequate to define the wave field, one could, with modest effort, use SPM (1984) guidance to estimate

the contribution of each regime to a nearshore process like sediment transport and then estimate the long-term net transport by adding all the individual contributions weighted by their occurrence fractions as depicted in Figure 7. Though beyond the scope of this report, one could then assess the importance of long, low waves that do not move much sediment individually but occur so often that their contributions over a year's time may be comparable to the net transport of rarer, more intense storm events. Alternatively, one could use information given herein to drive a suite of tests in a frequency-direction-capable, sediment transporting wave basin to achieve a similar assessment.

Harvest Platform Results

Observations at the FRF site are relatively easy to interpret because of a wealth of ancillary climatological data gathered at that site and reported on its World Wide Web site *http://www.frf.usace.army.mil* and in reports listed therein. For the Harvest Platform site, only wave data are available, and interpretation is somewhat more challenging and subjective. However, conditions at Harvest Platform form a simpler pattern than do those at the FRF, so the challenge is not severe. Joint wave height-frequency-direction statistics for Harvest Platform are shown in Figure 9 as a sequence of H_{mo} classed surfaces showing percent occurrences as functions of f_p and θ_0, following the display pattern used for FRF results. Contour plots of these surfaces are shown in Figure 10, with contour intervals the same as those used in Figure 8, 0.1 percent for all observations, with additional contours at 0.001 and 0.01 percent to reveal bins populated with only one observation. Table 4 lists the parameter range and increment constants used in the computation of the percent occurrence matrix for Harvest Platform.

Recalling that the θ_0 axis shows directions from which waves come relative to an origin at true north, and increasing in the counterclockwise sense, a marked characteristic of the Harvest Platform climate is the confinement of most of the observations to θ_0 in the range 40 to 90 deg, corresponding to waves from northwest to west in Figure 2. Approximately 95 percent of observations, covering all H_{mo} and f_p classes, reside in this range of mean direction, a result that was suggested in the marginal wave height-direction distribution shown in Figure 6. Because water depth at this gauge is approximately 200 m, and is greater to seaward, little refraction is expected for waves arriving at this site from the open Pacific Ocean, and waves have likely traveled in nearly straight lines from their sources. This condition suggests that primary energy sources lie in a roughly 50-deg-wide wedge radiating westward from Harvest Platform and originating on its south side by the site's latitude. Within this arc of mean directions, there appears to be a slight tendency for low-frequency waves to arrive more nearly from just north of due west than do high-frequency waves, which appear to arrive mostly from the northwest, though there is considerable scatter about this trend.

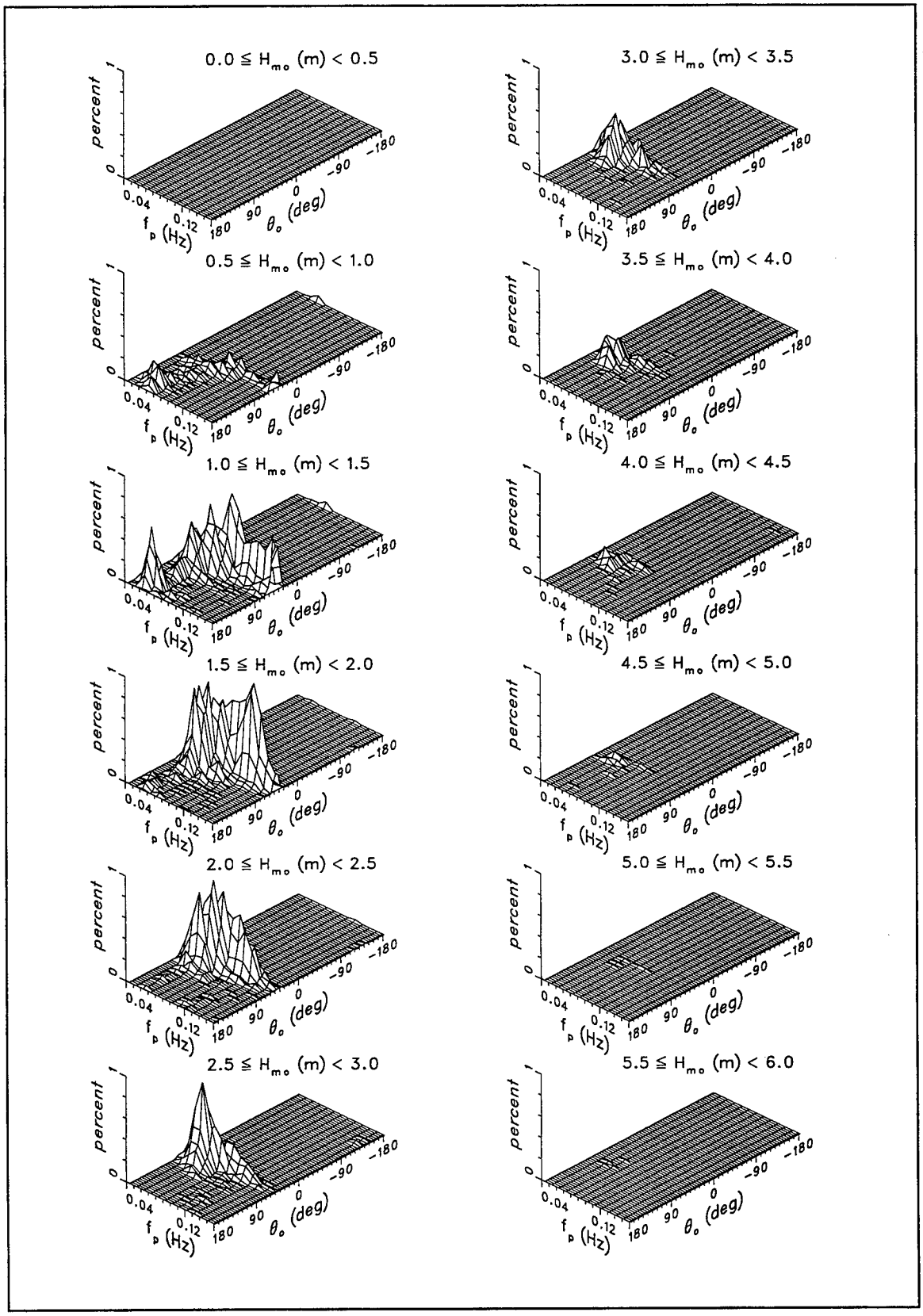

Figure 9. Joint height-frequency-direction probability function for Harvest Platform

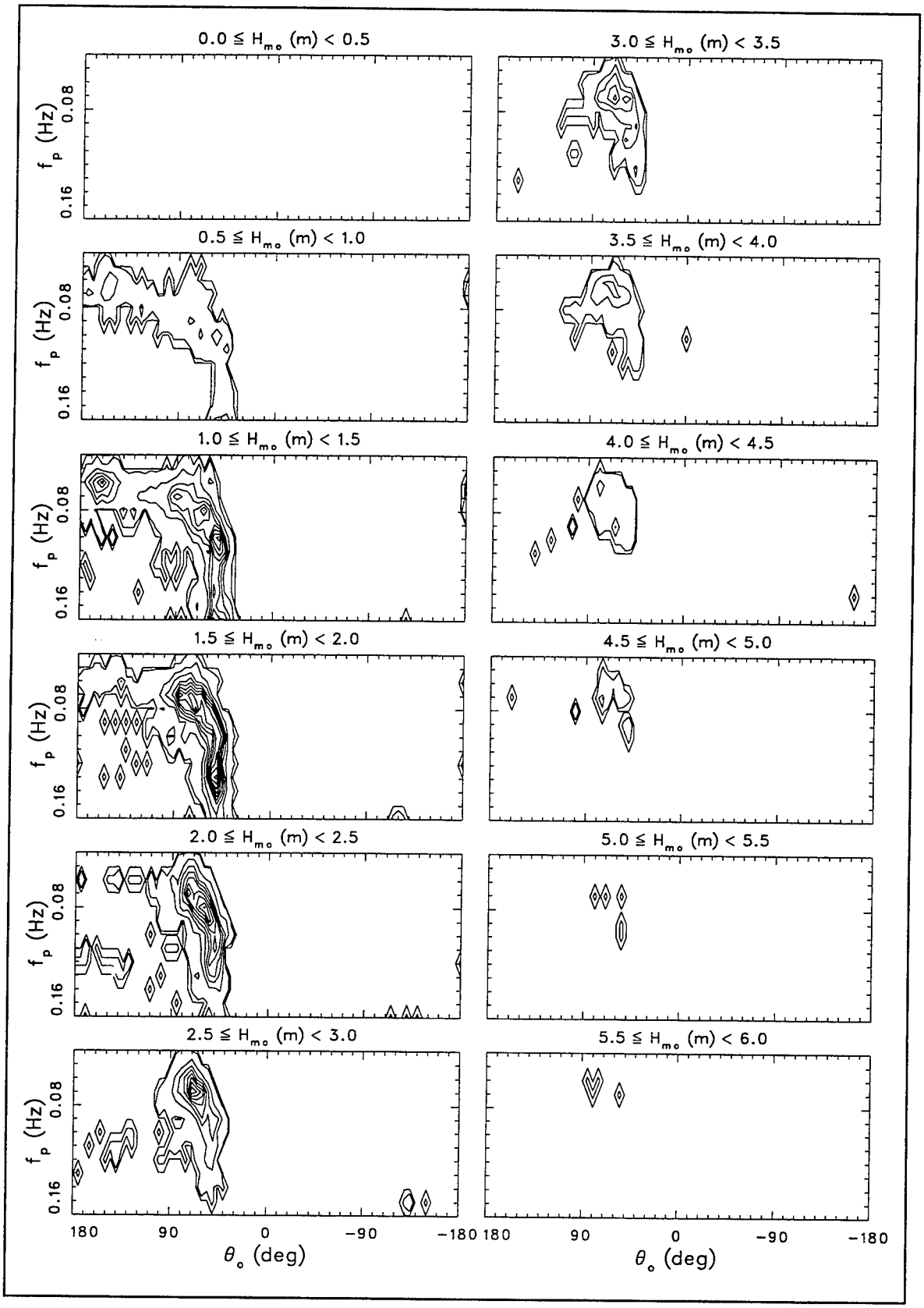

Figure 10. Contour plots of surfaces shown in Figure 9

Though primary waves tend to be bound in a relatively narrow range of direction, subtle variations of peak direction within this range are not inconsequential. A major interest is to use Harvest Platform observations to represent open ocean conditions for use in models of wave transformation through the Channel Islands, and subsequent wave migration to the coast of the Southern California Bight to characterize wave conditions along that economically important region. Several such models were examined by O'Reilly and Guza (1991, 1993), and it was found that minor variations in open ocean wave approach direction result in major variations in the amount of wave energy reaching various California coastal locations. Thus, details of the probability function relating to the bulk of Harvest Platform observations are important.

There are three regions in probability space away from the main lobes of Harvest Platform results containing results that are important either statistically or dynamically. One of these regions that is important in both senses is seen in Figures 9 and 10 as a maximum of probability centered near θ_0 = 160 deg and f_p = 0.06 Hz in the H_{mo} bin spanning 1.0 to 1.5 m. These parameters are characteristic of southern swell, long-traveled waves originating in the south Pacific Ocean. The probability peak associated with this maximum appears to extend over mean directions from 140 to 180 deg, spectral peak frequencies from 0.04 to 0.08 Hz, and in all of the four lowest, energy-containing H_{mo} bins (note that there are no observations in the Harvest Platform data set of $H_{mo} \leq$ 0.5 m). It is quite possible that not all of these observations are associated with southern swell, as low-frequency waves from long-duration storms more local to Harvest Platform might also appear in this parameter grouping.

For mean wave direction to exist in this high-probability lobe, southerly waves (from any source) must dominate the individual frequency-direction spectra from which the characterizing parameters are derived. It often happened, however, that swell waves from the south would coexist with swell at the same frequency from the west or northwest. In these cases, mean direction assumes a value somewhere between the individual swell peak directions, and its value depends on the relative strengths of these peaks. The statistical accumulation of these cases results in a ridge of finite probability extending from the main peak of westerly waves to the southern swell peak. Such ridges are evident in all the wave height bins exhibiting southern swell, as can be seen especially well in Figure 10. These results are somewhat artificial, as neither of the energetic peak directions are well represented, and are a hazard of characterizing directionally multi-modal frequency-direction spectra with a single directional parameter. Where such conditions are considered important to a particular study, it is suggested that individual frequency-direction spectra be examined to refine further their directional characterization.

Aside from probabilities associated with the main data grouping and the southern swell mode, there are two other significant probability groupings. There are not a large number of observations for these cases, yet they are important because they represent moderate to high energy. The most populous of these two groupings resides at moderate- to high-energy, intermediate frequencies, and in the direction arc from west through southwest to south.

These are the data in the lower left corners of the contour plots in Figure 10, and they are suggestive of storms in the quadrant to the southwest of Harvest Platform that are much more local than sources of southern swell. A much less populous group is located in the region of intermediate energy levels, near the high end of the frequency axis, and with θ_0 in the range -120 to -150 deg, indicating sources in the southeast. Referring to Figure 2, these waves appear to originate in the channel between the offshore islands and the mainland and are probably very local owing to their high characteristic frequencies and the restricted fetch in those directions.

As with southern swell cases that coexist with western swell to give a curious mix of characteristic parameters, there are cases where local seas coexist with swell to yield combinations of parameters that do not appear sensible, but are still consistent with the rather crude way that complicated wave fields are parameterized in this report. One such observation is in the 4.0- to 4.5-m wave height bin, with f_p near 0.14 Hz, and a θ_0 bin of -160 deg. According to Figure 2, this direction puts the wave source in line with San Miguel or Santa Rosa Island, which should constrain the fetch over which such waves could be generated and the heights they can achieve. Furthermore, 4-m waves at 0.14 Hz would be unnaturally steep. Examination of the detailed frequency-direction spectrum from which this set of parameters arose reveals a condition of mixed sea and swell, with the frequency spectral density at 0.14 Hz slightly higher than that for the swell peak. The directional spectrum at 0.14 Hz has two well-separated directional modes, one indicating waves from the east-southeast, and the other indicating waves from the south. Referring again to Figure 2, these conditions suggest a local storm, possibly non-stationary over the duration of the wave record for this case, forcing waves around the northern Channel Islands so that high-frequency waves sensibly approach Harvest Platform from the south and east-southeast directions, all in the presence of deep ocean swell from the west. Thus, the mix of sea and swell gives a high H_{mo}, and the directionally broad sea spectrum yields a mean wave direction that appears suspicious but is legitimate in the sense that it is the average direction for two widely separated directional modes. This is another case where considerable care must be exercised in interpreting ocean wave conditions characterized by only three parameters.

In comparison, wave conditions at the FRF and Harvest Platform are typically very different, though this is not surprising. Each site is subject to the forcing and boundary conditions imposed by prevailing weather systems in and on the edges of its major ocean basin, as well as bathymetrically induced wave blockage, steering, and transformation. The FRF site is on the west side of its major ocean basin and separated therefrom by a broad, shallow continental shelf. Barring tropical storms, most high-energy weather systems move from west to east, so that the FRF is in the weather lee of the North American continent. Local intense storms, mostly northeasters, are infrequent and relatively short-lived, so that the most common waves consist of low-energy, low-frequency swell from distant parts of the Atlantic Ocean. Harvest Platform is on the east side of its ocean basin, on the windward side of the continent, in relatively deep water, and in a much larger ocean. As such, it is exposed to waves of higher

energy that are relatively unattenuated or transformed by bathymetric effects, and which can originate anywhere in the vast region subtended by an arc of directions from south through west to northwest of the observation site.

Though each experiment site is different from the other, each site may be representative of other sites subject to the same types of forcing and boundary conditions. In this regard, the FRF results may characterize a number of U.S. east coast sites that are subject to both seasonal, wave-inducing frontal passages and infrequent hurricane waves and are separated from the deep Atlantic Ocean by a broad shallow continental shelf. Harvest Platform data may typify conditions in the open Pacific Ocean west of the islands that shelter the Southern California Bight. Without additional measurements or similar analysis of existing databases, these statements are, of course, conjectural. Lacking other guidance, however, and subject to care in interpretation, the statistical climates presented herein can be used to characterize other sites having comparable environments.

8 Summary

Based on a need for more complete wave statistical climatologies cited in the SPM (1984), joint probability functions of characteristic wave height, spectral peak frequency, and mean direction have been estimated empirically for two environmentally disparate U.S. coastal sites. One site is the FRF, on the northern Outer Banks of North Carolina, at which wave measurements have been made with a nine-element, high-resolution directional gauge in 8-m water depth, about 900 m offshore. The other site is the Texaco Oil Company production facility known as Harvest Platform, located at the northern end of the Southern California Bight, at which measurements have been made with a six-element, high-resolution directional wave gauge in 200-m water depth, about 20 km west of Point Conception, California.

Three-parameter joint statistics have been computed using conventional techniques described herein by Equation 5 for joint probability density, and Equation 12 for percent occurrence, with discrete independent variables wave height, peak frequency, and mean direction defined by Equations 6, 7, and 8, respectively. Fundamental to estimates of joint probability density and percent occurrence is the case-count matrix, defined in the text following Equation 5 and computed as described in Chapter 3. Observational data sets consisted of regularly spaced, nearly complete sequences of parameter triplets (H_{mo}, f_p, and θ_0) spanning 5 years (13,941 triplets) at the FRF, and 3 years (7,066 triplets) at Harvest Platform. Parameters used with the defining equations to discretize probability space are given in Table 4. This table and the case-count matrices tabulated in Appendixes A and B for the FRF and Harvest Platform, respectively, constitute the primary quantitative results of this study.

For historical interest, marginal probability distributions of H_{mo} alone were computed for the two sites and compared to five common, two-parameter, analytic probability functions. These functions are the modified exponential, log-normal, gamma, beta, and Weibull probability densities. Means and standard deviations of observed H_{mo} were used to set the parameters of these functions. All of the functions resembled, to some extent, the observed distributions near their modal peaks. In a subjective evaluation, the single function that compared most favorably with both data sets was log-normal. The modified exponential function, recommended by the SPM (1984) for nearshore sites, more nearly resembled FRF data than did the log-normal function, but did not compare as well with Harvest Platform data. Examination of the

high-energy, low-probability tail regions of the distributions again indicated that, with the exception of a region of depth-limited wave heights at extremely low probability, the modified exponential curve best represents FRF observations. The tail region of Harvest Platform data seems best represented by the gamma or beta functions.

These tests indicate that SPM (1984) guidance remains valid for shallow, nearshore sites, and that, with some additional effort, a separate function could be defined that would represent accurately the data at each site. Such an effort may prove moot, however, because there is no universal hypothesis that unifies wave height distributions for all sites. It is reasonable that a given site is subject both to local forcing and boundary conditions as well as radiative conditions from distant sources so that all sites cannot be treated the same way. Furthermore, H_{mo} alone is only a partial descriptor of wave conditions. When the suite of height conditions from a given incremental range is further distributed with respect to characteristic frequency and direction, any resemblance to a function defining the marginal distribution of wave height tends to be lost.

This latter statement is made credible by examining the marginal, two-parameter distributions relating wave height to peak frequency and wave height to mean direction, as done in Chapters 5 and 6, respectively. The first of these distributions ignores directional information and may provide useful guidance when, for example, designing a suite of model tests in a unidirectional wave flume. Empirical probability functions in the form of percent occurrences indicate that the FRF tends strongly to have wave heights near 0.4 m with peak frequencies of about 0.11 Hz, a shift downward of the modal peak of about 0.6 m when H_{mo} alone is examined. A broad variety of peak frequencies is possible for wave heights less than about 2 m, reflecting both initial storm conditions and persistent background swell. High-energy waves all tend to be restricted to low frequencies, as expected. Harvest Platform has a more uniform probability of H_{mo}-f_p pairs both at frequencies near 0.07 Hz and for wave heights between 1 and 2 m. These conditions are consistent with a rather even mix of swell waves and local seas.

Marginal distributions of H_{mo}-θ_0 pairs show primary modes that are relatively narrow in direction at both sites, spanning roughly 40 deg. FRF directional observations are centered just south of shore normal, the dominant direction of the low-frequency, low-energy swell seen in the height-frequency distribution for that site. Waves arriving at Harvest Platform cluster around the northwest direction, which appears to contain the primary energy sources for this site. Both sites have small secondary modes in their height-direction distributions, though for different reasons. For the FRF, a mode at H_{mo} near 1 m with waves coming from 20 to 30 deg north of shore normal is associated with local storm waves from the northeast, with such storms being the primary source of high-energy conditions. At Harvest Platform, the secondary mode appears for wave heights near 1 m and for directions slightly west of due south. These are low-frequency waves known as southern swell that originate, at least in part, in

the South Pacific Ocean in large storms arising in the southern hemisphere winter.

The clearest pictures of statistical wave climates at the two study sites are in the joint distributions of H_{mo}, f_p, and θ_0. The FRF observations show a strong limiting relationship between spectral peak frequency and mean direction. Low-energy, high-frequency wave conditions span almost the whole horizon of possible incident wave directions, but the range of incident directions narrows with decreasing frequency to the point where, at the lowest wind wave frequencies, incident directions are restricted to a 30-deg arc centered just south of shore normal. This behavior is consistent with the refractive nature of individual waves, and it is interesting that such behavior is retained in the parameters of highly filtered, processed data. Results show the climate at the FRF to be dominated by low-energy, low-frequency, nearly shore normal waves. Relatively rare wind events induce waves at all stages of spectral development, with northeaster-related conditions spanning sufficiently narrow ranges of parameter space to result in a secondary probability mode at low and intermediate energy levels. Even rarer events, associated with winds from the northwest, southwest, and southeast, result in waves from the northeast and southeast. Rarest among possible conditions are high-frequency waves from the shore normal direction.

The most common Harvest Platform waves at all energy levels and at all of the limited number of frequency bands arrive from a 50-deg range of directions spanning the arc from northwest to west. In the most populated wave-height bin, with H_{mo} between 1.5 and 2.0 m, the probability distribution in each θ_0 bin is nearly uniform. As energy levels increase, overall probabilities decrease, and, within one of these wave-height bins, probabilities drop rapidly with respect to θ_0 and more gradually with respect to f_p from maxima near 70 deg and 0.06 Hz. A secondary probability peak occurs at the three lowest energy-containing bins centered near θ_0 = 160 deg and f_p = 0.06 Hz. These are associated in part with the phenomenon known as southern swell. Far rarer are occurrences of intermediate-frequency waves from both the southwest and southeast at low and moderate energy levels. These conditions are probably associated with storms more local to the Harvest Platform site.

The primary purpose of this report is to publicize the information contained in Table 4 and Appendixes A and B from which can be deduced estimates of statistical wave climates for the two study sites and for sites having similar forcing and boundary conditions. Figures and extensive attendant discussion contained in this report are intended to help interpret these results in light of the simplicity of parameterization used for site characterization and the frequently complex nature of the more detailed observations from which the parameters were derived. Collectively, these results will help alleviate the need stated in the SPM (1984) for more detailed site characterizations, and should help project engineers and nearshore modelers to understand and make use of the nature of wind waves at these sites.

References

Abramowitz, M., and Stegun, I. A. (1970). *Handbook of mathematical functions*. Dover, New York.

Bendat, J. S., and Piersol, A. G. (1971). *Random data: Analysis and measurement procedures*. Wiley-Interscience, New York.

Kuik, A. J., van Vledder, G. Ph., and Holthuijsen, L. H. (1988). "A method for the routine analysis of pitch-and-roll buoy wave data," *Journal of Physical Oceanography* 18, 1020-34.

Leyden, M. L. (1997). "Probabilistic modeling of long-term wave climate," M.S. thesis, Florida Institute of Technology, Melbourne, FL.

Long, C. E. (1994). "Three-parameter characterization of shallow-water directional wind wave spectra," Technical Report CERC-94-1, U.S. Army Engineer Waterways Experiment Station, Vicksburg, MS.

_____. (1995). "Directional wind wave characteristics at Harvest Platform," Technical Report CERC-95-4, U.S. Army Engineer Waterways Experiment Station, Vicksburg, MS.

_____. (1997a). "Index and bulk parameters for frequency-direction spectra measured at CHL Field Research Facility, September 1995 to August 1996," Miscellaneous Paper CHL-97-8, U.S. Army Engineer Waterways Experiment Station, Vicksburg, MS.

_____. (1997b). "1996 Index of wind wave directional spectra measured at Harvest Platform," Miscellaneous Paper CHL-97-9, U.S. Army Engineer Waterways Experiment Station, Vicksburg, MS.

Long, C. E., and Oltman-Shay, J. M. (1991). "Directional characteristics of waves in shallow water," Technical Report CERC-91-1, U.S. Army Engineer Waterways Experiment Station, Vicksburg, MS.

Longuet-Higgins, M. S. (1952). "On the statistical distribution of the heights of sea waves," *Journal of Marine Research* 11, 245-66.

Miller, I., and Freund, J. E. (1985). *Probability and statistics for engineers*. Prentice-Hall, Englewood Cliffs, NJ.

O'Reilly, W. C., and Guza, R. T. (1991). "Comparison of spectral refraction and refraction-diffraction wave models," *Journal of Waterway, Port, Coastal, and Ocean Engineering* 117, 199-215.

_____. (1993). "A comparison of two spectral wave models in the Southern California Bight," *Coastal Engineering* 19, 263-82.

Pawka, S. S. (1983). "Island shadows in wave directional spectra," *Journal of Geophysical Research* 88, 2579-91.

Shore Protection Manual. (1984). 2 Vols, Coastal Engineering Research Center, U.S. Army Engineer Waterways Experiment Station, 4th ed., U.S. Government Printing Office, Washington, DC.

Appendix A
Case Counts for FRF 8-m Array

Tables A1 through A11 contain fundamental information for constructing discrete joint probability density or percent occurrence functions from the N = 13,941 observations used in this study from the FRF 8-m array directional wave gauge. A table entry is the number of observed cases having characteristic wave heights H_{mo}, peak frequencies f_p, and mean wave directions θ_0 within cells defined by ranges of height, frequency, and direction. Each table contains all information for cases with wave heights within a range ΔH = 0.5 m. Table columns are identified with center frequencies of cells having a frequency range Δf = 0.00977 Hz. Rows are labeled with center directions of cells with direction ranges $\Delta\theta$ = 5 deg.

Case counts are listed for simplicity of format. If all entries from all tables are summed, the result is simply N. To convert an entry to percent occurrence of cases in its height-frequency-direction cell, the entry number should be multiplied by 100 percent and divided by N, which is equivalent to multiplying the entry by 0.00717 percent. If all entries from all tables are thus normalized and then summed, the result is 100 percent. To convert an entry to the form of a discrete joint probability density, the entry number should be divided by the product $N\Delta H\Delta f\Delta\theta$, which is equivalent to multiplying the entry by the factor 0.00294 m^{-1} Hz^{-1} deg^{-1}. If all entries from all tables in this appendix are thus normalized, the result is the complete discrete approximation of the joint height-frequency-direction probability density function discussed in the body of this report for the FRF 8-m array.

Table A1
Case Counts for 0.0 m ≤ H_{mo} < 0.5 m

θ_0 (deg)	f_p (Hz)														
	0.044	0.054	0.064	0.074	0.084	0.093	0.103	0.113	0.123	0.132	0.142	0.152	0.162	0.171	0.181
-90	0	0	0	0	0	0	0	0	0	0	0	0	0	0	0
-85	0	0	0	0	0	0	0	0	0	0	0	0	0	0	0
-80	0	0	0	0	0	0	0	0	0	0	0	0	0	0	0
-75	0	0	0	0	0	0	0	0	0	0	0	0	0	0	0
-70	0	0	0	0	0	0	0	0	0	0	0	0	0	0	0
-65	0	0	0	0	0	0	0	0	0	0	0	0	0	0	0
-60	0	0	0	0	0	0	0	0	0	0	0	0	0	0	0
-55	0	0	0	0	0	0	0	0	0	0	0	0	0	0	0
-50	0	0	0	0	0	0	0	0	0	0	0	0	0	0	0
-45	0	0	0	0	0	0	0	0	0	0	0	1	0	7	6
-40	0	0	0	0	0	0	0	0	1	16	16	7	4	2	3
-35	0	1	0	0	0	0	0	2	18	42	50	13	4	2	1
-30	0	2	0	0	1	3	20	54	68	61	26	15	9	8	3
-25	0	0	1	0	1	9	64	239	81	47	17	5	4	0	0
-20	0	0	9	5	15	62	120	197	77	26	15	5	0	0	0
-15	0	0	22	37	46	102	107	130	77	23	7	2	1	2	0
-10	0	0	29	81	97	75	66	91	44	14	6	3	1	0	1
-5	0	6	58	88	101	83	64	34	18	9	5	2	0	0	0
0	0	3	14	30	79	64	24	9	5	6	7	4	3	0	0
5	0	0	0	2	18	5	1	2	1	5	9	3	1	1	0
10	0	0	0	0	2	0	0	3	3	2	12	1	2	3	1
15	0	0	0	0	0	0	0	1	0	1	9	1	2	1	1
20	0	0	0	0	0	0	0	0	0	1	5	2	4	2	3
25	0	0	0	0	0	0	0	0	0	0	0	0	1	1	1
30	0	0	0	0	0	0	0	0	0	0	0	0	0	1	5
35	0	0	0	0	0	0	0	0	0	0	0	0	0	3	2
40	0	0	0	0	0	0	0	0	0	0	0	0	0	0	0
45	0	0	0	0	0	0	0	0	0	0	0	0	0	0	0
50	0	0	0	0	0	0	0	0	0	0	0	0	0	0	0
55	0	0	0	0	0	0	0	0	0	0	0	0	0	0	0
60	0	0	0	0	0	0	0	0	0	0	0	0	0	0	0
65	0	0	0	0	0	0	0	0	0	0	0	0	0	0	0
70	0	0	0	0	0	0	0	0	0	0	0	0	0	0	0
75	0	0	0	0	0	0	0	0	0	0	0	0	0	0	0
80	0	0	0	0	0	0	0	0	0	0	0	0	0	0	0
85	0	0	0	0	0	0	0	0	0	0	0	0	0	0	0
90	0	0	0	0	0	0	0	0	0	0	0	0	0	0	0

(Continued)

Table A1 (Concluded)

θ_0 (deg)	f_p (Hz)													
	0.191	0.201	0.210	0.220	0.230	0.240	0.250	0.259	0.269	0.279	0.289	0.298	0.308	0.318
-90	0	0	0	0	0	0	0	0	0	0	0	0	0	0
-85	0	0	0	0	0	0	0	0	0	0	0	0	0	0
-80	0	0	0	0	0	0	0	0	0	0	0	0	0	0
-75	0	0	0	0	0	0	0	0	0	0	0	0	0	0
-70	0	0	0	0	0	0	0	0	0	0	0	0	0	0
-65	0	0	0	0	0	0	0	0	1	0	0	0	0	0
-60	0	0	0	1	0	0	0	1	1	1	1	0	1	0
-55	0	2	1	0	0	2	1	2	1	1	0	2	0	0
-50	1	2	3	0	0	0	1	0	1	0	1	1	1	3
-45	1	2	0	1	0	1	0	0	0	0	0	1	1	0
-40	1	1	2	0	2	0	0	0	0	0	0	0	0	0
-35	0	0	1	0	0	0	0	0	0	0	0	0	1	0
-30	0	1	1	1	0	0	0	0	0	0	0	0	0	0
-25	0	1	0	1	0	0	0	0	0	0	0	0	0	0
-20	1	1	0	1	1	0	0	0	0	0	0	0	0	0
-15	0	0	0	0	0	0	0	0	0	0	0	0	0	0
-10	1	1	0	0	0	0	0	0	0	0	0	0	0	0
-5	0	0	0	0	0	0	0	0	0	0	0	0	0	0
0	3	0	0	0	0	0	0	0	0	0	0	0	0	0
5	1	0	0	0	0	0	0	0	0	0	1	0	0	0
10	1	0	1	0	1	0	1	0	0	0	0	0	0	0
15	0	2	1	0	3	0	0	0	0	0	0	1	0	0
20	1	2	3	3	1	1	0	1	0	0	0	0	0	0
25	1	0	1	1	1	0	1	0	0	0	0	1	0	1
30	2	1	2	0	0	2	0	0	0	0	1	0	0	0
35	1	1	1	0	0	0	0	0	1	1	0	0	0	0
40	0	2	1	1	0	0	0	0	0	0	0	0	0	0
45	0	0	2	3	2	0	1	0	0	0	0	0	2	1
50	0	0	0	0	0	0	2	0	1	1	0	0	1	1
55	0	0	0	0	1	0	0	0	0	0	0	1	0	0
60	0	0	0	0	1	0	0	0	1	0	0	2	0	1
65	0	0	0	0	0	1	0	0	0	0	0	0	0	0
70	0	0	0	0	0	1	3	0	0	1	0	0	0	0
75	0	0	0	0	0	0	0	0	0	0	0	0	0	0
80	0	0	0	0	0	0	0	0	0	0	1	0	0	0
85	0	0	0	0	0	0	0	0	0	0	0	0	0	0
90	0	0	0	0	0	0	0	0	0	0	0	0	0	0

Table A2
Case Counts for 0.5 m ≤ H_{mo} < 1.0 m

θ_0 (deg)	f_p (Hz)														
	0.044	0.054	0.064	0.074	0.084	0.093	0.103	0.113	0.123	0.132	0.142	0.152	0.162	0.171	0.181
-90	0	0	0	0	0	0	0	0	0	0	0	0	0	0	0
-85	0	0	0	0	0	0	0	0	0	0	0	0	0	0	0
-80	0	0	0	0	0	0	0	0	0	0	0	0	0	0	0
-75	0	0	0	0	0	0	0	0	0	0	0	0	0	0	0
-70	0	0	0	0	0	0	0	0	0	0	0	0	0	0	0
-65	0	0	0	0	0	0	0	0	0	0	0	0	0	0	0
-60	0	0	0	0	0	0	0	0	0	0	0	0	0	0	0
-55	0	0	0	0	0	0	0	0	0	0	0	0	0	0	0
-50	0	0	0	0	0	0	0	0	0	0	0	0	0	0	1
-45	0	0	0	0	0	0	0	0	0	0	1	4	3	3	7
-40	0	0	0	0	0	0	0	0	0	3	9	14	18	9	11
-35	0	0	0	0	0	0	0	2	10	27	54	46	22	10	10
-30	0	0	4	5	1	14	16	41	50	60	59	42	26	13	7
-25	0	0	7	10	12	31	63	119	107	59	36	23	5	14	5
-20	0	0	4	17	20	54	121	134	72	42	23	11	4	4	2
-15	0	0	5	12	27	56	135	183	79	40	23	11	5	3	0
-10	0	2	26	43	85	106	170	191	63	22	11	7	6	0	2
-5	0	9	76	115	162	179	187	126	53	24	6	5	4	2	5
0	0	6	17	65	218	170	134	71	30	18	10	9	6	4	4
5	0	1	1	2	60	47	41	26	22	19	14	15	10	4	3
10	0	0	0	0	5	3	7	10	14	24	15	19	8	8	8
15	0	0	0	0	0	0	1	4	1	23	22	20	15	11	8
20	0	0	0	0	0	0	0	1	0	8	34	32	24	20	17
25	0	0	0	0	0	0	0	0	0	1	11	34	34	26	14
30	0	0	0	0	0	0	0	0	0	0	1	5	25	29	28
35	0	0	0	0	0	0	0	0	0	0	1	2	0	17	27
40	0	0	0	0	0	0	0	0	0	0	0	0	2	1	8
45	0	0	0	0	0	0	0	0	0	0	0	0	1	2	2
50	0	0	0	0	0	0	0	0	0	0	0	0	0	0	1
55	0	0	0	0	0	0	0	0	0	0	0	0	0	0	0
60	0	0	0	0	0	0	0	0	0	0	0	0	0	0	0
65	0	0	0	0	0	0	0	0	0	0	0	0	0	0	0
70	0	0	0	0	0	0	0	0	0	0	0	0	0	0	0
75	0	0	0	0	0	0	0	0	0	0	0	0	0	0	0
80	0	0	0	0	0	0	0	0	0	0	0	0	0	0	0
85	0	0	0	0	0	0	0	0	0	0	0	0	0	0	0
90	0	0	0	0	0	0	0	0	0	0	0	0	0	0	0

(Continued)

Table A2 (Concluded)

θ_0 (deg)	f_p (Hz)													
	0.191	0.201	0.210	0.220	0.230	0.240	0.250	0.259	0.269	0.279	0.289	0.298	0.308	0.318
-90	0	0	0	0	0	0	0	0	0	0	0	0	0	0
-85	0	0	0	0	0	0	0	0	0	0	0	0	0	0
-80	0	0	0	0	0	0	0	0	0	0	0	0	0	0
-75	0	0	0	0	0	0	0	0	0	0	0	0	0	0
-70	0	0	0	0	0	0	0	0	0	0	0	0	0	0
-65	0	0	0	0	0	0	0	0	0	1	0	0	0	0
-60	0	0	0	0	0	0	0	0	0	0	0	0	0	2
-55	0	0	0	0	0	3	0	1	1	0	1	0	2	4
-50	0	1	2	0	2	0	2	5	3	1	0	0	1	1
-45	4	3	1	2	1	1	0	0	1	1	1	1	0	1
-40	4	3	1	3	2	0	1	0	0	0	0	0	0	0
-35	9	4	3	3	0	0	0	0	0	1	0	0	0	2
-30	4	2	1	1	1	0	0	0	1	1	0	0	1	0
-25	2	3	1	1	1	1	1	0	1	0	0	0	0	0
-20	0	1	3	1	1	1	0	0	0	1	1	0	0	0
-15	1	1	2	0	3	0	0	3	0	1	0	0	0	0
-10	1	1	0	1	1	1	0	1	2	1	0	0	0	1
-5	2	1	2	2	1	1	1	2	2	0	0	1	0	0
0	1	2	2	2	2	1	1	0	1	0	0	0	0	1
5	4	1	2	1	3	4	1	1	1	0	1	0	0	0
10	1	1	2	1	0	2	1	1	2	1	0	0	0	0
15	5	2	4	1	4	3	0	0	1	1	1	0	0	1
20	8	0	7	4	3	4	2	5	1	1	1	0	0	1
25	5	7	5	7	1	3	0	1	5	0	2	1	0	0
30	14	9	5	7	2	5	1	4	3	1	0	2	1	1
35	17	9	16	8	6	1	4	5	3	1	1	0	0	0
40	12	13	7	4	6	5	3	2	3	0	0	2	2	0
45	9	11	11	9	9	5	3	0	2	1	1	1	0	0
50	1	2	6	7	6	6	4	6	4	3	1	1	2	1
55	1	0	2	4	0	9	3	4	2	0	0	3	0	0
60	0	1	0	2	4	0	1	0	2	1	0	0	0	1
65	0	0	0	0	2	4	0	0	0	0	0	0	0	0
70	0	0	0	0	0	1	0	1	1	1	0	0	1	0
75	0	0	0	0	0	0	0	0	0	0	0	0	0	0
80	0	0	0	0	0	0	0	0	0	0	0	0	0	0
85	0	0	0	0	0	0	0	0	0	0	0	0	0	0
90	0	0	0	0	0	0	0	0	0	0	0	0	0	0

Table A3
Case Counts for 1.0 m ≤ H_{mo} < 1.5 m

θ_0 (deg)	f_p (Hz)														
	0.044	0.054	0.064	0.074	0.084	0.093	0.103	0.113	0.123	0.132	0.142	0.152	0.162	0.171	0.181
-90	0	0	0	0	0	0	0	0	0	0	0	0	0	0	0
-85	0	0	0	0	0	0	0	0	0	0	0	0	0	0	0
-80	0	0	0	0	0	0	0	0	0	0	0	0	0	0	0
-75	0	0	0	0	0	0	0	0	0	0	0	0	0	0	0
-70	0	0	0	0	0	0	0	0	0	0	0	0	0	0	0
-65	0	0	0	0	0	0	0	0	0	0	0	0	0	0	0
-60	0	0	0	0	0	0	0	0	0	0	0	0	0	0	0
-55	0	0	0	0	0	0	0	0	0	0	0	0	0	0	0
-50	0	0	0	0	0	0	0	0	0	0	0	0	0	0	0
-45	0	0	0	0	0	0	0	0	0	0	0	0	1	0	0
-40	0	0	0	0	0	0	0	0	0	0	1	0	0	0	0
-35	0	0	0	0	0	0	0	1	1	2	8	4	0	1	0
-30	0	0	6	8	1	3	5	6	10	16	9	6	3	1	0
-25	0	0	11	24	1	10	12	13	17	13	11	3	3	0	0
-20	0	0	1	11	9	12	19	24	15	12	7	4	2	1	1
-15	0	0	0	11	20	30	25	22	19	14	4	1	3	4	1
-10	0	0	0	13	29	34	39	23	18	6	3	2	4	1	3
-5	0	0	0	40	76	67	60	37	18	7	3	1	2	6	2
0	0	0	1	16	71	86	56	35	18	8	6	5	6	3	5
5	0	0	0	0	32	55	23	22	19	14	6	7	7	7	3
10	0	0	0	0	4	8	16	18	21	16	22	9	13	3	9
15	0	0	0	0	0	0	0	4	16	12	18	12	11	8	7
20	0	0	0	0	0	0	0	0	3	13	26	19	19	14	12
25	0	0	0	0	0	0	0	0	0	1	27	47	28	17	16
30	0	0	0	0	0	0	0	0	0	0	4	27	27	40	15
35	0	0	0	0	0	0	0	0	0	0	1	4	23	20	17
40	0	0	0	0	0	0	0	0	0	0	0	3	4	16	14
45	0	0	0	0	0	0	0	0	0	0	0	0	1	3	3
50	0	0	0	0	0	0	0	0	0	0	0	0	0	0	1
55	0	0	0	0	0	0	0	0	0	0	0	0	0	0	0
60	0	0	0	0	0	0	0	0	0	0	0	0	0	0	0
65	0	0	0	0	0	0	0	0	0	0	0	0	0	0	0
70	0	0	0	0	0	0	0	0	0	0	0	0	0	0	0
75	0	0	0	0	0	0	0	0	0	0	0	0	0	0	0
80	0	0	0	0	0	0	0	0	0	0	0	0	0	0	0
85	0	0	0	0	0	0	0	0	0	0	0	0	0	0	0
90	0	0	0	0	0	0	0	0	0	0	0	0	0	0	0

(Continued)

Table A3 (Concluded)

θ_0 (deg)	f_p (Hz)													
	0.191	0.201	0.210	0.220	0.230	0.240	0.250	0.259	0.269	0.279	0.289	0.298	0.308	0.318
-90	0	0	0	0	0	0	0	0	0	0	0	0	0	0
-85	0	0	0	0	0	0	0	0	0	0	0	0	0	0
-80	0	0	0	0	0	0	0	0	0	0	0	0	0	0
-75	0	0	0	0	0	0	0	0	0	0	0	0	0	0
-70	0	0	0	0	0	0	0	0	0	0	0	0	0	0
-65	0	0	0	0	0	0	0	0	0	0	0	0	0	0
-60	0	0	0	0	0	0	0	0	0	0	0	0	0	0
-55	0	0	0	0	0	0	0	0	0	0	0	0	0	0
-50	0	0	0	0	0	0	0	0	0	0	0	0	0	0
-45	0	0	0	0	0	0	0	0	0	0	0	0	0	0
-40	1	0	0	0	0	0	0	0	0	0	0	0	0	0
-35	0	0	0	0	0	0	0	0	0	0	0	0	0	0
-30	0	0	0	0	0	0	0	0	0	0	0	0	0	0
-25	1	0	1	0	0	0	1	0	0	0	0	0	0	0
-20	0	0	0	1	1	0	0	0	0	0	0	0	0	0
-15	0	0	1	2	0	0	0	0	0	0	0	0	0	0
-10	1	0	1	1	0	0	0	0	0	0	0	0	0	0
-5	2	1	0	1	0	1	0	0	0	0	0	0	0	0
0	2	2	0	0	0	0	0	0	0	0	0	0	0	0
5	1	4	0	0	0	0	0	0	0	0	0	0	0	0
10	3	3	0	1	0	0	0	0	0	0	0	0	0	0
15	8	6	0	2	0	0	0	0	0	0	0	0	0	0
20	10	10	3	1	1	0	0	0	0	0	0	0	0	0
25	8	11	5	1	4	1	0	0	0	0	0	0	0	0
30	7	5	2	3	5	0	0	0	0	0	0	0	0	0
35	14	6	8	3	2	1	1	0	0	0	0	0	0	0
40	9	9	4	3	1	1	0	1	0	0	0	0	0	0
45	7	7	5	6	3	2	1	0	0	0	0	1	0	0
50	2	3	1	3	1	1	1	1	1	0	1	0	0	0
55	1	0	0	1	0	1	0	0	0	0	0	0	0	0
60	0	0	1	0	0	1	0	0	0	0	0	0	0	0
65	0	0	0	0	0	0	0	0	0	0	0	0	0	0
70	0	0	0	0	0	0	0	0	0	0	0	0	0	0
75	0	0	0	0	0	0	0	0	0	0	0	0	0	0
80	0	0	0	0	0	0	0	0	0	0	0	0	0	0
85	0	0	0	0	0	0	0	0	0	0	0	0	0	0
90	0	0	0	0	0	0	0	0	0	0	0	0	0	0

Table A4
Case Counts for 1.5 m ≤ H_{mo} < 2.0 m

θ_0 (deg)	f_p (Hz)														
	0.044	0.054	0.064	0.074	0.084	0.093	0.103	0.113	0.123	0.132	0.142	0.152	0.162	0.171	0.181
-90	0	0	0	0	0	0	0	0	0	0	0	0	0	0	0
-85	0	0	0	0	0	0	0	0	0	0	0	0	0	0	0
-80	0	0	0	0	0	0	0	0	0	0	0	0	0	0	0
-75	0	0	0	0	0	0	0	0	0	0	0	0	0	0	0
-70	0	0	0	0	0	0	0	0	0	0	0	0	0	0	0
-65	0	0	0	0	0	0	0	0	0	0	0	0	0	0	0
-60	0	0	0	0	0	0	0	0	0	0	0	0	0	0	0
-55	0	0	0	0	0	0	0	0	0	0	0	0	0	0	0
-50	0	0	0	0	0	0	0	0	0	0	0	0	0	0	0
-45	0	0	0	0	0	0	0	0	0	0	0	0	0	0	0
-40	0	0	0	0	0	0	0	0	0	0	0	0	0	0	0
-35	0	0	0	0	0	0	0	0	0	1	0	0	0	0	0
-30	0	1	2	2	0	2	1	0	4	0	0	0	1	0	0
-25	0	0	6	2	2	1	3	3	2	2	1	1	0	0	1
-20	0	0	8	4	3	7	7	11	8	1	0	0	0	0	0
-15	0	0	0	0	5	7	10	10	10	1	2	0	0	0	0
-10	0	0	0	10	12	20	17	6	6	4	1	1	0	1	0
-5	0	0	4	28	30	37	21	8	4	1	4	0	1	0	1
0	0	0	3	11	41	27	17	5	3	6	3	5	2	0	1
5	0	0	0	0	20	36	21	9	8	4	7	4	9	1	0
10	0	0	0	0	3	8	8	9	8	6	11	8	8	1	1
15	0	0	0	0	0	0	0	1	11	7	12	9	8	12	3
20	0	0	0	0	0	0	0	0	4	17	17	19	11	7	3
25	0	0	0	0	0	0	0	0	0	12	23	24	17	6	2
30	0	0	0	0	0	0	0	0	0	0	9	22	21	8	3
35	0	0	0	0	0	0	0	0	0	0	0	9	17	12	6
40	0	0	0	0	0	0	0	0	0	0	0	2	4	3	5
45	0	0	0	0	0	0	0	0	0	0	0	0	0	2	0
50	0	0	0	0	0	0	0	0	0	0	0	0	0	1	0
55	0	0	0	0	0	0	0	0	0	0	0	0	0	0	0
60	0	0	0	0	0	0	0	0	0	0	0	0	0	0	0
65	0	0	0	0	0	0	0	0	0	0	0	0	0	0	0
70	0	0	0	0	0	0	0	0	0	0	0	0	0	0	0
75	0	0	0	0	0	0	0	0	0	0	0	0	0	0	0
80	0	0	0	0	0	0	0	0	0	0	0	0	0	0	0
85	0	0	0	0	0	0	0	0	0	0	0	0	0	0	0
90	0	0	0	0	0	0	0	0	0	0	0	0	0	0	0

(Continued)

Table A4 (Concluded)

θ_0 (deg)	f_p (Hz)													
	0.191	0.201	0.210	0.220	0.230	0.240	0.250	0.259	0.269	0.279	0.289	0.298	0.308	0.318
-90	0	0	0	0	0	0	0	0	0	0	0	0	0	0
-85	0	0	0	0	0	0	0	0	0	0	0	0	0	0
-80	0	0	0	0	0	0	0	0	0	0	0	0	0	0
-75	0	0	0	0	0	0	0	0	0	0	0	0	0	0
-70	0	0	0	0	0	0	0	0	0	0	0	0	0	0
-65	0	0	0	0	0	0	0	0	0	0	0	0	0	0
-60	0	0	0	0	0	0	0	0	0	0	0	0	0	0
-55	0	0	0	0	0	0	0	0	0	0	0	0	0	0
-50	0	0	0	0	0	0	0	0	0	0	0	0	0	0
-45	0	0	0	0	0	0	0	0	0	0	0	0	0	0
-40	0	0	0	0	0	0	0	0	0	0	0	0	0	0
-35	0	0	0	0	0	0	0	0	0	0	0	0	0	0
-30	0	0	0	0	0	0	0	0	0	0	0	0	0	0
-25	0	0	0	0	0	0	0	0	0	0	0	0	0	0
-20	1	0	0	0	0	0	0	0	0	0	0	0	0	0
-15	0	0	0	0	0	0	0	0	0	0	0	0	0	0
-10	0	0	0	0	0	0	0	0	0	0	0	0	0	0
-5	0	0	0	0	0	0	0	0	0	0	0	0	0	0
0	1	0	0	0	0	0	0	0	0	0	0	0	0	0
5	0	0	0	0	0	0	0	0	0	0	0	0	0	0
10	0	0	0	0	0	0	0	0	0	0	0	0	0	0
15	2	0	0	0	0	0	0	0	0	0	0	0	0	0
20	3	0	0	1	0	0	0	0	0	0	0	0	0	0
25	1	0	0	0	0	0	0	0	0	0	0	0	0	0
30	0	0	1	0	0	0	0	0	0	0	0	0	0	0
35	2	1	0	1	0	0	0	0	0	0	0	0	0	0
40	2	0	0	0	0	0	0	0	0	0	0	0	0	0
45	1	0	0	0	0	0	0	0	0	0	0	0	0	1
50	0	0	0	0	0	0	0	0	0	0	0	0	0	0
55	0	0	0	0	0	0	0	0	0	0	0	0	0	0
60	0	0	0	0	0	0	0	0	0	0	0	0	0	0
65	0	0	0	0	0	0	0	0	0	0	0	0	0	0
70	0	0	0	0	0	0	0	0	0	0	0	0	0	0
75	0	0	0	0	0	0	0	0	0	0	0	0	0	0
80	0	0	0	0	0	0	0	0	0	0	0	0	0	0
85	0	0	0	0	0	0	0	0	0	0	0	0	0	0
90	0	0	0	0	0	0	0	0	0	0	0	0	0	0

Table A5
Case Counts for 2.0 m ≤ H_{mo} < 2.5 m

θ_0 (deg)	f_p (Hz)														
	0.044	0.054	0.064	0.074	0.084	0.093	0.103	0.113	0.123	0.132	0.142	0.152	0.162	0.171	0.181
-90	0	0	0	0	0	0	0	0	0	0	0	0	0	0	0
-85	0	0	0	0	0	0	0	0	0	0	0	0	0	0	0
-80	0	0	0	0	0	0	0	0	0	0	0	0	0	0	0
-75	0	0	0	0	0	0	0	0	0	0	0	0	0	0	0
-70	0	0	0	0	0	0	0	0	0	0	0	0	0	0	0
-65	0	0	0	0	0	0	0	0	0	0	0	0	0	0	0
-60	0	0	0	0	0	0	0	0	0	0	0	0	0	0	0
-55	0	0	0	0	0	0	0	0	0	0	0	0	0	0	0
-50	0	0	0	0	0	0	0	0	0	0	0	0	0	0	0
-45	0	0	0	0	0	0	0	0	0	0	0	0	0	0	0
-40	0	0	0	0	0	0	0	0	0	0	0	0	1	0	0
-35	0	0	0	0	0	0	0	0	0	0	0	0	0	0	0
-30	0	0	0	1	0	0	1	3	1	0	0	0	0	0	0
-25	0	1	1	6	1	0	5	2	0	1	0	0	0	0	0
-20	0	0	0	2	5	5	2	3	0	2	0	0	1	0	0
-15	0	0	0	0	5	5	3	3	0	0	0	0	0	0	0
-10	0	0	14	15	4	7	5	3	2	0	1	0	0	0	0
-5	0	0	6	25	9	7	10	5	3	2	1	1	0	0	0
0	0	0	5	10	28	13	7	6	3	5	3	0	0	0	0
5	0	0	0	1	6	10	9	7	7	4	4	1	0	0	0
10	0	0	0	0	4	7	3	3	6	2	8	8	1	0	0
15	0	0	0	0	0	2	1	0	2	5	7	7	1	0	0
20	0	0	0	0	0	0	0	0	2	10	9	4	0	0	0
25	0	0	0	0	0	0	0	0	0	1	8	6	2	0	0
30	0	0	0	0	0	0	0	0	0	0	4	5	3	0	0
35	0	0	0	0	0	0	0	0	0	0	0	4	0	0	0
40	0	0	0	0	0	0	0	0	0	0	0	0	1	1	0
45	0	0	0	0	0	0	0	0	0	0	0	0	0	0	0
50	0	0	0	0	0	0	0	0	0	0	0	0	0	0	0
55	0	0	0	0	0	0	0	0	0	0	0	0	0	0	0
60	0	0	0	0	0	0	0	0	0	0	0	0	0	0	0
65	0	0	0	0	0	0	0	0	0	0	0	0	0	0	0
70	0	0	0	0	0	0	0	0	0	0	0	0	0	0	0
75	0	0	0	0	0	0	0	0	0	0	0	0	0	0	0
80	0	0	0	0	0	0	0	0	0	0	0	0	0	0	0
85	0	0	0	0	0	0	0	0	0	0	0	0	0	0	0
90	0	0	0	0	0	0	0	0	0	0	0	0	0	0	0

(Continued)

Table A5 (Concluded)

θ_0 (deg)	f_p (Hz)													
	0.191	0.201	0.210	0.220	0.230	0.240	0.250	0.259	0.269	0.279	0.289	0.298	0.308	0.318
-90	0	0	0	0	0	0	0	0	0	0	0	0	0	0
-85	0	0	0	0	0	0	0	0	0	0	0	0	0	0
-80	0	0	0	0	0	0	0	0	0	0	0	0	0	0
-75	0	0	0	0	0	0	0	0	0	0	0	0	0	0
-70	0	0	0	0	0	0	0	0	0	0	0	0	0	0
-65	0	0	0	0	0	0	0	0	0	0	0	0	0	0
-60	0	0	0	0	0	0	0	0	0	0	0	0	0	0
-55	0	0	0	0	0	0	0	0	0	0	0	0	0	0
-50	0	0	0	0	0	0	0	0	0	0	0	0	0	0
-45	0	0	0	0	0	0	0	0	0	0	0	0	0	0
-40	0	0	0	0	0	0	0	0	0	0	0	0	0	0
-35	0	0	0	0	0	0	0	0	0	0	0	0	0	0
-30	0	0	0	0	0	0	0	0	0	0	0	0	0	0
-25	0	0	0	0	0	0	0	0	0	0	0	0	0	0
-20	0	0	0	0	0	0	0	0	0	0	0	0	0	0
-15	0	0	0	0	0	0	0	0	0	0	0	0	0	0
-10	0	0	0	0	0	0	0	0	0	0	0	0	0	0
-5	0	0	0	0	0	0	0	0	0	0	0	0	0	0
0	0	0	0	0	0	0	0	0	0	0	0	0	0	0
5	0	0	0	0	0	0	0	0	0	0	0	0	0	0
10	0	0	0	0	0	0	0	0	0	0	0	0	0	0
15	0	0	0	0	0	0	0	0	0	0	0	0	0	0
20	0	0	0	0	0	0	0	0	0	0	0	0	0	0
25	0	0	0	0	0	0	0	0	0	0	0	0	0	0
30	0	0	0	0	0	0	0	0	0	0	0	0	0	0
35	0	0	0	0	0	0	0	0	0	0	0	0	0	0
40	0	0	0	0	0	0	0	0	0	0	0	0	0	0
45	0	0	0	0	0	0	0	0	0	0	0	0	0	0
50	0	0	0	0	0	0	0	0	0	0	0	0	0	0
55	0	0	0	0	0	0	0	0	0	0	0	0	0	0
60	0	0	0	0	0	0	0	0	0	0	0	0	0	0
65	0	0	0	0	0	0	0	0	0	0	0	0	0	0
70	0	0	0	0	0	0	0	0	0	0	0	0	0	0
75	0	0	0	0	0	0	0	0	0	0	0	0	0	0
80	0	0	0	0	0	0	0	0	0	0	0	0	0	0
85	0	0	0	0	0	0	0	0	0	0	0	0	0	0
90	0	0	0	0	0	0	0	0	0	0	0	0	0	0

Table A6
Case Counts for 2.5 m ≤ H_{mo} < 3.0 m

θ_0 (deg)	f_p (Hz)														
	0.044	0.054	0.064	0.074	0.084	0.093	0.103	0.113	0.123	0.132	0.142	0.152	0.162	0.171	0.181
-90	0	0	0	0	0	0	0	0	0	0	0	0	0	0	0
-85	0	0	0	0	0	0	0	0	0	0	0	0	0	0	0
-80	0	0	0	0	0	0	0	0	0	0	0	0	0	0	0
-75	0	0	0	0	0	0	0	0	0	0	0	0	0	0	0
-70	0	0	0	0	0	0	0	0	0	0	0	0	0	0	0
-65	0	0	0	0	0	0	0	0	0	0	0	0	0	0	0
-60	0	0	0	0	0	0	0	0	0	0	0	0	0	0	0
-55	0	0	0	0	0	0	0	0	0	0	0	0	0	0	0
-50	0	0	0	0	0	0	0	0	0	0	0	0	0	0	0
-45	0	0	0	0	0	0	0	0	0	0	0	0	0	0	0
-40	0	0	0	0	0	0	0	0	0	0	0	0	0	0	0
-35	0	0	0	0	0	0	0	1	0	0	0	0	0	0	0
-30	0	0	0	1	1	1	1	0	0	0	0	0	0	0	0
-25	0	0	0	1	1	2	0	0	0	0	0	0	0	0	0
-20	0	0	0	3	4	0	3	3	0	0	0	0	0	0	0
-15	0	0	0	1	2	1	2	0	1	0	0	0	0	0	0
-10	0	0	7	2	4	1	1	2	0	0	0	0	0	0	0
-5	0	0	7	8	3	7	5	1	1	0	0	0	0	0	0
0	0	0	4	7	11	9	3	2	0	0	0	0	0	0	0
5	0	0	0	1	12	9	6	1	3	0	0	0	0	0	0
10	0	0	0	0	1	3	11	4	4	2	1	1	0	0	0
15	0	0	0	0	0	0	3	1	4	2	2	1	0	0	0
20	0	0	0	0	0	0	0	1	3	4	1	0	0	0	0
25	0	0	0	0	0	0	0	0	0	1	0	0	0	0	0
30	0	0	0	0	0	0	0	0	0	0	4	0	0	0	0
35	0	0	0	0	0	0	0	0	0	0	0	0	0	0	0
40	0	0	0	0	0	0	0	0	0	0	0	0	0	0	0
45	0	0	0	0	0	0	0	0	0	0	0	0	0	0	0
50	0	0	0	0	0	0	0	0	0	0	0	0	0	0	0
55	0	0	0	0	0	0	0	0	0	0	0	0	0	0	0
60	0	0	0	0	0	0	0	0	0	0	0	0	0	0	0
65	0	0	0	0	0	0	0	0	0	0	0	0	0	0	0
70	0	0	0	0	0	0	0	0	0	0	0	0	0	0	0
75	0	0	0	0	0	0	0	0	0	0	0	0	0	0	0
80	0	0	0	0	0	0	0	0	0	0	0	0	0	0	0
85	0	0	0	0	0	0	0	0	0	0	0	0	0	0	0
90	0	0	0	0	0	0	0	0	0	0	0	0	0	0	0

(Continued)

Table A6 (Concluded)

θ_0 (deg)	f_p (Hz)													
	0.191	0.201	0.210	0.220	0.230	0.240	0.250	0.259	0.269	0.279	0.289	0.298	0.308	0.318
-90	0	0	0	0	0	0	0	0	0	0	0	0	0	0
-85	0	0	0	0	0	0	0	0	0	0	0	0	0	0
-80	0	0	0	0	0	0	0	0	0	0	0	0	0	0
-75	0	0	0	0	0	0	0	0	0	0	0	0	0	0
-70	0	0	0	0	0	0	0	0	0	0	0	0	0	0
-65	0	0	0	0	0	0	0	0	0	0	0	0	0	0
-60	0	0	0	0	0	0	0	0	0	0	0	0	0	0
-55	0	0	0	0	0	0	0	0	0	0	0	0	0	0
-50	0	0	0	0	0	0	0	0	0	0	0	0	0	0
-45	0	0	0	0	0	0	0	0	0	0	0	0	0	0
-40	0	0	0	0	0	0	0	0	0	0	0	0	0	0
-35	0	0	0	0	0	0	0	0	0	0	0	0	0	0
-30	0	0	0	0	0	0	0	0	0	0	0	0	0	0
-25	0	0	0	0	0	0	0	0	0	0	0	0	0	0
-20	0	0	0	0	0	0	0	0	0	0	0	0	0	0
-15	0	0	0	0	0	0	0	0	0	0	0	0	0	0
-10	0	0	0	0	0	0	0	0	0	0	0	0	0	0
-5	0	0	0	0	0	0	0	0	0	0	0	0	0	0
0	0	0	0	0	0	0	0	0	0	0	0	0	0	0
5	0	0	0	0	0	0	0	0	0	0	0	0	0	0
10	0	0	0	0	0	0	0	0	0	0	0	0	0	0
15	0	0	0	0	0	0	0	0	0	0	0	0	0	0
20	0	0	0	0	0	0	0	0	0	0	0	0	0	0
25	0	0	0	0	0	0	0	0	0	0	0	0	0	0
30	0	0	0	0	0	0	0	0	0	0	0	0	0	0
35	0	0	0	0	0	0	0	0	0	0	0	0	0	0
40	0	0	0	0	0	0	0	0	0	0	0	0	0	0
45	0	0	0	0	0	0	0	0	0	0	0	0	0	0
50	0	0	0	0	0	0	0	0	0	0	0	0	0	0
55	0	0	0	0	0	0	0	0	0	0	0	0	0	0
60	0	0	0	0	0	0	0	0	0	0	0	0	0	0
65	0	0	0	0	0	0	0	0	0	0	0	0	0	0
70	0	0	0	0	0	0	0	0	0	0	0	0	0	0
75	0	0	0	0	0	0	0	0	0	0	0	0	0	0
80	0	0	0	0	0	0	0	0	0	0	0	0	0	0
85	0	0	0	0	0	0	0	0	0	0	0	0	0	0
90	0	0	0	0	0	0	0	0	0	0	0	0	0	0

Table A7
Case Counts for 3.0 m ≤ H_{mo} < 3.5 m

θ_0 (deg)	f_p (Hz)														
	0.044	0.054	0.064	0.074	0.084	0.093	0.103	0.113	0.123	0.132	0.142	0.152	0.162	0.171	0.181
-90	0	0	0	0	0	0	0	0	0	0	0	0	0	0	0
-85	0	0	0	0	0	0	0	0	0	0	0	0	0	0	0
-80	0	0	0	0	0	0	0	0	0	0	0	0	0	0	0
-75	0	0	0	0	0	0	0	0	0	0	0	0	0	0	0
-70	0	0	0	0	0	0	0	0	0	0	0	0	0	0	0
-65	0	0	0	0	0	0	0	0	0	0	0	0	0	0	0
-60	0	0	0	0	0	0	0	0	0	0	0	0	0	0	0
-55	0	0	0	0	0	0	0	0	0	0	0	0	0	0	0
-50	0	0	0	0	0	0	0	0	0	0	0	0	0	0	0
-45	0	0	0	0	0	0	0	0	0	0	0	0	0	0	0
-40	0	0	0	0	0	0	0	0	0	0	0	0	0	0	0
-35	0	0	0	0	0	0	0	0	0	0	0	0	0	0	0
-30	0	0	0	0	0	0	0	0	1	0	0	0	0	0	0
-25	0	0	0	0	3	3	1	2	0	0	0	0	0	0	0
-20	0	0	0	0	0	1	3	1	0	0	0	0	0	0	0
-15	0	0	1	5	1	5	4	0	0	0	0	0	0	0	0
-10	0	0	0	2	1	3	1	0	0	0	0	0	0	0	0
-5	0	1	2	0	4	1	2	1	0	0	0	0	0	0	0
0	0	0	0	13	1	4	0	1	0	0	0	0	0	0	0
5	0	0	0	1	2	8	4	1	0	0	0	0	0	0	0
10	0	0	0	0	0	1	4	2	0	0	0	0	0	0	0
15	0	0	0	0	0	0	0	1	0	0	0	0	0	0	0
20	0	0	0	0	0	0	0	0	0	1	0	0	0	0	0
25	0	0	0	0	0	0	0	0	0	0	0	0	0	0	0
30	0	0	0	0	0	0	0	0	0	0	0	0	0	0	0
35	0	0	0	0	0	0	0	0	0	0	0	0	0	0	0
40	0	0	0	0	0	0	0	0	0	0	0	0	0	0	0
45	0	0	0	0	0	0	0	0	0	0	0	0	0	0	0
50	0	0	0	0	0	0	0	0	0	0	0	0	0	0	0
55	0	0	0	0	0	0	0	0	0	0	0	0	0	0	0
60	0	0	0	0	0	0	0	0	0	0	0	0	0	0	0
65	0	0	0	0	0	0	0	0	0	0	0	0	0	0	0
70	0	0	0	0	0	0	0	0	0	0	0	0	0	0	0
75	0	0	0	0	0	0	0	0	0	0	0	0	0	0	0
80	0	0	0	0	0	0	0	0	0	0	0	0	0	0	0
85	0	0	0	0	0	0	0	0	0	0	0	0	0	0	0
90	0	0	0	0	0	0	0	0	0	0	0	0	0	0	0

(Continued)

Table A7 (Concluded)

θ_0 (deg)	f_p (Hz)													
	0.191	0.201	0.210	0.220	0.230	0.240	0.250	0.259	0.269	0.279	0.289	0.298	0.308	0.318
-90	0	0	0	0	0	0	0	0	0	0	0	0	0	0
-85	0	0	0	0	0	0	0	0	0	0	0	0	0	0
-80	0	0	0	0	0	0	0	0	0	0	0	0	0	0
-75	0	0	0	0	0	0	0	0	0	0	0	0	0	0
-70	0	0	0	0	0	0	0	0	0	0	0	0	0	0
-65	0	0	0	0	0	0	0	0	0	0	0	0	0	0
-60	0	0	0	0	0	0	0	0	0	0	0	0	0	0
-55	0	0	0	0	0	0	0	0	0	0	0	0	0	0
-50	0	0	0	0	0	0	0	0	0	0	0	0	0	0
-45	0	0	0	0	0	0	0	0	0	0	0	0	0	0
-40	0	0	0	0	0	0	0	0	0	0	0	0	0	0
-35	0	0	0	0	0	0	0	0	0	0	0	0	0	0
-30	0	0	0	0	0	0	0	0	0	0	0	0	0	0
-25	0	0	0	0	0	0	0	0	0	0	0	0	0	0
-20	0	0	0	0	0	0	0	0	0	0	0	0	0	0
-15	0	0	0	0	0	0	0	0	0	0	0	0	0	0
-10	0	0	0	0	0	0	0	0	0	0	0	0	0	0
-5	0	0	0	0	0	0	0	0	0	0	0	0	0	0
0	0	0	0	0	0	0	0	0	0	0	0	0	0	0
5	0	0	0	0	0	0	0	0	0	0	0	0	0	0
10	0	0	0	0	0	0	0	0	0	0	0	0	0	0
15	0	0	0	0	0	0	0	0	0	0	0	0	0	0
20	0	0	0	0	0	0	0	0	0	0	0	0	0	0
25	0	0	0	0	0	0	0	0	0	0	0	0	0	0
30	0	0	0	0	0	0	0	0	0	0	0	0	0	0
35	0	0	0	0	0	0	0	0	0	0	0	0	0	0
40	0	0	0	0	0	0	0	0	0	0	0	0	0	0
45	0	0	0	0	0	0	0	0	0	0	0	0	0	0
50	0	0	0	0	0	0	0	0	0	0	0	0	0	0
55	0	0	0	0	0	0	0	0	0	0	0	0	0	0
60	0	0	0	0	0	0	0	0	0	0	0	0	0	0
65	0	0	0	0	0	0	0	0	0	0	0	0	0	0
70	0	0	0	0	0	0	0	0	0	0	0	0	0	0
75	0	0	0	0	0	0	0	0	0	0	0	0	0	0
80	0	0	0	0	0	0	0	0	0	0	0	0	0	0
85	0	0	0	0	0	0	0	0	0	0	0	0	0	0
90	0	0	0	0	0	0	0	0	0	0	0	0	0	0

Table A8
Case Counts for 3.5 m ≤ H_{mo} < 4.0 m

θ_0 (deg)	f_p (Hz)														
	0.044	0.054	0.064	0.074	0.084	0.093	0.103	0.113	0.123	0.132	0.142	0.152	0.162	0.171	0.181
-90	0	0	0	0	0	0	0	0	0	0	0	0	0	0	0
-85	0	0	0	0	0	0	0	0	0	0	0	0	0	0	0
-80	0	0	0	0	0	0	0	0	0	0	0	0	0	0	0
-75	0	0	0	0	0	0	0	0	0	0	0	0	0	0	0
-70	0	0	0	0	0	0	0	0	0	0	0	0	0	0	0
-65	0	0	0	0	0	0	0	0	0	0	0	0	0	0	0
-60	0	0	0	0	0	0	0	0	0	0	0	0	0	0	0
-55	0	0	0	0	0	0	0	0	0	0	0	0	0	0	0
-50	0	0	0	0	0	0	0	0	0	0	0	0	0	0	0
-45	0	0	0	0	0	0	0	0	0	0	0	0	0	0	0
-40	0	0	0	0	0	0	0	0	0	0	0	0	0	0	0
-35	0	0	0	0	0	0	0	0	0	0	0	0	0	0	0
-30	0	0	0	0	0	0	0	0	0	0	0	0	0	0	0
-25	0	0	0	0	1	2	0	0	0	0	0	0	0	0	0
-20	0	0	1	1	5	0	0	0	0	0	0	0	0	0	0
-15	0	0	1	3	1	0	0	0	0	0	0	0	0	0	0
-10	0	0	1	4	2	3	2	0	0	0	0	0	0	0	0
-5	0	0	5	1	0	1	0	1	0	0	0	0	0	0	0
0	0	0	1	2	0	3	0	1	0	0	0	0	0	0	0
5	0	0	0	0	0	4	0	1	0	0	0	0	0	0	0
10	0	0	0	0	0	1	1	0	0	1	0	0	0	0	0
15	0	0	0	0	0	0	0	0	0	0	0	0	0	0	0
20	0	0	0	0	0	0	0	0	0	0	0	0	0	0	0
25	0	0	0	0	0	0	0	0	0	0	0	0	0	0	0
30	0	0	0	0	0	0	0	0	0	0	0	0	0	0	0
35	0	0	0	0	0	0	0	0	0	0	0	0	0	0	0
40	0	0	0	0	0	0	0	0	0	0	0	0	0	0	0
45	0	0	0	0	0	0	0	0	0	0	0	0	0	0	0
50	0	0	0	0	0	0	0	0	0	0	0	0	0	0	0
55	0	0	0	0	0	0	0	0	0	0	0	0	0	0	0
60	0	0	0	0	0	0	0	0	0	0	0	0	0	0	0
65	0	0	0	0	0	0	0	0	0	0	0	0	0	0	0
70	0	0	0	0	0	0	0	0	0	0	0	0	0	0	0
75	0	0	0	0	0	0	0	0	0	0	0	0	0	0	0
80	0	0	0	0	0	0	0	0	0	0	0	0	0	0	0
85	0	0	0	0	0	0	0	0	0	0	0	0	0	0	0
90	0	0	0	0	0	0	0	0	0	0	0	0	0	0	0

(Continued)

Table A8 (Concluded)

θ_0 (deg)	f_p (Hz)													
	0.191	0.201	0.210	0.220	0.230	0.240	0.250	0.259	0.269	0.279	0.289	0.298	0.308	0.318
-90	0	0	0	0	0	0	0	0	0	0	0	0	0	0
-85	0	0	0	0	0	0	0	0	0	0	0	0	0	0
-80	0	0	0	0	0	0	0	0	0	0	0	0	0	0
-75	0	0	0	0	0	0	0	0	0	0	0	0	0	0
-70	0	0	0	0	0	0	0	0	0	0	0	0	0	0
-65	0	0	0	0	0	0	0	0	0	0	0	0	0	0
-60	0	0	0	0	0	0	0	0	0	0	0	0	0	0
-55	0	0	0	0	0	0	0	0	0	0	0	0	0	0
-50	0	0	0	0	0	0	0	0	0	0	0	0	0	0
-45	0	0	0	0	0	0	0	0	0	0	0	0	0	0
-40	0	0	0	0	0	0	0	0	0	0	0	0	0	0
-35	0	0	0	0	0	0	0	0	0	0	0	0	0	0
-30	0	0	0	0	0	0	0	0	0	0	0	0	0	0
-25	0	0	0	0	0	0	0	0	0	0	0	0	0	0
-20	0	0	0	0	0	0	0	0	0	0	0	0	0	0
-15	0	0	0	0	0	0	0	0	0	0	0	0	0	0
-10	0	0	0	0	0	0	0	0	0	0	0	0	0	0
-5	0	0	0	0	0	0	0	0	0	0	0	0	0	0
0	0	0	0	0	0	0	0	0	0	0	0	0	0	0
5	0	0	0	0	0	0	0	0	0	0	0	0	0	0
10	0	0	0	0	0	0	0	0	0	0	0	0	0	0
15	0	0	0	0	0	0	0	0	0	0	0	0	0	0
20	0	0	0	0	0	0	0	0	0	0	0	0	0	0
25	0	0	0	0	0	0	0	0	0	0	0	0	0	0
30	0	0	0	0	0	0	0	0	0	0	0	0	0	0
35	0	0	0	0	0	0	0	0	0	0	0	0	0	0
40	0	0	0	0	0	0	0	0	0	0	0	0	0	0
45	0	0	0	0	0	0	0	0	0	0	0	0	0	0
50	0	0	0	0	0	0	0	0	0	0	0	0	0	0
55	0	0	0	0	0	0	0	0	0	0	0	0	0	0
60	0	0	0	0	0	0	0	0	0	0	0	0	0	0
65	0	0	0	0	0	0	0	0	0	0	0	0	0	0
70	0	0	0	0	0	0	0	0	0	0	0	0	0	0
75	0	0	0	0	0	0	0	0	0	0	0	0	0	0
80	0	0	0	0	0	0	0	0	0	0	0	0	0	0
85	0	0	0	0	0	0	0	0	0	0	0	0	0	0
90	0	0	0	0	0	0	0	0	0	0	0	0	0	0

Table A9
Case Counts for 4.0 m ≤ H_{mo} < 4.5 m

θ_0 (deg)	f_p (Hz)														
	0.044	0.054	0.064	0.074	0.084	0.093	0.103	0.113	0.123	0.132	0.142	0.152	0.162	0.171	0.181
-90	0	0	0	0	0	0	0	0	0	0	0	0	0	0	0
-85	0	0	0	0	0	0	0	0	0	0	0	0	0	0	0
-80	0	0	0	0	0	0	0	0	0	0	0	0	0	0	0
-75	0	0	0	0	0	0	0	0	0	0	0	0	0	0	0
-70	0	0	0	0	0	0	0	0	0	0	0	0	0	0	0
-65	0	0	0	0	0	0	0	0	0	0	0	0	0	0	0
-60	0	0	0	0	0	0	0	0	0	0	0	0	0	0	0
-55	0	0	0	0	0	0	0	0	0	0	0	0	0	0	0
-50	0	0	0	0	0	0	0	0	0	0	0	0	0	0	0
-45	0	0	0	0	0	0	0	0	0	0	0	0	0	0	0
-40	0	0	0	0	0	0	0	0	0	0	0	0	0	0	0
-35	0	0	0	0	0	0	0	0	0	0	0	0	0	0	0
-30	0	0	0	0	0	0	0	0	0	0	0	0	0	0	0
-25	0	0	0	0	0	0	0	0	0	0	0	0	0	0	0
-20	0	0	0	1	0	0	0	0	0	0	0	0	0	0	0
-15	0	0	1	3	0	0	0	0	0	0	0	0	0	0	0
-10	0	0	0	7	1	0	0	0	0	0	0	0	0	0	0
-5	0	0	5	1	1	1	0	0	0	0	0	0	0	0	0
0	0	0	1	0	0	1	0	0	0	0	0	0	0	0	0
5	0	0	0	0	0	0	0	0	0	0	0	0	0	0	0
10	0	0	0	0	0	0	1	0	0	0	0	0	0	0	0
15	0	0	0	0	0	0	0	0	0	0	0	0	0	0	0
20	0	0	0	0	0	0	0	0	0	0	0	0	0	0	0
25	0	0	0	0	0	0	0	0	0	0	0	0	0	0	0
30	0	0	0	0	0	0	0	0	0	0	0	0	0	0	0
35	0	0	0	0	0	0	0	0	0	0	0	0	0	0	0
40	0	0	0	0	0	0	0	0	0	0	0	0	0	0	0
45	0	0	0	0	0	0	0	0	0	0	0	0	0	0	0
50	0	0	0	0	0	0	0	0	0	0	0	0	0	0	0
55	0	0	0	0	0	0	0	0	0	0	0	0	0	0	0
60	0	0	0	0	0	0	0	0	0	0	0	0	0	0	0
65	0	0	0	0	0	0	0	0	0	0	0	0	0	0	0
70	0	0	0	0	0	0	0	0	0	0	0	0	0	0	0
75	0	0	0	0	0	0	0	0	0	0	0	0	0	0	0
80	0	0	0	0	0	0	0	0	0	0	0	0	0	0	0
85	0	0	0	0	0	0	0	0	0	0	0	0	0	0	0
90	0	0	0	0	0	0	0	0	0	0	0	0	0	0	0

(Continued)

Table A9 (Concluded)

θ_0 (deg)	f_p (Hz)													
	0.191	0.201	0.210	0.220	0.230	0.240	0.250	0.259	0.269	0.279	0.289	0.298	0.308	0.318
-90	0	0	0	0	0	0	0	0	0	0	0	0	0	0
-85	0	0	0	0	0	0	0	0	0	0	0	0	0	0
-80	0	0	0	0	0	0	0	0	0	0	0	0	0	0
-75	0	0	0	0	0	0	0	0	0	0	0	0	0	0
-70	0	0	0	0	0	0	0	0	0	0	0	0	0	0
-65	0	0	0	0	0	0	0	0	0	0	0	0	0	0
-60	0	0	0	0	0	0	0	0	0	0	0	0	0	0
-55	0	0	0	0	0	0	0	0	0	0	0	0	0	0
-50	0	0	0	0	0	0	0	0	0	0	0	0	0	0
-45	0	0	0	0	0	0	0	0	0	0	0	0	0	0
-40	0	0	0	0	0	0	0	0	0	0	0	0	0	0
-35	0	0	0	0	0	0	0	0	0	0	0	0	0	0
-30	0	0	0	0	0	0	0	0	0	0	0	0	0	0
-25	0	0	0	0	0	0	0	0	0	0	0	0	0	0
-20	0	0	0	0	0	0	0	0	0	0	0	0	0	0
-15	0	0	0	0	0	0	0	0	0	0	0	0	0	0
-10	0	0	0	0	0	0	0	0	0	0	0	0	0	0
-5	0	0	0	0	0	0	0	0	0	0	0	0	0	0
0	0	0	0	0	0	0	0	0	0	0	0	0	0	0
5	0	0	0	0	0	0	0	0	0	0	0	0	0	0
10	0	0	0	0	0	0	0	0	0	0	0	0	0	0
15	0	0	0	0	0	0	0	0	0	0	0	0	0	0
20	0	0	0	0	0	0	0	0	0	0	0	0	0	0
25	0	0	0	0	0	0	0	0	0	0	0	0	0	0
30	0	0	0	0	0	0	0	0	0	0	0	0	0	0
35	0	0	0	0	0	0	0	0	0	0	0	0	0	0
40	0	0	0	0	0	0	0	0	0	0	0	0	0	0
45	0	0	0	0	0	0	0	0	0	0	0	0	0	0
50	0	0	0	0	0	0	0	0	0	0	0	0	0	0
55	0	0	0	0	0	0	0	0	0	0	0	0	0	0
60	0	0	0	0	0	0	0	0	0	0	0	0	0	0
65	0	0	0	0	0	0	0	0	0	0	0	0	0	0
70	0	0	0	0	0	0	0	0	0	0	0	0	0	0
75	0	0	0	0	0	0	0	0	0	0	0	0	0	0
80	0	0	0	0	0	0	0	0	0	0	0	0	0	0
85	0	0	0	0	0	0	0	0	0	0	0	0	0	0
90	0	0	0	0	0	0	0	0	0	0	0	0	0	0

Table A10
Case Counts for 4.5 m ≤ H_{mo} < 5.0 m

θ_0 (deg)	f_p (Hz)														
	0.044	0.054	0.064	0.074	0.084	0.093	0.103	0.113	0.123	0.132	0.142	0.152	0.162	0.171	0.181
-90	0	0	0	0	0	0	0	0	0	0	0	0	0	0	0
-85	0	0	0	0	0	0	0	0	0	0	0	0	0	0	0
-80	0	0	0	0	0	0	0	0	0	0	0	0	0	0	0
-75	0	0	0	0	0	0	0	0	0	0	0	0	0	0	0
-70	0	0	0	0	0	0	0	0	0	0	0	0	0	0	0
-65	0	0	0	0	0	0	0	0	0	0	0	0	0	0	0
-60	0	0	0	0	0	0	0	0	0	0	0	0	0	0	0
-55	0	0	0	0	0	0	0	0	0	0	0	0	0	0	0
-50	0	0	0	0	0	0	0	0	0	0	0	0	0	0	0
-45	0	0	0	0	0	0	0	0	0	0	0	0	0	0	0
-40	0	0	0	0	0	0	0	0	0	0	0	0	0	0	0
-35	0	0	0	0	0	0	0	0	0	0	0	0	0	0	0
-30	0	0	0	0	0	0	0	0	0	0	0	0	0	0	0
-25	0	0	0	0	0	0	0	0	0	0	0	0	0	0	0
-20	0	0	0	0	0	0	0	0	0	0	0	0	0	0	0
-15	0	0	0	0	0	0	0	0	0	0	0	0	0	0	0
-10	0	0	1	0	0	0	0	0	0	0	0	0	0	0	0
-5	0	0	0	0	0	0	0	0	0	0	0	0	0	0	0
0	0	0	0	0	0	0	0	0	0	0	0	0	0	0	0
5	0	0	0	0	0	0	0	0	0	0	0	0	0	0	0
10	0	0	0	0	0	0	0	0	0	0	0	0	0	0	0
15	0	0	0	0	0	0	0	0	0	0	0	0	0	0	0
20	0	0	0	0	0	0	0	0	0	0	0	0	0	0	0
25	0	0	0	0	0	0	0	0	0	0	0	0	0	0	0
30	0	0	0	0	0	0	0	0	0	0	0	0	0	0	0
35	0	0	0	0	0	0	0	0	0	0	0	0	0	0	0
40	0	0	0	0	0	0	0	0	0	0	0	0	0	0	0
45	0	0	0	0	0	0	0	0	0	0	0	0	0	0	0
50	0	0	0	0	0	0	0	0	0	0	0	0	0	0	0
55	0	0	0	0	0	0	0	0	0	0	0	0	0	0	0
60	0	0	0	0	0	0	0	0	0	0	0	0	0	0	0
65	0	0	0	0	0	0	0	0	0	0	0	0	0	0	0
70	0	0	0	0	0	0	0	0	0	0	0	0	0	0	0
75	0	0	0	0	0	0	0	0	0	0	0	0	0	0	0
80	0	0	0	0	0	0	0	0	0	0	0	0	0	0	0
85	0	0	0	0	0	0	0	0	0	0	0	0	0	0	0
90	0	0	0	0	0	0	0	0	0	0	0	0	0	0	0

(Continued)

Table A10 (Concluded)

θ_0 (deg)	f_p (Hz)													
	0.191	0.201	0.210	0.220	0.230	0.240	0.250	0.259	0.269	0.279	0.289	0.298	0.308	0.318
-90	0	0	0	0	0	0	0	0	0	0	0	0	0	0
-85	0	0	0	0	0	0	0	0	0	0	0	0	0	0
-80	0	0	0	0	0	0	0	0	0	0	0	0	0	0
-75	0	0	0	0	0	0	0	0	0	0	0	0	0	0
-70	0	0	0	0	0	0	0	0	0	0	0	0	0	0
-65	0	0	0	0	0	0	0	0	0	0	0	0	0	0
-60	0	0	0	0	0	0	0	0	0	0	0	0	0	0
-55	0	0	0	0	0	0	0	0	0	0	0	0	0	0
-50	0	0	0	0	0	0	0	0	0	0	0	0	0	0
-45	0	0	0	0	0	0	0	0	0	0	0	0	0	0
-40	0	0	0	0	0	0	0	0	0	0	0	0	0	0
-35	0	0	0	0	0	0	0	0	0	0	0	0	0	0
-30	0	0	0	0	0	0	0	0	0	0	0	0	0	0
-25	0	0	0	0	0	0	0	0	0	0	0	0	0	0
-20	0	0	0	0	0	0	0	0	0	0	0	0	0	0
-15	0	0	0	0	0	0	0	0	0	0	0	0	0	0
-10	0	0	0	0	0	0	0	0	0	0	0	0	0	0
-5	0	0	0	0	0	0	0	0	0	0	0	0	0	0
0	0	0	0	0	0	0	0	0	0	0	0	0	0	0
5	0	0	0	0	0	0	0	0	0	0	0	0	0	0
10	0	0	0	0	0	0	0	0	0	0	0	0	0	0
15	0	0	0	0	0	0	0	0	0	0	0	0	0	0
20	0	0	0	0	0	0	0	0	0	0	0	0	0	0
25	0	0	0	0	0	0	0	0	0	0	0	0	0	0
30	0	0	0	0	0	0	0	0	0	0	0	0	0	0
35	0	0	0	0	0	0	0	0	0	0	0	0	0	0
40	0	0	0	0	0	0	0	0	0	0	0	0	0	0
45	0	0	0	0	0	0	0	0	0	0	0	0	0	0
50	0	0	0	0	0	0	0	0	0	0	0	0	0	0
55	0	0	0	0	0	0	0	0	0	0	0	0	0	0
60	0	0	0	0	0	0	0	0	0	0	0	0	0	0
65	0	0	0	0	0	0	0	0	0	0	0	0	0	0
70	0	0	0	0	0	0	0	0	0	0	0	0	0	0
75	0	0	0	0	0	0	0	0	0	0	0	0	0	0
80	0	0	0	0	0	0	0	0	0	0	0	0	0	0
85	0	0	0	0	0	0	0	0	0	0	0	0	0	0
90	0	0	0	0	0	0	0	0	0	0	0	0	0	0

Table A11
Case Counts for 5.0 m ≤ H_{mo} < 5.5 m

θ_0 (deg)	f_p (Hz)														
	0.044	0.054	0.064	0.074	0.084	0.093	0.103	0.113	0.123	0.132	0.142	0.152	0.162	0.171	0.181
-90	0	0	0	0	0	0	0	0	0	0	0	0	0	0	0
-85	0	0	0	0	0	0	0	0	0	0	0	0	0	0	0
-80	0	0	0	0	0	0	0	0	0	0	0	0	0	0	0
-75	0	0	0	0	0	0	0	0	0	0	0	0	0	0	0
-70	0	0	0	0	0	0	0	0	0	0	0	0	0	0	0
-65	0	0	0	0	0	0	0	0	0	0	0	0	0	0	0
-60	0	0	0	0	0	0	0	0	0	0	0	0	0	0	0
-55	0	0	0	0	0	0	0	0	0	0	0	0	0	0	0
-50	0	0	0	0	0	0	0	0	0	0	0	0	0	0	0
-45	0	0	0	0	0	0	0	0	0	0	0	0	0	0	0
-40	0	0	0	0	0	0	0	0	0	0	0	0	0	0	0
-35	0	0	0	0	0	0	0	0	0	0	0	0	0	0	0
-30	0	0	0	0	0	0	0	0	0	0	0	0	0	0	0
-25	0	0	0	0	0	0	0	0	0	0	0	0	0	0	0
-20	0	0	0	0	0	0	0	0	0	0	0	0	0	0	0
-15	0	0	0	0	0	0	0	0	0	0	0	0	0	0	0
-10	0	0	0	2	0	0	0	0	0	0	0	0	0	0	0
-5	0	0	0	0	0	0	0	0	0	0	0	0	0	0	0
0	0	0	0	0	0	0	0	0	0	0	0	0	0	0	0
5	0	0	0	0	0	0	0	0	0	0	0	0	0	0	0
10	0	0	0	0	0	0	0	0	0	0	0	0	0	0	0
15	0	0	0	0	0	0	0	0	0	0	0	0	0	0	0
20	0	0	0	0	0	0	0	0	0	0	0	0	0	0	0
25	0	0	0	0	0	0	0	0	0	0	0	0	0	0	0
30	0	0	0	0	0	0	0	0	0	0	0	0	0	0	0
35	0	0	0	0	0	0	0	0	0	0	0	0	0	0	0
40	0	0	0	0	0	0	0	0	0	0	0	0	0	0	0
45	0	0	0	0	0	0	0	0	0	0	0	0	0	0	0
50	0	0	0	0	0	0	0	0	0	0	0	0	0	0	0
55	0	0	0	0	0	0	0	0	0	0	0	0	0	0	0
60	0	0	0	0	0	0	0	0	0	0	0	0	0	0	0
65	0	0	0	0	0	0	0	0	0	0	0	0	0	0	0
70	0	0	0	0	0	0	0	0	0	0	0	0	0	0	0
75	0	0	0	0	0	0	0	0	0	0	0	0	0	0	0
80	0	0	0	0	0	0	0	0	0	0	0	0	0	0	0
85	0	0	0	0	0	0	0	0	0	0	0	0	0	0	0
90	0	0	0	0	0	0	0	0	0	0	0	0	0	0	0

(Continued)

Table A11 (Concluded)

θ_0 (deg)	f_p (Hz)													
	0.191	0.201	0.210	0.220	0.230	0.240	0.250	0.259	0.269	0.279	0.289	0.298	0.308	0.318
-90	0	0	0	0	0	0	0	0	0	0	0	0	0	0
-85	0	0	0	0	0	0	0	0	0	0	0	0	0	0
-80	0	0	0	0	0	0	0	0	0	0	0	0	0	0
-75	0	0	0	0	0	0	0	0	0	0	0	0	0	0
-70	0	0	0	0	0	0	0	0	0	0	0	0	0	0
-65	0	0	0	0	0	0	0	0	0	0	0	0	0	0
-60	0	0	0	0	0	0	0	0	0	0	0	0	0	0
-55	0	0	0	0	0	0	0	0	0	0	0	0	0	0
-50	0	0	0	0	0	0	0	0	0	0	0	0	0	0
-45	0	0	0	0	0	0	0	0	0	0	0	0	0	0
-40	0	0	0	0	0	0	0	0	0	0	0	0	0	0
-35	0	0	0	0	0	0	0	0	0	0	0	0	0	0
-30	0	0	0	0	0	0	0	0	0	0	0	0	0	0
-25	0	0	0	0	0	0	0	0	0	0	0	0	0	0
-20	0	0	0	0	0	0	0	0	0	0	0	0	0	0
-15	0	0	0	0	0	0	0	0	0	0	0	0	0	0
-10	0	0	0	0	0	0	0	0	0	0	0	0	0	0
-5	0	0	0	0	0	0	0	0	0	0	0	0	0	0
0	0	0	0	0	0	0	0	0	0	0	0	0	0	0
5	0	0	0	0	0	0	0	0	0	0	0	0	0	0
10	0	0	0	0	0	0	0	0	0	0	0	0	0	0
15	0	0	0	0	0	0	0	0	0	0	0	0	0	0
20	0	0	0	0	0	0	0	0	0	0	0	0	0	0
25	0	0	0	0	0	0	0	0	0	0	0	0	0	0
30	0	0	0	0	0	0	0	0	0	0	0	0	0	0
35	0	0	0	0	0	0	0	0	0	0	0	0	0	0
40	0	0	0	0	0	0	0	0	0	0	0	0	0	0
45	0	0	0	0	0	0	0	0	0	0	0	0	0	0
50	0	0	0	0	0	0	0	0	0	0	0	0	0	0
55	0	0	0	0	0	0	0	0	0	0	0	0	0	0
60	0	0	0	0	0	0	0	0	0	0	0	0	0	0
65	0	0	0	0	0	0	0	0	0	0	0	0	0	0
70	0	0	0	0	0	0	0	0	0	0	0	0	0	0
75	0	0	0	0	0	0	0	0	0	0	0	0	0	0
80	0	0	0	0	0	0	0	0	0	0	0	0	0	0
85	0	0	0	0	0	0	0	0	0	0	0	0	0	0
90	0	0	0	0	0	0	0	0	0	0	0	0	0	0

Appendix B
Case Counts for Harvest Platform

Tables B1 through B11 contain fundamental information for constructing discrete joint probability density or percent occurrence functions from the N = 7,066 observations used in this study from the Harvest Platform directional wave gauge. A table entry is the number of observed cases having characteristic wave heights H_{mo}, peak frequencies f_p, and mean wave directions θ_0 within cells defined by ranges of height, frequency, and direction. Each table contains all information for cases with wave heights within a range ΔH = 0.5 m. Table columns are identified with center frequencies of cells having a frequency range Δf = 0.00977 Hz. Rows are labeled with center directions of cells with direction ranges $\Delta\theta$ = 5 deg.

Case counts are listed for simplicity of format. If all entries from all tables are summed, the result is simply N. To convert an entry to percent occurrence of cases in its height-frequency-direction cell, the entry number should be multiplied by 100 percent and divided by N, which is equivalent to multiplying the entry by 0.0142 percent. If all entries from all tables are thus normalized and then summed, the result is 100 percent. To convert an entry to the form of a discrete joint probability density, the entry number should be divided by the product $N\Delta H\Delta f\Delta\theta$, which is equivalent to multiplying the entry by the factor 0.00580 m^{-1} Hz^{-1} deg^{-1}. If all entries from all tables in this appendix are thus normalized, the result is the complete discrete approximation of the joint height-frequency-direction probability density function discussed in the body of this report for Harvest Platform.

Table B1
Case Counts for 0.5 m ≤ H_{mo} < 1.0 m

θ_0 (deg)	f_p (Hz)												
	0.044	0.054	0.064	0.074	0.084	0.093	0.103	0.113	0.123	0.132	0.142	0.152	0.162
-180	0	0	1	4	0	0	0	0	0	0	0	0	0
-175	0	0	0	0	0	0	0	0	0	0	0	0	0
-170	0	0	0	0	0	0	0	0	0	0	0	0	0
-165	0	0	0	0	0	0	0	0	0	0	0	0	0
-160	0	0	0	0	0	0	0	0	0	0	0	0	0
-155	0	0	0	0	0	0	0	0	0	0	0	0	0
-150	0	0	0	0	0	0	0	0	0	0	0	0	0
-145	0	0	0	0	0	0	0	0	0	0	0	0	0
-140	0	0	0	0	0	0	0	0	0	0	0	0	0
-135	0	0	0	0	0	0	0	0	0	0	0	0	0
-130	0	0	0	0	0	0	0	0	0	0	0	0	0
-125	0	0	0	0	0	0	0	0	0	0	0	0	0
-120	0	0	0	0	0	0	0	0	0	0	0	0	0
-115	0	0	0	0	0	0	0	0	0	0	0	0	0
-110	0	0	0	0	0	0	0	0	0	0	0	0	0
-105	0	0	0	0	0	0	0	0	0	0	0	0	0
-100	0	0	0	0	0	0	0	0	0	0	0	0	0
-95	0	0	0	0	0	0	0	0	0	0	0	0	0
-90	0	0	0	0	0	0	0	0	0	0	0	0	0
-85	0	0	0	0	0	0	0	0	0	0	0	0	0
-80	0	0	0	0	0	0	0	0	0	0	0	0	0
-75	0	0	0	0	0	0	0	0	0	0	0	0	0
-70	0	0	0	0	0	0	0	0	0	0	0	0	0
-65	0	0	0	0	0	0	0	0	0	0	0	0	0
-60	0	0	0	0	0	0	0	0	0	0	0	0	0
-55	0	0	0	0	0	0	0	0	0	0	0	0	0
-50	0	0	0	0	0	0	0	0	0	0	0	0	0
-45	0	0	0	0	0	0	0	0	0	0	0	0	0
-40	0	0	0	0	0	0	0	0	0	0	0	0	0
-35	0	0	0	0	0	0	0	0	0	0	0	0	0
-30	0	0	0	0	0	0	0	0	0	0	0	0	0
-25	0	0	0	0	0	0	0	0	0	0	0	0	0
-20	0	0	0	0	0	0	0	0	0	0	0	0	0
-15	0	0	0	0	0	0	0	0	0	0	0	0	0
-10	0	0	0	0	0	0	0	0	0	0	0	0	0
-5	0	0	0	0	0	0	0	0	0	0	0	0	0

(Continued)

Table B1 (Concluded)

θ_0 (deg)	f_p (Hz)												
	0.044	0.054	0.064	0.074	0.084	0.093	0.103	0.113	0.123	0.132	0.142	0.152	0.162
0	0	0	0	0	0	0	0	0	0	0	0	0	0
5	0	0	0	0	0	0	0	0	0	0	0	0	0
10	0	0	0	0	0	0	0	0	0	0	0	0	0
15	0	0	0	0	0	0	0	0	0	0	0	0	0
20	0	0	0	0	0	0	0	0	0	0	0	0	0
25	0	0	0	0	0	0	0	0	0	0	0	0	0
30	0	0	0	0	0	0	0	0	0	0	0	0	0
35	0	0	0	0	0	0	0	0	0	0	0	0	0
40	0	0	0	0	0	0	0	0	0	0	1	1	3
45	0	0	0	0	0	0	3	10	0	2	1	1	12
50	0	0	0	0	0	1	7	6	3	5	1	1	9
55	0	0	0	0	0	0	13	5	1	1	1	2	8
60	0	0	0	1	0	2	7	4	0	0	0	0	6
65	0	0	0	1	1	3	4	5	0	0	0	0	0
70	0	1	0	4	3	5	9	2	0	0	0	0	0
75	0	0	1	7	3	7	2	2	0	0	0	0	0
80	0	1	4	4	5	8	4	0	0	0	0	0	0
85	0	0	1	3	4	5	1	0	0	0	0	0	0
90	0	0	0	1	5	2	1	0	0	0	0	0	0
95	0	0	0	0	4	3	1	0	0	0	0	0	0
100	0	0	1	3	3	3	0	0	0	0	0	0	0
105	0	0	0	0	4	3	0	0	0	0	0	0	0
110	0	0	0	0	4	0	1	0	0	0	0	0	0
115	0	0	0	4	1	0	0	0	0	0	0	0	0
120	0	0	0	1	3	0	0	0	0	0	0	0	0
125	0	0	1	3	0	1	0	0	0	0	0	0	0
130	0	0	0	2	2	0	0	0	0	0	0	0	0
135	0	0	1	6	0	1	0	0	0	0	0	0	0
140	0	0	2	2	0	0	0	0	0	0	0	0	0
145	0	0	5	6	0	0	0	0	0	0	0	0	0
150	0	0	9	6	1	1	0	0	0	0	0	0	0
155	0	2	14	11	3	0	0	0	0	0	0	0	0
160	0	5	6	14	1	1	0	0	0	0	0	0	0
165	0	1	7	4	0	0	0	0	0	0	0	0	0
170	0	0	0	7	0	0	0	0	0	0	0	0	0
175	0	0	3	9	0	0	0	0	0	0	0	0	0
180	0	0	1	4	0	0	0	0	0	0	0	0	0

Table B2
Case Counts for 1.0 m ≤ H_{mo} < 1.5 m

θ_0 (deg)	f_p (Hz)												
	0.044	0.054	0.064	0.074	0.084	0.093	0.103	0.113	0.123	0.132	0.142	0.152	0.162
-180	0	0	1	1	4	0	0	0	0	0	0	0	0
-175	0	0	0	0	0	0	0	0	0	0	0	0	0
-170	0	0	0	0	0	0	0	0	0	0	0	0	0
-165	0	0	0	0	0	0	0	0	0	0	0	0	0
-160	0	0	0	0	0	0	0	0	0	0	0	0	0
-155	0	0	0	0	0	0	0	0	0	0	0	0	0
-150	0	0	0	0	0	0	0	0	0	0	0	0	0
-145	0	0	0	0	0	0	0	0	0	0	0	0	0
-140	0	0	0	0	0	0	0	0	0	0	0	0	0
-135	0	0	0	0	0	0	0	0	0	0	0	0	0
-130	0	0	0	0	0	0	0	0	0	0	0	0	0
-125	0	0	0	0	0	0	0	0	0	0	0	0	1
-120	0	0	0	0	0	0	0	0	0	0	0	0	0
-115	0	0	0	0	0	0	0	0	0	0	0	0	0
-110	0	0	0	0	0	0	0	0	0	0	0	0	0
-105	0	0	0	0	0	0	0	0	0	0	0	0	0
-100	0	0	0	0	0	0	0	0	0	0	0	0	0
-95	0	0	0	0	0	0	0	0	0	0	0	0	0
-90	0	0	0	0	0	0	0	0	0	0	0	0	0
-85	0	0	0	0	0	0	0	0	0	0	0	0	0
-80	0	0	0	0	0	0	0	0	0	0	0	0	0
-75	0	0	0	0	0	0	0	0	0	0	0	0	0
-70	0	0	0	0	0	0	0	0	0	0	0	0	0
-65	0	0	0	0	0	0	0	0	0	0	0	0	0
-60	0	0	0	0	0	0	0	0	0	0	0	0	0
-55	0	0	0	0	0	0	0	0	0	0	0	0	0
-50	0	0	0	0	0	0	0	0	0	0	0	0	0
-45	0	0	0	0	0	0	0	0	0	0	0	0	0
-40	0	0	0	0	0	0	0	0	0	0	0	0	0
-35	0	0	0	0	0	0	0	0	0	0	0	0	0
-30	0	0	0	0	0	0	0	0	0	0	0	0	0
-25	0	0	0	0	0	0	0	0	0	0	0	0	0
-20	0	0	0	0	0	0	0	0	0	0	0	0	0
-15	0	0	0	0	0	0	0	0	0	0	0	0	0
-10	0	0	0	0	0	0	0	0	0	0	0	0	0
-5	0	0	0	0	0	0	0	0	0	0	0	0	0

(Continued)

Table B2 (Concluded)

θ_0 (deg)	f_p (Hz)												
	0.044	0.054	0.064	0.074	0.084	0.093	0.103	0.113	0.123	0.132	0.142	0.152	0.162
0	0	0	0	0	0	0	0	0	0	0	0	0	0
5	0	0	0	0	0	0	0	0	0	0	0	0	0
10	0	0	0	0	0	0	0	0	0	0	0	0	0
15	0	0	0	0	0	0	0	0	0	0	0	0	0
20	0	0	0	0	0	0	0	0	0	0	0	0	0
25	0	0	0	0	0	0	0	0	0	0	0	0	0
30	0	0	0	0	0	0	0	0	0	0	0	0	0
35	0	0	0	0	0	0	0	0	0	0	0	0	4
40	0	0	0	0	0	0	2	4	1	1	1	12	15
45	0	0	0	0	0	1	15	31	8	3	7	14	29
50	0	0	0	0	1	15	52	42	23	20	24	16	30
55	0	0	1	2	9	27	48	31	24	27	30	26	37
60	0	2	0	8	29	28	26	6	12	14	8	7	12
65	0	0	3	11	43	23	18	9	4	6	3	7	5
70	0	11	9	12	31	32	11	2	3	0	3	0	2
75	0	1	14	18	28	23	10	1	0	0	1	3	0
80	1	5	11	27	20	15	2	0	0	0	0	0	0
85	0	7	13	28	22	2	1	1	1	0	0	0	1
90	0	1	12	33	14	2	1	0	0	1	0	0	0
95	0	0	9	26	15	2	1	1	0	0	0	0	1
100	0	1	7	11	8	6	4	0	0	1	0	0	0
105	0	0	7	12	6	3	0	1	1	0	0	0	0
110	0	0	3	12	1	1	0	0	1	0	0	0	0
115	0	0	5	12	2	0	0	0	0	0	0	0	0
120	0	0	2	10	0	0	0	0	0	0	0	0	0
125	0	0	3	9	2	0	0	0	0	0	1	0	0
130	0	0	3	4	0	1	0	0	0	0	0	0	0
135	0	0	2	2	1	1	0	0	0	0	0	0	0
140	0	0	6	4	0	1	0	0	0	0	0	0	0
145	0	2	8	4	1	0	0	0	0	0	0	0	0
150	0	4	15	10	0	0	2	0	0	0	0	0	0
155	0	1	24	15	0	0	0	0	0	0	0	0	0
160	0	1	39	10	0	0	2	0	0	0	0	0	0
165	0	7	28	19	0	4	0	0	0	0	0	0	0
170	0	1	19	3	2	0	0	0	0	1	0	0	0
175	0	1	9	1	2	2	0	0	1	0	0	0	0
180	0	0	1	1	4	0	0	0	0	0	0	0	0

Table B3
Case Counts for 1.5 m ≤ H_{mo} < 2.0 m

θ_0 (deg)	f_p (Hz)												
	0.044	0.054	0.064	0.074	0.084	0.093	0.103	0.113	0.123	0.132	0.142	0.152	0.162
-180	0	1	0	0	0	0	0	0	1	0	0	0	0
-175	0	0	0	0	0	0	0	0	0	0	0	0	0
-170	0	0	0	0	0	0	0	0	0	0	0	0	0
-165	0	0	0	0	0	0	0	0	0	0	0	0	0
-160	0	0	0	0	0	0	0	0	0	0	0	0	0
-155	0	0	0	0	0	0	0	0	0	0	0	0	0
-150	0	0	0	0	0	0	0	0	0	0	0	0	0
-145	0	0	0	0	0	0	0	0	0	0	0	0	0
-140	0	0	0	0	0	0	0	0	0	0	0	0	0
-135	0	0	0	0	0	0	0	0	0	0	0	0	0
-130	0	0	0	0	0	0	0	0	0	0	0	0	0
-125	0	0	0	0	0	0	0	0	0	0	0	0	1
-120	0	0	0	0	0	0	0	0	0	0	0	0	2
-115	0	0	0	0	0	0	0	0	0	0	0	0	1
-110	0	0	0	0	0	0	0	0	0	0	0	0	0
-105	0	0	0	0	0	0	0	0	0	0	0	0	0
-100	0	0	0	0	0	0	0	0	0	0	0	0	0
-95	0	0	0	0	0	0	0	0	0	0	0	0	0
-90	0	0	0	0	0	0	0	0	0	0	0	0	0
-85	0	0	0	0	0	0	0	0	0	0	0	0	0
-80	0	0	0	0	0	0	0	0	0	0	0	0	0
-75	0	0	0	0	0	0	0	0	0	0	0	0	0
-70	0	0	0	0	0	0	0	0	0	0	0	0	0
-65	0	0	0	0	0	0	0	0	0	0	0	0	0
-60	0	0	0	0	0	0	0	0	0	0	0	0	0
-55	0	0	0	0	0	0	0	0	0	0	0	0	0
-50	0	0	0	0	0	0	0	0	0	0	0	0	0
-45	0	0	0	0	0	0	0	0	0	0	0	0	0
-40	0	0	0	0	0	0	0	0	0	0	0	0	0
-35	0	0	0	0	0	0	0	0	0	0	0	0	0
-30	0	0	0	0	0	0	0	0	0	0	0	0	0
-25	0	0	0	0	0	0	0	0	0	0	0	0	0
-20	0	0	0	0	0	0	0	0	0	0	0	0	0
-15	0	0	0	0	0	0	0	0	0	0	0	0	0
-10	0	0	0	0	0	0	0	0	0	0	0	0	0
-5	0	0	0	0	0	0	0	0	0	0	0	0	0

(Continued)

Table B3 (Concluded)

θ_0 (deg)	f_p (Hz)												
	0.044	0.054	0.064	0.074	0.084	0.093	0.103	0.113	0.123	0.132	0.142	0.152	0.162
0	0	0	0	0	0	0	0	0	0	0	0	0	0
5	0	0	0	0	0	0	0	0	0	0	0	0	0
10	0	0	0	0	0	0	0	0	0	0	0	0	0
15	0	0	0	0	0	0	0	0	0	0	0	0	0
20	0	0	0	0	0	0	0	0	0	0	0	0	0
25	0	0	0	0	0	0	0	0	0	0	0	0	0
30	0	0	0	0	0	0	0	0	0	0	0	0	0
35	0	0	0	0	0	0	1	0	1	0	1	0	1
40	0	0	0	0	0	3	6	6	3	2	4	4	2
45	0	0	0	0	0	11	41	24	14	31	25	8	11
50	0	0	1	0	12	41	48	49	53	66	47	20	12
55	0	0	2	6	37	47	25	29	43	61	21	14	7
60	0	0	7	22	47	43	21	8	19	20	12	2	0
65	0	1	10	45	38	33	13	4	4	3	4	0	0
70	0	11	13	43	59	14	6	4	2	3	1	0	0
75	1	7	26	55	40	13	5	2	0	1	0	0	1
80	0	7	20	44	39	6	12	3	0	0	0	0	0
85	0	1	21	55	24	7	5	0	0	0	0	0	0
90	0	1	15	25	5	1	0	2	0	0	0	0	0
95	0	0	7	17	5	2	0	1	0	0	0	0	0
100	0	0	5	13	0	6	2	0	0	0	0	0	0
105	0	0	6	5	1	2	0	0	0	0	0	0	0
110	0	0	4	1	0	1	0	0	0	0	0	0	0
115	0	0	3	2	0	1	1	0	1	0	0	0	0
120	0	0	3	2	0	0	0	0	0	0	0	0	0
125	0	0	0	5	0	1	0	0	1	0	0	0	0
130	0	0	1	1	0	0	0	0	0	0	0	0	0
135	0	0	1	0	0	1	0	1	0	0	0	0	0
140	0	3	0	1	0	0	0	0	0	1	0	0	0
145	0	5	1	0	0	1	0	0	0	0	0	0	0
150	0	3	3	0	0	0	0	0	0	0	0	0	0
155	0	0	4	0	0	1	0	0	0	1	0	0	0
160	0	1	3	1	0	0	0	0	0	0	0	0	0
165	0	1	3	0	0	0	0	0	0	0	0	0	0
170	0	0	5	3	0	0	0	0	0	0	0	0	0
175	0	0	4	0	2	0	0	0	0	0	0	0	0
180	0	0	1	0	0	0	0	0	1	0	0	0	0

Table B4
Case Counts for 2.0 m ≤ H_{mo} < 2.5 m

θ_0 (deg)	f_p (Hz)												
	0.044	0.054	0.064	0.074	0.084	0.093	0.103	0.113	0.123	0.132	0.142	0.152	0.162
-180	0	0	0	0	0	0	0	0	1	0	0	0	0
-175	0	0	0	0	0	0	0	0	0	0	0	0	0
-170	0	0	0	0	0	0	0	0	0	0	0	0	0
-165	0	0	0	0	0	0	0	0	0	0	0	0	0
-160	0	0	0	0	0	0	0	0	0	0	0	0	0
-155	0	0	0	0	0	0	0	0	0	0	0	0	0
-150	0	0	0	0	0	0	0	0	0	0	0	0	0
-145	0	0	0	0	0	0	0	0	0	0	0	0	0
-140	0	0	0	0	0	0	0	0	0	0	0	0	1
-135	0	0	0	0	0	0	0	0	0	0	0	0	0
-130	0	0	0	0	0	0	0	0	0	0	0	0	1
-125	0	0	0	0	0	0	0	0	0	0	0	0	0
-120	0	0	0	0	0	0	0	0	0	0	0	0	0
-115	0	0	0	0	0	0	0	0	0	0	0	0	1
-110	0	0	0	0	0	0	0	0	0	0	0	0	0
-105	0	0	0	0	0	0	0	0	0	0	0	0	0
-100	0	0	0	0	0	0	0	0	0	0	0	0	0
-95	0	0	0	0	0	0	0	0	0	0	0	0	0
-90	0	0	0	0	0	0	0	0	0	0	0	0	0
-85	0	0	0	0	0	0	0	0	0	0	0	0	0
-80	0	0	0	0	0	0	0	0	0	0	0	0	0
-75	0	0	0	0	0	0	0	0	0	0	0	0	0
-70	0	0	0	0	0	0	0	0	0	0	0	0	0
-65	0	0	0	0	0	0	0	0	0	0	0	0	0
-60	0	0	0	0	0	0	0	0	0	0	0	0	0
-55	0	0	0	0	0	0	0	0	0	0	0	0	0
-50	0	0	0	0	0	0	0	0	0	0	0	0	0
-45	0	0	0	0	0	0	0	0	0	0	0	0	0
-40	0	0	0	0	0	0	0	0	0	0	0	0	0
-35	0	0	0	0	0	0	0	0	0	0	0	0	0
-30	0	0	0	0	0	0	0	0	0	0	0	0	0
-25	0	0	0	0	0	0	0	0	0	0	0	0	0
-20	0	0	0	0	0	0	0	0	0	0	0	0	0
-15	0	0	0	0	0	0	0	0	0	0	0	0	0
-10	0	0	0	0	0	0	0	0	0	0	0	0	0
-5	0	0	0	0	0	0	0	0	0	0	0	0	0

(Continued)

Table B4 (Concluded)

θ_0 (deg)	f_p (Hz)												
	0.044	0.054	0.064	0.074	0.084	0.093	0.103	0.113	0.123	0.132	0.142	0.152	0.162
0	0	0	0	0	0	0	0	0	0	0	0	0	0
5	0	0	0	0	0	0	0	0	0	0	0	0	0
10	0	0	0	0	0	0	0	0	0	0	0	0	0
15	0	0	0	0	0	0	0	0	0	0	0	0	0
20	0	0	0	0	0	0	0	0	0	0	0	0	0
25	0	0	0	0	0	0	0	0	0	0	0	0	0
30	0	0	0	0	0	0	0	0	0	0	0	0	0
35	0	0	0	0	0	0	2	0	0	0	0	0	0
40	0	0	0	0	0	8	13	0	0	2	2	0	1
45	0	0	0	0	3	10	30	26	19	12	8	2	1
50	0	0	0	6	14	39	35	40	24	23	5	4	1
55	0	0	6	14	40	52	27	22	32	20	5	1	0
60	0	0	8	32	58	31	11	12	12	6	2	0	1
65	0	4	13	41	50	23	6	3	3	0	3	0	0
70	0	14	31	34	37	12	6	4	4	1	1	0	0
75	1	14	31	50	17	4	1	2	0	0	0	0	0
80	0	7	19	24	19	0	0	0	0	0	0	0	0
85	0	4	6	9	10	3	0	1	0	0	0	1	0
90	0	0	11	6	3	3	0	1	0	0	0	0	0
95	0	0	1	7	3	3	0	1	0	0	0	0	0
100	0	0	3	2	1	3	0	0	0	1	0	0	0
105	0	0	0	1	0	0	0	0	0	0	0	0	0
110	0	0	2	1	0	0	1	0	0	0	1	0	0
115	0	0	0	0	0	0	0	0	0	0	0	0	0
120	0	0	1	0	0	0	0	0	0	0	0	0	0
125	0	0	1	0	0	0	0	0	0	0	0	0	0
130	0	0	1	0	0	0	0	0	2	0	0	0	0
135	0	0	0	0	0	0	0	0	0	1	0	0	0
140	0	0	3	0	0	0	0	0	1	1	0	0	0
145	0	0	1	0	0	0	0	0	1	0	0	0	0
150	0	0	1	0	0	0	0	0	1	0	0	0	0
155	0	0	0	0	0	0	0	0	1	0	0	0	0
160	0	0	0	0	0	0	0	1	0	0	0	0	0
165	0	0	0	0	0	0	0	0	0	0	0	0	0
170	0	0	0	0	0	0	0	2	1	0	0	0	1
175	0	0	2	0	0	0	0	0	1	0	0	0	0
180	0	0	0	0	0	0	0	0	1	0	0	0	0

Table B5
Case Counts for 2.5 m ≤ H_{mo} < 3.0 m

θ_0 (deg)	f_p (Hz)												
	0.044	0.054	0.064	0.074	0.084	0.093	0.103	0.113	0.123	0.132	0.142	0.152	0.162
-180	0	0	0	0	0	0	0	0	0	0	0	0	0
-175	0	0	0	0	0	0	0	0	0	0	0	0	0
-170	0	0	0	0	0	0	0	0	0	0	0	0	0
-165	0	0	0	0	0	0	0	0	0	0	0	0	0
-160	0	0	0	0	0	0	0	0	0	0	0	0	0
-155	0	0	0	0	0	0	0	0	0	0	0	0	0
-150	0	0	0	0	0	0	0	0	0	0	0	1	0
-145	0	0	0	0	0	0	0	0	0	0	0	0	0
-140	0	0	0	0	0	0	0	0	0	0	0	0	0
-135	0	0	0	0	0	0	0	0	0	0	0	2	0
-130	0	0	0	0	0	0	0	0	0	0	0	1	0
-125	0	0	0	0	0	0	0	0	0	0	0	0	0
-120	0	0	0	0	0	0	0	0	0	0	0	0	0
-115	0	0	0	0	0	0	0	0	0	0	0	0	0
-110	0	0	0	0	0	0	0	0	0	0	0	0	0
-105	0	0	0	0	0	0	0	0	0	0	0	0	0
-100	0	0	0	0	0	0	0	0	0	0	0	0	0
-95	0	0	0	0	0	0	0	0	0	0	0	0	0
-90	0	0	0	0	0	0	0	0	0	0	0	0	0
-85	0	0	0	0	0	0	0	0	0	0	0	0	0
-80	0	0	0	0	0	0	0	0	0	0	0	0	0
-75	0	0	0	0	0	0	0	0	0	0	0	0	0
-70	0	0	0	0	0	0	0	0	0	0	0	0	0
-65	0	0	0	0	0	0	0	0	0	0	0	0	0
-60	0	0	0	0	0	0	0	0	0	0	0	0	0
-55	0	0	0	0	0	0	0	0	0	0	0	0	0
-50	0	0	0	0	0	0	0	0	0	0	0	0	0
-45	0	0	0	0	0	0	0	0	0	0	0	0	0
-40	0	0	0	0	0	0	0	0	0	0	0	0	0
-35	0	0	0	0	0	0	0	0	0	0	0	0	0
-30	0	0	0	0	0	0	0	0	0	0	0	0	0
-25	0	0	0	0	0	0	0	0	0	0	0	0	0
-20	0	0	0	0	0	0	0	0	0	0	0	0	0
-15	0	0	0	0	0	0	0	0	0	0	0	0	0
-10	0	0	0	0	0	0	0	0	0	0	0	0	0
-5	0	0	0	0	0	0	0	0	0	0	0	0	0

(Continued)

Table B5 (Concluded)

θ_0 (deg)	f_p (Hz)												
	0.044	0.054	0.064	0.074	0.084	0.093	0.103	0.113	0.123	0.132	0.142	0.152	0.162
0	0	0	0	0	0	0	0	0	0	0	0	0	0
5	0	0	0	0	0	0	0	0	0	0	0	0	0
10	0	0	0	0	0	0	0	0	0	0	0	0	0
15	0	0	0	0	0	0	0	0	0	0	0	0	0
20	0	0	0	0	0	0	0	0	0	0	0	0	0
25	0	0	0	0	0	0	0	0	0	0	0	0	0
30	0	0	0	0	0	0	0	0	0	0	0	0	0
35	0	0	0	0	0	0	0	0	0	0	0	0	0
40	0	0	0	0	0	4	3	0	0	0	1	0	0
45	0	0	0	0	2	15	5	7	0	4	0	0	0
50	0	0	0	2	9	18	18	12	10	6	1	1	0
55	0	0	2	16	16	13	10	8	9	5	1	0	0
60	0	0	9	39	28	21	8	2	5	1	2	0	0
65	0	3	17	49	26	8	1	3	1	0	0	0	0
70	0	11	37	56	15	1	3	0	0	0	0	0	0
75	2	7	25	25	9	1	2	0	1	0	0	0	0
80	1	3	16	16	7	0	1	1	0	0	0	0	0
85	0	3	8	13	4	0	1	2	0	0	0	0	0
90	0	0	3	4	1	1	0	1	0	0	0	0	0
95	0	0	0	5	1	0	0	0	1	0	0	0	0
100	0	0	0	1	3	0	1	0	1	0	0	0	0
105	0	0	0	0	0	0	0	0	0	0	0	0	0
110	0	0	0	0	0	0	0	0	0	0	0	0	0
115	0	0	0	0	0	0	0	0	0	0	0	0	0
120	0	0	0	0	0	0	0	0	0	0	0	0	0
125	0	0	0	0	0	0	1	1	0	0	0	0	0
130	0	0	0	0	0	0	1	0	0	0	0	0	0
135	0	0	0	0	0	0	0	1	0	0	0	0	0
140	0	0	0	0	0	0	0	1	2	0	0	0	0
145	0	0	0	0	0	0	0	1	0	0	0	0	0
150	0	0	0	0	0	0	0	0	1	0	0	0	0
155	0	0	0	0	0	0	1	0	0	0	0	0	0
160	0	0	0	0	0	0	0	0	0	0	0	0	0
165	0	0	0	0	0	0	0	1	0	0	0	0	0
170	0	0	0	0	0	0	0	0	0	0	0	0	0
175	0	0	0	0	0	0	0	0	0	1	0	0	0
180	0	0	0	0	0	0	0	0	0	0	0	0	0

Table B6
Case Counts for 3.0 m ≤ H_{mo} < 3.5 m

θ_0 (deg)	f_p (Hz)												
	0.044	0.054	0.064	0.074	0.084	0.093	0.103	0.113	0.123	0.132	0.142	0.152	0.162
-180	0	0	0	0	0	0	0	0	0	0	0	0	0
-175	0	0	0	0	0	0	0	0	0	0	0	0	0
-170	0	0	0	0	0	0	0	0	0	0	0	0	0
-165	0	0	0	0	0	0	0	0	0	0	0	0	0
-160	0	0	0	0	0	0	0	0	0	0	0	0	0
-155	0	0	0	0	0	0	0	0	0	0	0	0	0
-150	0	0	0	0	0	0	0	0	0	0	0	0	0
-145	0	0	0	0	0	0	0	0	0	0	0	0	0
-140	0	0	0	0	0	0	0	0	0	0	0	0	0
-135	0	0	0	0	0	0	0	0	0	0	0	0	0
-130	0	0	0	0	0	0	0	0	0	0	0	0	0
-125	0	0	0	0	0	0	0	0	0	0	0	0	0
-120	0	0	0	0	0	0	0	0	0	0	0	0	0
-115	0	0	0	0	0	0	0	0	0	0	0	0	0
-110	0	0	0	0	0	0	0	0	0	0	0	0	0
-105	0	0	0	0	0	0	0	0	0	0	0	0	0
-100	0	0	0	0	0	0	0	0	0	0	0	0	0
-95	0	0	0	0	0	0	0	0	0	0	0	0	0
-90	0	0	0	0	0	0	0	0	0	0	0	0	0
-85	0	0	0	0	0	0	0	0	0	0	0	0	0
-80	0	0	0	0	0	0	0	0	0	0	0	0	0
-75	0	0	0	0	0	0	0	0	0	0	0	0	0
-70	0	0	0	0	0	0	0	0	0	0	0	0	0
-65	0	0	0	0	0	0	0	0	0	0	0	0	0
-60	0	0	0	0	0	0	0	0	0	0	0	0	0
-55	0	0	0	0	0	0	0	0	0	0	0	0	0
-50	0	0	0	0	0	0	0	0	0	0	0	0	0
-45	0	0	0	0	0	0	0	0	0	0	0	0	0
-40	0	0	0	0	0	0	0	0	0	0	0	0	0
-35	0	0	0	0	0	0	0	0	0	0	0	0	0
-30	0	0	0	0	0	0	0	0	0	0	0	0	0
-25	0	0	0	0	0	0	0	0	0	0	0	0	0
-20	0	0	0	0	0	0	0	0	0	0	0	0	0
-15	0	0	0	0	0	0	0	0	0	0	0	0	0
-10	0	0	0	0	0	0	0	0	0	0	0	0	0
-5	0	0	0	0	0	0	0	0	0	0	0	0	0

(Continued)

Table B6 (Concluded)

θ_0 (deg)	f_p (Hz)												
	0.044	0.054	0.064	0.074	0.084	0.093	0.103	0.113	0.123	0.132	0.142	0.152	0.162
0	0	0	0	0	0	0	0	0	0	0	0	0	0
5	0	0	0	0	0	0	0	0	0	0	0	0	0
10	0	0	0	0	0	0	0	0	0	0	0	0	0
15	0	0	0	0	0	0	0	0	0	0	0	0	0
20	0	0	0	0	0	0	0	0	0	0	0	0	0
25	0	0	0	0	0	0	0	0	0	0	0	0	0
30	0	0	0	0	0	0	0	0	0	0	0	0	0
35	0	0	0	0	0	0	0	0	0	0	0	0	0
40	0	0	0	0	0	0	0	0	0	0	0	0	0
45	0	0	0	0	2	1	2	4	3	1	0	0	0
50	0	0	0	2	8	16	7	4	0	1	0	0	0
55	0	0	4	21	13	6	12	3	2	0	0	0	0
60	0	0	4	25	13	6	16	1	0	0	0	0	0
65	0	1	12	19	12	5	1	4	0	0	0	0	0
70	1	13	21	31	9	1	0	2	1	0	0	0	0
75	0	4	20	24	4	1	0	0	0	0	0	0	0
80	0	3	12	18	5	1	0	0	0	0	0	0	0
85	0	0	8	19	0	0	0	0	0	0	0	0	0
90	0	0	3	6	1	1	0	0	0	0	0	0	0
95	0	0	3	4	1	0	0	0	0	0	0	0	0
100	0	0	1	0	1	0	0	0	0	0	0	0	0
105	0	0	0	0	1	0	0	1	0	0	0	0	0
110	0	0	0	0	1	0	0	1	0	0	0	0	0
115	0	0	0	0	1	0	0	0	0	0	0	0	0
120	0	0	0	0	0	1	0	0	0	0	0	0	0
125	0	0	0	0	0	0	0	0	0	0	0	0	0
130	0	0	0	0	0	0	0	0	0	0	0	0	0
135	0	0	0	0	0	0	0	0	0	0	0	0	0
140	0	0	0	0	0	0	0	0	0	0	0	0	0
145	0	0	0	0	0	0	0	0	0	0	0	0	0
150	0	0	0	0	0	0	0	0	0	0	0	0	0
155	0	0	0	0	0	0	0	0	0	0	0	0	0
160	0	0	0	0	0	0	0	0	0	1	0	0	0
165	0	0	0	0	0	0	0	0	0	0	0	0	0
170	0	0	0	0	0	0	0	0	0	0	0	0	0
175	0	0	0	0	0	0	0	0	0	0	0	0	0
180	0	0	0	0	0	0	0	0	0	0	0	0	0

Table B7
Case Counts for 3.5 m ≤ H_{mo} < 4.0 m

θ_0 (deg)	f_p (Hz)												
	0.044	0.054	0.064	0.074	0.084	0.093	0.103	0.113	0.123	0.132	0.142	0.152	0.162
-180	0	0	0	0	0	0	0	0	0	0	0	0	0
-175	0	0	0	0	0	0	0	0	0	0	0	0	0
-170	0	0	0	0	0	0	0	0	0	0	0	0	0
-165	0	0	0	0	0	0	0	0	0	0	0	0	0
-160	0	0	0	0	0	0	0	0	0	0	0	0	0
-155	0	0	0	0	0	0	0	0	0	0	0	0	0
-150	0	0	0	0	0	0	0	0	0	0	0	0	0
-145	0	0	0	0	0	0	0	0	0	0	0	0	0
-140	0	0	0	0	0	0	0	0	0	0	0	0	0
-135	0	0	0	0	0	0	0	0	0	0	0	0	0
-130	0	0	0	0	0	0	0	0	0	0	0	0	0
-125	0	0	0	0	0	0	0	0	0	0	0	0	0
-120	0	0	0	0	0	0	0	0	0	0	0	0	0
-115	0	0	0	0	0	0	0	0	0	0	0	0	0
-110	0	0	0	0	0	0	0	0	0	0	0	0	0
-105	0	0	0	0	0	0	0	0	0	0	0	0	0
-100	0	0	0	0	0	0	0	0	0	0	0	0	0
-95	0	0	0	0	0	0	0	0	0	0	0	0	0
-90	0	0	0	0	0	0	0	0	0	0	0	0	0
-85	0	0	0	0	0	0	0	0	0	0	0	0	0
-80	0	0	0	0	0	0	0	0	0	0	0	0	0
-75	0	0	0	0	0	0	0	0	0	0	0	0	0
-70	0	0	0	0	0	0	0	0	0	0	0	0	0
-65	0	0	0	0	0	0	0	0	0	0	0	0	0
-60	0	0	0	0	0	0	0	0	0	0	0	0	0
-55	0	0	0	0	0	0	0	0	0	0	0	0	0
-50	0	0	0	0	0	0	0	0	0	0	0	0	0
-45	0	0	0	0	0	0	0	0	0	0	0	0	0
-40	0	0	0	0	0	0	0	0	0	0	0	0	0
-35	0	0	0	0	0	0	0	0	0	0	0	0	0
-30	0	0	0	0	0	0	0	0	0	0	0	0	0
-25	0	0	0	0	0	0	0	0	0	0	0	0	0
-20	0	0	0	0	0	0	0	0	0	0	0	0	0
-15	0	0	0	0	0	0	0	0	0	0	0	0	0
-10	0	0	0	0	0	0	0	0	0	0	0	0	0
-5	0	0	0	0	0	0	0	0	0	0	0	0	0

(Continued)

Table B7 (Concluded)

θ_0 (deg)	f_p (Hz)												
	0.044	0.054	0.064	0.074	0.084	0.093	0.103	0.113	0.123	0.132	0.142	0.152	0.162
0	0	0	0	0	0	0	1	0	0	0	0	0	0
5	0	0	0	0	0	0	0	0	0	0	0	0	0
10	0	0	0	0	0	0	0	0	0	0	0	0	0
15	0	0	0	0	0	0	0	0	0	0	0	0	0
20	0	0	0	0	0	0	0	0	0	0	0	0	0
25	0	0	0	0	0	0	0	0	0	0	0	0	0
30	0	0	0	0	0	0	0	0	0	0	0	0	0
35	0	0	0	0	0	0	0	0	0	0	0	0	0
40	0	0	0	0	0	0	0	0	0	0	0	0	0
45	0	0	0	0	1	0	4	2	1	0	0	0	0
50	0	0	0	1	3	6	3	1	1	0	0	0	0
55	0	0	2	11	2	4	1	1	0	0	0	0	0
60	0	0	5	13	3	1	0	0	1	0	0	0	0
65	0	1	5	15	5	1	0	0	0	0	0	0	0
70	0	2	15	14	4	3	0	1	0	0	0	0	0
75	0	0	16	7	1	2	0	0	0	0	0	0	0
80	0	0	14	10	1	0	0	0	0	0	0	0	0
85	0	0	9	13	4	0	0	0	0	0	0	0	0
90	0	0	3	8	1	0	0	0	0	0	0	0	0
95	0	0	0	1	1	0	0	0	0	0	0	0	0
100	0	0	0	0	1	1	0	0	0	0	0	0	0
105	0	0	0	0	2	0	1	0	0	0	0	0	0
110	0	0	0	0	1	0	0	0	0	0	0	0	0
115	0	0	0	0	1	0	0	0	0	0	0	0	0
120	0	0	0	0	0	0	0	0	0	0	0	0	0
125	0	0	0	0	0	0	0	0	0	0	0	0	0
130	0	0	0	0	0	0	0	0	0	0	0	0	0
135	0	0	0	0	0	0	0	0	0	0	0	0	0
140	0	0	0	0	0	0	0	0	0	0	0	0	0
145	0	0	0	0	0	0	0	0	0	0	0	0	0
150	0	0	0	0	0	0	0	0	0	0	0	0	0
155	0	0	0	0	0	0	0	0	0	0	0	0	0
160	0	0	0	0	0	0	0	0	0	0	0	0	0
165	0	0	0	0	0	0	0	0	0	0	0	0	0
170	0	0	0	0	0	0	0	0	0	0	0	0	0
175	0	0	0	0	0	0	0	0	0	0	0	0	0
180	0	0	0	0	0	0	0	0	0	0	0	0	0

Table B8
Case Counts for 4.0 m ≤ H_{mo} < 4.5 m

θ_0 (deg)	f_p (Hz)												
	0.044	0.054	0.064	0.074	0.084	0.093	0.103	0.113	0.123	0.132	0.142	0.152	0.162
-180	0	0	0	0	0	0	0	0	0	0	0	0	0
-175	0	0	0	0	0	0	0	0	0	0	0	0	0
-170	0	0	0	0	0	0	0	0	0	0	0	0	0
-165	0	0	0	0	0	0	0	0	0	0	0	0	0
-160	0	0	0	0	0	0	0	0	0	0	1	0	0
-155	0	0	0	0	0	0	0	0	0	0	0	0	0
-150	0	0	0	0	0	0	0	0	0	0	0	0	0
-145	0	0	0	0	0	0	0	0	0	0	0	0	0
-140	0	0	0	0	0	0	0	0	0	0	0	0	0
-135	0	0	0	0	0	0	0	0	0	0	0	0	0
-130	0	0	0	0	0	0	0	0	0	0	0	0	0
-125	0	0	0	0	0	0	0	0	0	0	0	0	0
-120	0	0	0	0	0	0	0	0	0	0	0	0	0
-115	0	0	0	0	0	0	0	0	0	0	0	0	0
-110	0	0	0	0	0	0	0	0	0	0	0	0	0
-105	0	0	0	0	0	0	0	0	0	0	0	0	0
-100	0	0	0	0	0	0	0	0	0	0	0	0	0
-95	0	0	0	0	0	0	0	0	0	0	0	0	0
-90	0	0	0	0	0	0	0	0	0	0	0	0	0
-85	0	0	0	0	0	0	0	0	0	0	0	0	0
-80	0	0	0	0	0	0	0	0	0	0	0	0	0
-75	0	0	0	0	0	0	0	0	0	0	0	0	0
-70	0	0	0	0	0	0	0	0	0	0	0	0	0
-65	0	0	0	0	0	0	0	0	0	0	0	0	0
-60	0	0	0	0	0	0	0	0	0	0	0	0	0
-55	0	0	0	0	0	0	0	0	0	0	0	0	0
-50	0	0	0	0	0	0	0	0	0	0	0	0	0
-45	0	0	0	0	0	0	0	0	0	0	0	0	0
-40	0	0	0	0	0	0	0	0	0	0	0	0	0
-35	0	0	0	0	0	0	0	0	0	0	0	0	0
-30	0	0	0	0	0	0	0	0	0	0	0	0	0
-25	0	0	0	0	0	0	0	0	0	0	0	0	0
-20	0	0	0	0	0	0	0	0	0	0	0	0	0
-15	0	0	0	0	0	0	0	0	0	0	0	0	0
-10	0	0	0	0	0	0	0	0	0	0	0	0	0
-5	0	0	0	0	0	0	0	0	0	0	0	0	0

(Continued)

Table B8 (Concluded)

θ_0 (deg)	f_p (Hz)												
	0.044	0.054	0.064	0.074	0.084	0.093	0.103	0.113	0.123	0.132	0.142	0.152	0.162
0	0	0	0	0	0	0	0	0	0	0	0	0	0
5	0	0	0	0	0	0	0	0	0	0	0	0	0
10	0	0	0	0	0	0	0	0	0	0	0	0	0
15	0	0	0	0	0	0	0	0	0	0	0	0	0
20	0	0	0	0	0	0	0	0	0	0	0	0	0
25	0	0	0	0	0	0	0	0	0	0	0	0	0
30	0	0	0	0	0	0	0	0	0	0	0	0	0
35	0	0	0	0	0	0	0	0	0	0	0	0	0
40	0	0	0	0	0	0	0	0	0	0	0	0	0
45	0	0	0	0	0	0	0	0	0	0	0	0	0
50	0	0	0	4	3	3	2	0	0	0	0	0	0
55	0	0	0	5	1	4	3	0	0	0	0	0	0
60	0	0	3	5	2	1	1	0	0	0	0	0	0
65	0	0	5	5	1	0	1	0	0	0	0	0	0
70	0	0	6	6	2	1	0	0	0	0	0	0	0
75	0	0	6	5	1	1	0	0	0	0	0	0	0
80	0	1	11	6	1	2	0	0	0	0	0	0	0
85	0	0	4	7	1	0	0	0	0	0	0	0	0
90	0	0	0	3	0	0	0	0	0	0	0	0	0
95	0	0	0	0	0	0	0	0	0	0	0	0	0
100	0	0	0	1	0	0	0	0	0	0	0	0	0
105	0	0	0	0	0	2	0	0	0	0	0	0	0
110	0	0	0	0	0	0	0	0	0	0	0	0	0
115	0	0	0	0	0	0	0	0	0	0	0	0	0
120	0	0	0	0	0	0	0	0	0	0	0	0	0
125	0	0	0	0	0	0	1	0	0	0	0	0	0
130	0	0	0	0	0	0	0	0	0	0	0	0	0
135	0	0	0	0	0	0	0	0	0	0	0	0	0
140	0	0	0	0	0	0	0	1	0	0	0	0	0
145	0	0	0	0	0	0	0	0	0	0	0	0	0
150	0	0	0	0	0	0	0	0	0	0	0	0	0
155	0	0	0	0	0	0	0	0	0	0	0	0	0
160	0	0	0	0	0	0	0	0	0	0	0	0	0
165	0	0	0	0	0	0	0	0	0	0	0	0	0
170	0	0	0	0	0	0	0	0	0	0	0	0	0
175	0	0	0	0	0	0	0	0	0	0	0	0	0
180	0	0	0	0	0	0	0	0	0	0	0	0	0

Table B9
Case Counts for 4.5 m ≤ H_{mo} < 5.0 m

θ_0 (deg)	f_p (Hz)												
	0.044	0.054	0.064	0.074	0.084	0.093	0.103	0.113	0.123	0.132	0.142	0.152	0.162
-180	0	0	0	0	0	0	0	0	0	0	0	0	0
-175	0	0	0	0	0	0	0	0	0	0	0	0	0
-170	0	0	0	0	0	0	0	0	0	0	0	0	0
-165	0	0	0	0	0	0	0	0	0	0	0	0	0
-160	0	0	0	0	0	0	0	0	0	0	0	0	0
-155	0	0	0	0	0	0	0	0	0	0	0	0	0
-150	0	0	0	0	0	0	0	0	0	0	0	0	0
-145	0	0	0	0	0	0	0	0	0	0	0	0	0
-140	0	0	0	0	0	0	0	0	0	0	0	0	0
-135	0	0	0	0	0	0	0	0	0	0	0	0	0
-130	0	0	0	0	0	0	0	0	0	0	0	0	0
-125	0	0	0	0	0	0	0	0	0	0	0	0	0
-120	0	0	0	0	0	0	0	0	0	0	0	0	0
-115	0	0	0	0	0	0	0	0	0	0	0	0	0
-110	0	0	0	0	0	0	0	0	0	0	0	0	0
-105	0	0	0	0	0	0	0	0	0	0	0	0	0
-100	0	0	0	0	0	0	0	0	0	0	0	0	0
-95	0	0	0	0	0	0	0	0	0	0	0	0	0
-90	0	0	0	0	0	0	0	0	0	0	0	0	0
-85	0	0	0	0	0	0	0	0	0	0	0	0	0
-80	0	0	0	0	0	0	0	0	0	0	0	0	0
-75	0	0	0	0	0	0	0	0	0	0	0	0	0
-70	0	0	0	0	0	0	0	0	0	0	0	0	0
-65	0	0	0	0	0	0	0	0	0	0	0	0	0
-60	0	0	0	0	0	0	0	0	0	0	0	0	0
-55	0	0	0	0	0	0	0	0	0	0	0	0	0
-50	0	0	0	0	0	0	0	0	0	0	0	0	0
-45	0	0	0	0	0	0	0	0	0	0	0	0	0
-40	0	0	0	0	0	0	0	0	0	0	0	0	0
-35	0	0	0	0	0	0	0	0	0	0	0	0	0
-30	0	0	0	0	0	0	0	0	0	0	0	0	0
-25	0	0	0	0	0	0	0	0	0	0	0	0	0
-20	0	0	0	0	0	0	0	0	0	0	0	0	0
-15	0	0	0	0	0	0	0	0	0	0	0	0	0
-10	0	0	0	0	0	0	0	0	0	0	0	0	0
-5	0	0	0	0	0	0	0	0	0	0	0	0	0

(Continued)

Table B9 (Concluded)

θ_0 (deg)	f_p (Hz)												
	0.044	0.054	0.064	0.074	0.084	0.093	0.103	0.113	0.123	0.132	0.142	0.152	0.162
0	0	0	0	0	0	0	0	0	0	0	0	0	0
5	0	0	0	0	0	0	0	0	0	0	0	0	0
10	0	0	0	0	0	0	0	0	0	0	0	0	0
15	0	0	0	0	0	0	0	0	0	0	0	0	0
20	0	0	0	0	0	0	0	0	0	0	0	0	0
25	0	0	0	0	0	0	0	0	0	0	0	0	0
30	0	0	0	0	0	0	0	0	0	0	0	0	0
35	0	0	0	0	0	0	0	0	0	0	0	0	0
40	0	0	0	0	0	0	0	0	0	0	0	0	0
45	0	0	0	0	0	0	0	0	0	0	0	0	0
50	0	0	0	1	0	2	1	0	0	0	0	0	0
55	0	0	0	2	0	1	0	0	0	0	0	0	0
60	0	0	5	3	0	0	0	0	0	0	0	0	0
65	0	0	1	0	0	0	0	0	0	0	0	0	0
70	0	0	2	3	0	0	0	0	0	0	0	0	0
75	0	1	3	0	1	0	0	0	0	0	0	0	0
80	0	0	0	1	0	0	0	0	0	0	0	0	0
85	0	0	0	0	0	0	0	0	0	0	0	0	0
90	0	0	0	0	0	0	0	0	0	0	0	0	0
95	0	0	0	0	0	0	0	0	0	0	0	0	0
100	0	0	0	0	2	0	0	0	0	0	0	0	0
105	0	0	0	0	0	0	0	0	0	0	0	0	0
110	0	0	0	0	0	0	0	0	0	0	0	0	0
115	0	0	0	0	0	0	0	0	0	0	0	0	0
120	0	0	0	0	0	0	0	0	0	0	0	0	0
125	0	0	0	0	0	0	0	0	0	0	0	0	0
130	0	0	0	0	0	0	0	0	0	0	0	0	0
135	0	0	0	0	0	0	0	0	0	0	0	0	0
140	0	0	0	0	0	0	0	0	0	0	0	0	0
145	0	0	0	0	0	0	0	0	0	0	0	0	0
150	0	0	0	0	0	0	0	0	0	0	0	0	0
155	0	0	0	0	0	0	0	0	0	0	0	0	0
160	0	0	0	1	0	0	0	0	0	0	0	0	0
165	0	0	0	0	0	0	0	0	0	0	0	0	0
170	0	0	0	0	0	0	0	0	0	0	0	0	0
175	0	0	0	0	0	0	0	0	0	0	0	0	0
180	0	0	0	0	0	0	0	0	0	0	0	0	0

Table B10
Case Counts for 5.0 m ≤ H_{mo} < 5.5 m

θ_0 (deg)	f_p (Hz)												
	0.044	0.054	0.064	0.074	0.084	0.093	0.103	0.113	0.123	0.132	0.142	0.152	0.162
-180	0	0	0	0	0	0	0	0	0	0	0	0	0
-175	0	0	0	0	0	0	0	0	0	0	0	0	0
-170	0	0	0	0	0	0	0	0	0	0	0	0	0
-165	0	0	0	0	0	0	0	0	0	0	0	0	0
-160	0	0	0	0	0	0	0	0	0	0	0	0	0
-155	0	0	0	0	0	0	0	0	0	0	0	0	0
-150	0	0	0	0	0	0	0	0	0	0	0	0	0
-145	0	0	0	0	0	0	0	0	0	0	0	0	0
-140	0	0	0	0	0	0	0	0	0	0	0	0	0
-135	0	0	0	0	0	0	0	0	0	0	0	0	0
-130	0	0	0	0	0	0	0	0	0	0	0	0	0
-125	0	0	0	0	0	0	0	0	0	0	0	0	0
-120	0	0	0	0	0	0	0	0	0	0	0	0	0
-115	0	0	0	0	0	0	0	0	0	0	0	0	0
-110	0	0	0	0	0	0	0	0	0	0	0	0	0
-105	0	0	0	0	0	0	0	0	0	0	0	0	0
-100	0	0	0	0	0	0	0	0	0	0	0	0	0
-95	0	0	0	0	0	0	0	0	0	0	0	0	0
-90	0	0	0	0	0	0	0	0	0	0	0	0	0
-85	0	0	0	0	0	0	0	0	0	0	0	0	0
-80	0	0	0	0	0	0	0	0	0	0	0	0	0
-75	0	0	0	0	0	0	0	0	0	0	0	0	0
-70	0	0	0	0	0	0	0	0	0	0	0	0	0
-65	0	0	0	0	0	0	0	0	0	0	0	0	0
-60	0	0	0	0	0	0	0	0	0	0	0	0	0
-55	0	0	0	0	0	0	0	0	0	0	0	0	0
-50	0	0	0	0	0	0	0	0	0	0	0	0	0
-45	0	0	0	0	0	0	0	0	0	0	0	0	0
-40	0	0	0	0	0	0	0	0	0	0	0	0	0
-35	0	0	0	0	0	0	0	0	0	0	0	0	0
-30	0	0	0	0	0	0	0	0	0	0	0	0	0
-25	0	0	0	0	0	0	0	0	0	0	0	0	0
-20	0	0	0	0	0	0	0	0	0	0	0	0	0
-15	0	0	0	0	0	0	0	0	0	0	0	0	0
-10	0	0	0	0	0	0	0	0	0	0	0	0	0
-5	0	0	0	0	0	0	0	0	0	0	0	0	0

(Continued)

Table B10 (Concluded)

θ_0 (deg)	f_p (Hz)												
	0.044	0.054	0.064	0.074	0.084	0.093	0.103	0.113	0.123	0.132	0.142	0.152	0.162
0	0	0	0	0	0	0	0	0	0	0	0	0	0
5	0	0	0	0	0	0	0	0	0	0	0	0	0
10	0	0	0	0	0	0	0	0	0	0	0	0	0
15	0	0	0	0	0	0	0	0	0	0	0	0	0
20	0	0	0	0	0	0	0	0	0	0	0	0	0
25	0	0	0	0	0	0	0	0	0	0	0	0	0
30	0	0	0	0	0	0	0	0	0	0	0	0	0
35	0	0	0	0	0	0	0	0	0	0	0	0	0
40	0	0	0	0	0	0	0	0	0	0	0	0	0
45	0	0	0	0	0	0	0	0	0	0	0	0	0
50	0	0	0	0	0	0	0	0	0	0	0	0	0
55	0	0	0	1	0	1	1	0	0	0	0	0	0
60	0	0	0	0	0	0	0	0	0	0	0	0	0
65	0	0	0	0	0	0	0	0	0	0	0	0	0
70	0	0	0	1	0	0	0	0	0	0	0	0	0
75	0	0	0	0	0	0	0	0	0	0	0	0	0
80	0	0	0	1	0	0	0	0	0	0	0	0	0
85	0	0	0	0	0	0	0	0	0	0	0	0	0
90	0	0	0	0	0	0	0	0	0	0	0	0	0
95	0	0	0	0	0	0	0	0	0	0	0	0	0
100	0	0	0	0	0	0	0	0	0	0	0	0	0
105	0	0	0	0	0	0	0	0	0	0	0	0	0
110	0	0	0	0	0	0	0	0	0	0	0	0	0
115	0	0	0	0	0	0	0	0	0	0	0	0	0
120	0	0	0	0	0	0	0	0	0	0	0	0	0
125	0	0	0	0	0	0	0	0	0	0	0	0	0
130	0	0	0	0	0	0	0	0	0	0	0	0	0
135	0	0	0	0	0	0	0	0	0	0	0	0	0
140	0	0	0	0	0	0	0	0	0	0	0	0	0
145	0	0	0	0	0	0	0	0	0	0	0	0	0
150	0	0	0	0	0	0	0	0	0	0	0	0	0
155	0	0	0	0	0	0	0	0	0	0	0	0	0
160	0	0	0	0	0	0	0	0	0	0	0	0	0
165	0	0	0	0	0	0	0	0	0	0	0	0	0
170	0	0	0	0	0	0	0	0	0	0	0	0	0
175	0	0	0	0	0	0	0	0	0	0	0	0	0
180	0	0	0	0	0	0	0	0	0	0	0	0	0

Table B11
Case Counts for 5.5 m ≤ H_{mo} < 6.0 m

θ_0 (deg)	f_p (Hz)												
	0.044	0.054	0.064	0.074	0.084	0.093	0.103	0.113	0.123	0.132	0.142	0.152	0.162
-180	0	0	0	0	0	0	0	0	0	0	0	0	0
-175	0	0	0	0	0	0	0	0	0	0	0	0	0
-170	0	0	0	0	0	0	0	0	0	0	0	0	0
-165	0	0	0	0	0	0	0	0	0	0	0	0	0
-160	0	0	0	0	0	0	0	0	0	0	0	0	0
-155	0	0	0	0	0	0	0	0	0	0	0	0	0
-150	0	0	0	0	0	0	0	0	0	0	0	0	0
-145	0	0	0	0	0	0	0	0	0	0	0	0	0
-140	0	0	0	0	0	0	0	0	0	0	0	0	0
-135	0	0	0	0	0	0	0	0	0	0	0	0	0
-130	0	0	0	0	0	0	0	0	0	0	0	0	0
-125	0	0	0	0	0	0	0	0	0	0	0	0	0
-120	0	0	0	0	0	0	0	0	0	0	0	0	0
-115	0	0	0	0	0	0	0	0	0	0	0	0	0
-110	0	0	0	0	0	0	0	0	0	0	0	0	0
-105	0	0	0	0	0	0	0	0	0	0	0	0	0
-100	0	0	0	0	0	0	0	0	0	0	0	0	0
-95	0	0	0	0	0	0	0	0	0	0	0	0	0
-90	0	0	0	0	0	0	0	0	0	0	0	0	0
-85	0	0	0	0	0	0	0	0	0	0	0	0	0
-80	0	0	0	0	0	0	0	0	0	0	0	0	0
-75	0	0	0	0	0	0	0	0	0	0	0	0	0
-70	0	0	0	0	0	0	0	0	0	0	0	0	0
-65	0	0	0	0	0	0	0	0	0	0	0	0	0
-60	0	0	0	0	0	0	0	0	0	0	0	0	0
-55	0	0	0	0	0	0	0	0	0	0	0	0	0
-50	0	0	0	0	0	0	0	0	0	0	0	0	0
-45	0	0	0	0	0	0	0	0	0	0	0	0	0
-40	0	0	0	0	0	0	0	0	0	0	0	0	0
-35	0	0	0	0	0	0	0	0	0	0	0	0	0
-30	0	0	0	0	0	0	0	0	0	0	0	0	0
-25	0	0	0	0	0	0	0	0	0	0	0	0	0
-20	0	0	0	0	0	0	0	0	0	0	0	0	0
-15	0	0	0	0	0	0	0	0	0	0	0	0	0
-10	0	0	0	0	0	0	0	0	0	0	0	0	0
-5	0	0	0	0	0	0	0	0	0	0	0	0	0

(Continued)

Table B11 (Concluded)

θ_0 (deg)	f_p (Hz)												
	0.044	0.054	0.064	0.074	0.084	0.093	0.103	0.113	0.123	0.132	0.142	0.152	0.162
0	0	0	0	0	0	0	0	0	0	0	0	0	0
5	0	0	0	0	0	0	0	0	0	0	0	0	0
10	0	0	0	0	0	0	0	0	0	0	0	0	0
15	0	0	0	0	0	0	0	0	0	0	0	0	0
20	0	0	0	0	0	0	0	0	0	0	0	0	0
25	0	0	0	0	0	0	0	0	0	0	0	0	0
30	0	0	0	0	0	0	0	0	0	0	0	0	0
35	0	0	0	0	0	0	0	0	0	0	0	0	0
40	0	0	0	0	0	0	0	0	0	0	0	0	0
45	0	0	0	0	0	0	0	0	0	0	0	0	0
50	0	0	0	0	0	0	0	0	0	0	0	0	0
55	0	0	0	1	0	0	0	0	0	0	0	0	0
60	0	0	0	0	0	0	0	0	0	0	0	0	0
65	0	0	0	0	0	0	0	0	0	0	0	0	0
70	0	0	0	0	0	0	0	0	0	0	0	0	0
75	0	0	1	0	0	0	0	0	0	0	0	0	0
80	0	0	0	1	0	0	0	0	0	0	0	0	0
85	0	0	1	0	0	0	0	0	0	0	0	0	0
90	0	0	0	0	0	0	0	0	0	0	0	0	0
95	0	0	0	0	0	0	0	0	0	0	0	0	0
100	0	0	0	0	0	0	0	0	0	0	0	0	0
105	0	0	0	0	0	0	0	0	0	0	0	0	0
110	0	0	0	0	0	0	0	0	0	0	0	0	0
115	0	0	0	0	0	0	0	0	0	0	0	0	0
120	0	0	0	0	0	0	0	0	0	0	0	0	0
125	0	0	0	0	0	0	0	0	0	0	0	0	0
130	0	0	0	0	0	0	0	0	0	0	0	0	0
135	0	0	0	0	0	0	0	0	0	0	0	0	0
140	0	0	0	0	0	0	0	0	0	0	0	0	0
145	0	0	0	0	0	0	0	0	0	0	0	0	0
150	0	0	0	0	0	0	0	0	0	0	0	0	0
155	0	0	0	0	0	0	0	0	0	0	0	0	0
160	0	0	0	0	0	0	0	0	0	0	0	0	0
165	0	0	0	0	0	0	0	0	0	0	0	0	0
170	0	0	0	0	0	0	0	0	0	0	0	0	0
175	0	0	0	0	0	0	0	0	0	0	0	0	0
180	0	0	0	0	0	0	0	0	0	0	0	0	0

Appendix C
Notation

d	Water depth
f_1, f_2	Arbitrary values bounding a range of frequencies in probability parameter space
f_j	Element j of an array of J discrete frequencies used to define probability parameter space
f_{min}	Minimum frequency in an array of discrete frequencies
f_p	Peak frequency of a wave energy spectrum; defines wind wave characteristic frequency
f_r	Element r of an array of R discrete frequencies used to define a wave energy spectrum
$H_{1/3}$	Characteristic wave height based on zero up-crossings in a wave record time series
H_1, H_2	Arbitrary values bounding a range of wave heights in probability parameter space
H_i	Element i of an array of I discrete wave heights used to define probability parameter space
H_{max}	Depth-limited wave height
H_{mo}	Characteristic wave height based on a wave energy spectrum
i	Index associated with discrete wave height
I	Upper limit of index i

j	Index associated with discrete frequency in probability parameter space
J	Upper limit of index j
k	Index associated with discrete wave direction in probability parameter space
K	Upper limit of index k
m	Index associated with discrete wave direction in a frequency-direction spectrum
M	Upper limit of index m
n	Index associated with measured triplets of characteristic wave height, frequency, and direction
$nint[\ ]$	Nearest integer operator
n_i	Element i of a one-dimensional case count matrix associated with characteristic wave height
n_{ijk}	Element of a three-dimensional case count matrix containing the number of coincident observations of H_{mo} in discrete wave height bin i, f_p in discrete frequency bin j, and θ_0 in discrete direction bin k
N	Total number of height-frequency-direction triplets in a data set
p	Analytic probability density
$\hat{p}$	Estimated probability density
$\hat{p}_i$	Discrete, estimated, wave height probability density
$\hat{p}_{ij}$	Discrete, estimated, joint wave height-frequency probability density
$\hat{p}_{ijk}$	Discrete, estimated, joint wave height-frequency-direction probability density
$\hat{p}_{ik}$	Discrete, estimated, joint wave height-direction probability density
$Prob[\ ]$	Probability that expression in brackets is true
Q	Analytic exceedance probability

$\hat{Q}$	Estimated exceedance probability
r	Index associated with discrete frequency in a wave energy spectrum
R	Upper limit of index r
$S(f_r)$	Discrete wave energy frequency spectrum
$S(f_r, \theta_m)$	Discrete wave energy frequency-direction spectrum
x	Dummy variable of integration
α, β	Parameters in an analytic, two-parameter probability function
Γ	Gamma function
Δf	Discrete frequency increment
ΔH	Discrete wave height increment
$\Delta\theta$	Discrete direction increment
θ_0	Mean of wave directions at spectral peak frequency; defines characteristic wave direction
θ_1, θ_2	Arbitrary values bounding a range of wave directions in probability parameter space
θ_k	Element k of an array of K discrete directions associated with probability parameter space
θ_m	Element m of an array of M discrete directions associated with a wave energy spectrum
θ_{min}	Minimum direction in an array of discrete directions
μ	Mean value of a set of observations
σ	Standard deviation of a set of observations

REPORT DOCUMENTATION PAGE

Form Approved
OMB No. 0704-0188

1. AGENCY USE ONLY *(Leave blank)*	2. REPORT DATE	3. REPORT TYPE AND DATES COVERED
	May 1998	Final report

4. TITLE AND SUBTITLE
Joint Wind Wave Height-Frequency-Direction Statistics at Two Disparate Sites

5. FUNDING NUMBERS

6. AUTHOR(S)
Charles E. Long

7. PERFORMING ORGANIZATION NAME(S) AND ADDRESS(ES)
U.S. Army Engineer Waterways Experiment Station
3909 Halls Ferry Road
Vicksburg, MS 39180-6199

8. PERFORMING ORGANIZATION REPORT NUMBER
Technical Report CHL-98-10

9. SPONSORING/MONITORING AGENCY NAME(S) AND ADDRESS(ES)
U.S. Army Corps of Engineers
Washington, DC 20314-1000

10. SPONSORING/MONITORING AGENCY REPORT NUMBER

11. SUPPLEMENTARY NOTES
Available from National Technical Information Service, 5285 Port Royal Road, Springfield, VA 22161.

12a. DISTRIBUTION/AVAILABILITY STATEMENT
Approved for public release; distribution is unlimited.

12b. DISTRIBUTION CODE

13. ABSTRACT ***(Maximum 200 words)***

Joint probability functions associating wind wave characteristics height, spectral peak frequency, and mean wave direction at the peak frequency are estimated based on observations at two sites with distinctively different wave climates. One of the data sources is a directional wave gauge in approximately 8-m water depth, 900 m offshore of the U.S. Army Engineer Waterways Experiment Station Coastal and Hydraulics Laboratory Field Research Facility on the northern Outer Banks of North Carolina. The other data source is a directional wave gauge mounted on the Texaco Oil Company production facility known as Harvest Platform located in about 200 m of water approximately 20 km west of Point Conception, California. The objective is to provide a simple three-parameter statistical characterization of these two sites so that meaningful combinations of these parameters can be used with conventional coastal engineering analysis tools. In addition to three-parameter joint statistics, marginal distributions with wave height-frequency, and joint height-direction are also presented.

14. SUBJECT TERMS
Joint statistics
Wave climate
Wave database
Wind waves

15. NUMBER OF PAGES
107

16. PRICE CODE

17. SECURITY CLASSIFICATION OF REPORT	18. SECURITY CLASSIFICATION OF THIS PAGE	19. SECURITY CLASSIFICATION OF ABSTRACT	20. LIMITATION OF ABSTRACT
UNCLASSIFIED	UNCLASSIFIED		